PFC/JA–86–61

KINETIC EQUILIBRIUM AND STABILITY PROPERTIES OF HIGH–CURRENT BETATRONS

John J. Petillo and Ronald C. Davidson
Plasma Fusion Center
Massachusetts Institute of Technology
Cambridge, Massachusetts 02139

KINETIC EQUILIBRIUM AND STABILITY PROPERTIES OF HIGH–CURRENT BETATRONS

John J. Petillo and Ronald C. Davidson
Plasma Fusion Center
Massachusetts Institute of Technology, Cambridge, Massachusetts 02139

ABSTRACT

Kinetic stability properties of an intense relativistic electron ring in modified and conventional betatron configurations are investigated using the linearized Vlasov–Maxwell equations. Included is the important influence of intense equilibrium self fields. It is assumed that the the ring is thin, and that $\nu/\gamma_b \ll 1$, where ν is Budker's parameter and $\gamma_b mc^2$ is the characteristic electron energy. The stability analysis is carried out for eigenfrequency ω close to harmonics of the cyclotron frequency ω_{cz} in the vertical betatron field. Also included in the analysis is the influence of transverse electromagnetic effects and surface–wave perturbations. Dispersion relations for longitudinal perturbations are obtained, where it is assumed that the ring is located inside a perfectly conducting toroidal shell. There are several noteworthy points. First, transverse electromagnetic effects can completely stabilize the negative–mass instability for sufficiently high–current rings when betatron focusing forces exceed defocusing self–field forces ($\omega_{cz}^2 > \omega_{pe}^2/\gamma_b^2$). Second, for $\omega_{cz}^2 > \omega_{pe}^2/\gamma_b^2$ with no charge neutralization or stabilizing spread in canonical angular momentum ($f = 0$ and $\Delta = 0$), surface–wave instabilities can be completely stabilized at sufficiently low transverse beam temperature. Third, for $\omega_{cz}^2 < \omega_{pe}^2/\gamma_b^2$, sufficiently low transverse temperature together with surface effects combine to drive a radial kink instability. Finally, the dispersion relation is analyzed numerically for parameters representative of the Naval Research Laboratory's modified betatron and the Los Alamos National Laboratory's Liner Driven Ring Accelerator and Phermex Injected Conventional Betatron. Detailed stability results are presented for the projected operating regimes of these devices, including the effects of canonical angular momentum spread, inverse aspect ratio, slowly varying accelerating fields, location of the conducting wall, and radial elongation of the minor ring cross section.

I. INTRODUCTION

High–energy accelerators capable of producing high–current electron beams have been an active and growing area of research. In recent years, there has been considerable effort to improve and modify the technology of existing acceleration schemes[1–4]. Cyclic induction accelerators appear to be very promising, which include the conventional high–current betatron as well as the modified betatron (Fig. 1). In the conventional betatron, a relativistic toroidal electron ring is confined by an external mirror (or betatron) magnetic field, and the change of this magnetic field with time is responsible for the acceleration. In the modified betatron, a strong applied toroidal magnetic field is added to the mirror field of the conventional betatron[5–14]. This has the effect of considerably increasing the limiting beam current over that of the conventional betatron. Denoting the applied fields at the beam center by B_{0z} and $B_{0\theta}$, it is found that the limiting beam current is increased by a factor of $(1/2)(B_{0\theta}/B_{0z})^2$, when $B_{0\theta}/B_{0z} \gg 1$[14]. Also, the stability of the accelerated beam is substantially improved[7–9,11,12].

Detailed analyses of the modified betatron configuration are relatively recent. However, previous theoretical studies have been carried out using kinetic[7–9], single–particle[10–12], and macroscopic fluid[13] models. This paper uses a kinetic model based on the Vlasov–Maxwell equations to investigate longitudinal stability properties over a wide parameter range. Included in the analysis are the important effects of intense self–electric and self–magnetic fields.

Also included in the equilibrium and stability analysis are the important effects of slowly–varying accelerating betatron fields. In this regard, the major radius of the electron ring (R_0) is assumed to remain constant during acceleration. Therefore, when including the effects of time–varying betatron fields, the 2:1 betatron flux condition is assumed to exist[5,15]. This flux rule provides acceleration of particles at constant radius, and the notation 2:1 corresponds to the condition that $2B_z(r,t) =< B_z(t) >$. Here, $B_z(r,t)$ denotes the vertical field at radius r, and $< B_z(t) >$ represents the space–averaged vertical field (averaged from the axis of the torus out to the radius of circulation r).

A summary of kinetic equilibrium properties for both the modified and conventional betatrons is presented in Sec. II. In Sec. III, the longitudinal kinetic dispersion relations are obtained for (a) a betatron with a circular cross section

beam ($a = b$) and without slowly–varying accelerating fields, and (b) a betatron with a noncircular beam and slowly–varying accelerating fields. In both cases, the equilibrium distribution function includes the effects of an immobile, partially neutralizing ion background, and a spread in canonical angular momentum Δ. These dispersion relations, derived in recent calculations[7–9] using the linearized Vlasov–Maxwell equations, are fully electromagnetic, and lowest order toroidal effects have been taken into account in calculating the perturbed charge and current densities. In particular, surface–charge and surface–current perturbations, corresponding to a kink–type perturbation of the ring ($\partial/\partial\phi \neq 0$), are incorporated in the analysis. Perturbed quantities are assumed to have frequency ω approximately equal to a harmonic of the relativistic cyclotron frequency in the vertical betatron field ω_{cz}. Also, the eigenvalue equation has been solved in the limit of large aspect ratio.

In the present work, the dispersion relation is analyzed analytically in Sec. IV for both the modified and conventional betatrons, and exact expressions are derived describing the stability boundaries. In Sec. V, the dispersion relation is solved numerically and the results are applied to the Phase I and Phase II betatrons at the Naval Research Laboratory (NRL) and the Phermex and Liner betatrons at the Los Alamos National Laboratory (LANL).

In Sec. IV, detailed stability properties are first investigated with emphasis on the influence of a spread in canonical angular momentum, transverse electromagnetic effects, and surface–wave perturbations. First, in Sec. IV.A, a small spread (Δ) in canonical angular momentum is shown to have a strong stabilizing influence. Second, in Sec. IV.B, the stabilizing influence of transverse electromagnetic effects is illustrated when the conductor is close to the beam surface ($a_c \simeq a$), allowing surface–wave contributions to be neglected. In the conventional betatron regime ($\omega_{cz}^2 > \omega_{pe}^2/\gamma_b^2$), where betatron focusing forces exceed self–field defocusing forces, the negative–mass instability in both the modified and conventional betatrons is found to be completely stabilized by electromagnetic effects for sufficiently high beam currents. However, in the modified betatron regime ($\omega_{cz}^2 < \omega_{pe}^2/\gamma_b^2$), where betatron focusing forces are exceeded by self–field defocusing forces, the traditional criterion for negative–mass stabilization is recovered.

In Sec. IV.C, the influence of surface–wave perturbations on stability behavior is investigated by assuming a moderate beam energy so that the stabilizing influence of transverse electromagnetic effects can be neglected in the dispersion relation. For

$f = 0$ and $\Delta = 0$, the results divide naturally into two cases. First, when betatron focusing forces exceed self–field defocusing forces ($\omega_{cz}^2 > \omega_{pe}^2/\gamma_b^2$: conventional betatron regime), it is found that the negative–mass instability for a moderate energy modified betatron is absent for sufficiently low transverse beam temperatures. For the conventional betatron in this regime, a sufficiently high density is required to provide stabilization. Second, when betatron focusing forces are exceeded by self–field defocusing forces ($\omega_{cz}^2 < \omega_{pe}^2/\gamma_b^2$: modified betatron regime), it is found that reducing the transverse beam temperature to sufficiently low values results in instability. This instability originates from the inclusion of surface–wave contributions in the dispersion relation and corresponds to a radial kink instability. Finally, in Secs. IV.D and IV.E, exact analytical expressions that determine the stability boundaries for the transverse beam temperature and the inverse aspect ratio are obtained from the dispersion relation.

Section V presents a full numerical investigation of the dispersion relation. Equilibrium and stability boundaries are calculated from the exact analytical expressions in Sec. IV, including effects such as nonneutrality, noncircular minor cross section, canonical angular momentum spread, and time–varying external accelerating fields. Particular emphasis is placed on determining the equilibrium and stability behavior for the projected operating regimes of three betatron devices of current interest. These devices include the Naval Research Laboratory's (NRL) modified betatron (Phase I and Phase II) in Sec. V.B, and the Los Alamos National Laboratory's (LANL) Liner and Phermex conventional betatrons in Sec. V.C. The projected operating parameters for these devices are listed in Table 1. The investigation shows, in the modified betatron regime ($\omega_{cz}^2 < \omega_{pe}^2/\gamma_b^2$), that surface–wave effects tend to be dominant, and a sufficiently high transverse beam temperature is required for stabilization. On the other hand, in the conventional betatron regime ($\omega_{cz}^2 > \omega_{pe}^2/\gamma_b^2$), surface–wave effects require a sufficiently low transverse beam temperature for stabilization. However, when the beam energy is large and the current is sufficiently high, it is found that the system is stabilized by electromagnetic effects for all values of transverse temperature.

Of particular note in Sec. V, for the NRL modified betatron, it is found that transverse beam temperature has a very strong influence on stability behavior. As indicated earlier, in the modified betatron regime, the beam can be stabilized by sufficiently large transverse temperature. Moreover, when a particular operating

point is found to be unstable (e.g., at higher energy), the increase in transverse beam temperature required for stabilization is very modest.

The influence of inverse aspect ratio a/R_0 on stability behavior is also studied in Sec. V for both the NRL modified betatron and the LANL conventional betatrons. It is found that increasing the inverse aspect ratio a/R_0 has a stabilizing effect on the negative–mass instability, where stabilization is due to transverse electromagnetic effects. Generally speaking, the aspect ratio has a weak influence on stability behavior in comparison with the transverse beam temperature.

The stabilizing influence of a spread Δ in canonical angular momentum is also investigated numerically in Sec. V. For the NRL modified betatron, it is found that a very small spread Δ in canonical angular momentum has a strong stabilizing effect.

The influence of noncircular beam cross section on stability behavior is also analyzed in Sec. V for the LANL Phermex conventional betatron. It is found that the negative–mass instability can be stabilized by radially elongating the ring in the minor dimension. However, the degree of radial or axial elongation of the ring is strongly limited by the condition for existence of equilibrium.

The influence of the location of the conducting wall (a_c) is also investigated in Sec. V. For the NRL modified betatron, as the conducting wall radius a_c approaches the beam radius a, it is found that the requirements on transverse beam temperature for stabilization of the radial kink instability decrease. Moreover, for $a_c = a$, surface–wave perturbations do not exist, and the radial kink instability is absent. For the LANL Phermex conventional betatron, as a_c approaches a, the ring can become unstable. For Phermex, this is a weak influence on stability compared with the inverse aspect ratio.

The final effect studied in Sec. V is the influence of slowly–varying accelerating fields on stability behavior for the LANL Liner conventional betatron. It is found that the largest (stabilizing) effect occurs when the acceleration process is just beginning.

II. THEORETICAL MODEL AND EQUILIBRIUM PROPERTIES

This section gives a brief description of the theoretical model and self–consistent equilibrium constraints derived from the Vlasov–Maxwell equations for the modified and conventional betatron configurations.

A. Theoretical Model and Assumptions

The equilibrium configuration used to model the modified and conventional betatrons is illustrated in Fig. 1. It consists of a relativistic electron ring located at the midplane of an externally applied betatron (mirror) magnetic field $B_{0r}^{ext}(r,z)\hat{\mathbf{e}}_r + B_{0z}^{ext}(r,z)\hat{\mathbf{e}}_z$. Moreover, there is an external toroidal magnetic field $B_{0\theta}^{ext}(r,z)\hat{\mathbf{e}}_\theta$, together with the external betatron field, which act to confine the electrons both axially and radially. The equilibrium radius of the electron ring is denoted by R_0 and the minor dimensions of the ring are denoted by $2a$ (radial dimension) and $2b$ (axial dimension). In addition, the electron ring is concentrically located inside a toroidal conductor with minor radius a_c. The electron current in the toroidal direction produces a poloidal self–magnetic field. Furthermore, for $B_{0\theta}^{ext}(r,z) = 0$, the conventional betatron configuration is recovered.

The equilibrium fields provide both focusing and defocusing forces on the electrons in the ring. As indicated earlier, the electrons travel at relativistic velocities in the positive θ–direction. This gives an associated ring current in the negative θ–direction, which produces a poloidal self–magnetic field $\mathbf{B}_0^s(\mathbf{x})$ with the polarity indicated in Fig. 1. This self–magnetic field, by virtue of the Lorentz force on the electrons, produces a focusing force which acts to compress the ring in the minor dimensions.

The electron ring is assumed to be partially neutralized by a positive ion background. The excess electrons form a potential well for the ions. For the electrons, however, the electrostatic forces are repulsive. Thus, the self–electric field produced by a nonneutral ring ($f < 1$) acts as a defocusing field which tends to increase the minor dimensions of the ring.

The modified betatron equilibrium possesses an average equilibrium poloidal rotation of the ring electrons. This rotation, together with the externally applied toroidal magnetic field, provides an additional Lorentz focusing force acting to confine the electrons.

To make the theoretical analysis tractable, we make the following simplifying assumptions, which are consistent with the operating parameters for present and planned betatron experiments [see Tables 1 and 2].

1. The electron ring is immersed in an immobile ($m_i \to \infty$), partially neutralizing ion background. The equilibrium ion density is

$$n_i^0(r,z) = f n_e^0(r,z), \tag{1}$$

where the fractional charge neutralization f is assumed to be constant, and $n_e^0(r,z)$ is the equilibrium electron density. This approximation may be highly idealized, but it provides a good qualitative indication of the effects of a neutralizing ion background on equilibrium properties of the electron ring.

2. The minor dimensions of the electron ring and the conducting wall are small compared to the major radius, i.e.,

$$a, b \ll R_0, \quad a_c \ll R_0. \tag{2}$$

3. Furthermore, it is assumed that

$$\frac{\nu}{\gamma_b} = \frac{N_e}{2\pi R_0} \frac{e^2}{mc^2} \frac{1}{\gamma_b} \ll 1, \tag{3}$$

where ν is Budker's parameter, N_e is the total number of electrons in the ring, $-e$ is the electron charge, m is the electron rest mass, c is the speed of light *in vacuo*, e^2/mc^2 is the classical electron radius, and $\gamma_b mc^2$ is the characteristic energy of the beam electrons. For an electron beam with uniform density $\bar{n}_e = N_e/2\pi^2 ab R_0$, it can be shown that

$$\frac{\nu}{\gamma_b} = \frac{\omega_{pe}^2 ab}{4c^2}, \tag{4}$$

where $\omega_{pe}^2 \equiv 4\pi e^2 \bar{n}_e/\gamma_b m$ is the relativistic electron plasma frequency–squared.

4. The characteristic transverse (r,z) kinetic energy of the beam electrons is small compared to the characteristic azimuthal energy, i.e.,

$$\frac{p_r^2 + p_z^2}{2\gamma_b m} \ll \gamma_b mc^2, \tag{5}$$

where $p_\theta \simeq \gamma_b m \beta_b c$ is the characteristic azimuthal momentum.

5. The spread in canonical angular momentum $\delta P_\theta = P_\theta - P_0$ is assumed to be sufficiently small that $|\delta P_\theta| \ll \gamma_b m \beta_b c R_0$. For the modified betatron, it is further assumed that[7-9]

$$\frac{|\delta P_\theta|}{\gamma_b m \beta_b c R_0} \ll \frac{\hat{B}_\theta}{\hat{B}_z}\left|\frac{p_\perp}{p_\theta}\right|, \tag{6}$$

where $p_\perp = (p_r^2 + p_z^2)^{1/2}$ is the characteristic transverse momentum, p_θ is the characteristic azimuthal momentum, and $\hat{B}_z = B_{0z}^{ext}(R_0, 0)$ and $\hat{B}_\theta = B_{0\theta}^{ext}(R_0, 0)$. For the modified betatron, Eq. (6) together with the assumption of circular cross section, i.e.,

$$\begin{aligned} a &= b, \\ n &= 1/2, \end{aligned} \tag{7}$$

are sufficient to assure that the poloidal canonical angular momentum P_ϕ is a good approximate invariant. In Eq. (7), the external field index n is defined by

$$n = -\left[\frac{r}{B_{0z}^{ext}(r,z)}\frac{\partial B_{0z}^{ext}(r,z)}{\partial r}\right]_{(R_0,0)}. \tag{8}$$

B. Self–Consistent Vlasov Equilibrium

A particular choice of Vlasov equilibrium which incorporates the essential properties of both types of betatron configurations is given by[7-9]

$$f_e^0(H, P_\phi, P_\theta) = \frac{\bar{n}_e R_0 \Delta}{2\pi^2 \gamma_b m} \frac{\delta(H - \omega_b P_\phi - \hat{\gamma} m c^2)}{\left[(P_\theta - P_0)^2 + \Delta^2\right]}. \tag{9}$$

Here, $\bar{n}_e$, R_0, Δ, ω_b, P_0, and $\hat{\gamma}$ are constants, and ω_b is the poloidal rotation frequency of the ring electrons. In addition, the relativistic factors evaluated at the reference orbit position $(R_0, 0)$ are defined by

$$\gamma_b = \gamma(R_0, 0), \quad \beta_b = \beta(R_0, 0), \tag{10}$$

where $\beta(r,z) = V_{0\theta}(r,z)/c$. Also, the canonical angular momentum at the reference orbit is defined by

$$P_0 = P_\theta(R_0, 0) = \frac{e\hat{B}_z}{2c} R_0^2. \tag{11}$$

For the modified betatron, the distribution function in Eq. (9) gives a ring equilibrium with uniform beam density, a constant toroidal current density, and a rigid–rotor poloidal current density. For the conventional betatron, the poloidal rotation frequency ω_b is set equal to zero in Eq. (9), and no poloidal current is included in the analysis. Moreover, for both types of betatron configurations, a Lorentzian spread in canonical angular momentum P_θ has been incorporated in the distribution function in Eq. (9).

For the equilibrium configuration illustrated in Fig. 1, the total energy H and the canonical angular momentum P_θ are exact single–particle constants of the motion in the equilibrium fields. Here, H and P_θ are defined by

$$\begin{aligned} H &= \left[m^2c^4 + c^2\mathbf{p}^2\right]^{1/2} - e\phi_0(r,z), \\ P_\theta &= r\left[p_\theta - \frac{e}{c}A_{0\theta}(r,z)\right]. \end{aligned} \tag{12}$$

In Eq. (12), $\phi_0(r,z)$ is the equilibrium electrostatic potential, $A_{0\theta}(r,z) = A_{0\theta}^{ext}(r,z) + A_{0\theta}^{s}(r,z)$ is the θ–component of the vector potential for the total equilibrium magnetic field, and $\mathbf{p}$ is the mechanical momentum, where

$$\mathbf{v} = \frac{\mathbf{p}}{\gamma m} = \frac{\mathbf{p}/m}{(1 + \mathbf{p}^2/m^2c^2)^{1/2}}, \tag{13}$$

with $\mathbf{p}^2 = (p_r^2 + p_\theta^2 + p_z^2)$.

When $a = b$ (circular cross section) and the inequality in Eq. (6) is satisfied, an additional *approximate* single particle constant of the motion is the canonical angular momentum P_ϕ in the poloidal direction. Here, P_ϕ is defined by

$$P_\phi = \rho p_\phi - \frac{e\hat{B}_\theta}{2c}\rho^2, \tag{14}$$

where p_ϕ is the ϕ–component of the mechanical momentum, and (ρ, ϕ) denotes the coordinate transformation

$$\begin{aligned} r' &= r - R_0 = \rho\cos\phi, \\ z &= \rho\sin\phi. \end{aligned} \tag{15}$$

C. General Equilibrium Properties

The distribution function in Eq. (9) can be used to calculate several equilibrium properties common to both the modified and conventional betatron configurations. For example, the equilibrium electron density $n_e^0(r,z) = \int d^3p\, f_e^0$ obtained from Eq. (9) for a thin electron ring is given by

$$n_e^0(r,z) = \bar{n}_e U_{-1}\left[1 - \left(\frac{r'^2}{a^2} + \frac{z^2}{b^2}\right)\right], \tag{16}$$

where $U_{-1}(x)$ is the Heaviside step function defined by

$$U_{-1}(x) = \begin{cases} 1, & \text{if} \quad x \geq 0, \\ 0, & \text{if} \quad x < 0. \end{cases} \tag{17}$$

From Eq. (16), the electron density is constant ($\bar{n}_e$) within the elliptical boundary defined by $r'^2/a^2 + z^2/b^2 = 1$ and equal to zero outside. The minor dimensions a and b are defined by

$$\begin{aligned} a &= \left[\frac{2(\hat{\gamma} - \gamma_b)c^2}{\gamma_b \Omega_r^2}\right]^{1/2}, \\ b &= \left[\frac{2(\hat{\gamma} - \gamma_b)c^2}{\gamma_b \Omega_z^2}\right]^{1/2}, \end{aligned} \tag{18}$$

where $\hat{\gamma} > \gamma_b$, $\Omega_r^2 > 0$, and $\Omega_z^2 > 0$ are required for existence of the equilibrium. Here, the effective transverse focusing frequencies, Ω_r and Ω_z, are defined by

$$\begin{aligned} \Omega_r^2 &= \omega_b\omega_{c\theta} - \omega_b^2 + \omega_r^2, \\ \Omega_z^2 &= \omega_b\omega_{c\theta} - \omega_b^2 + \omega_z^2. \end{aligned} \tag{19}$$

Moreover, the radial and axial betatron frequencies, ω_r and ω_z, in Eq. (19) are expressed as

$$\omega_r^2 = \omega_{cz}^2(1-n) + \omega_{pe}^2 \frac{b}{a+b}\Big[\beta_b^2 - (1-f)\Big],$$

$$\omega_z^2 = \omega_{cz}^2 n + \omega_{pe}^2 \frac{a}{a+b}\Big[\beta_b^2 - (1-f)\Big]. \tag{20}$$

The betatron frequencies, ω_r and ω_z, correspond to the transverse oscillation frequencies of the electron orbits in a conventional betatron. The first term on the right–hand sides of Eq. (20) represents the focusing effect of the external betatron fields, whereas the second term represents the defocusing ($\beta_b^2 < 1-f$) effect produced by the equilibrium self–fields. In Eqs. (19) and (20), $\omega_{pe} = (4\pi\bar{n}_e e^2/\gamma_b m)^{1/2}$ is the relativistic electron plasma frequency, and ω_{cz} and $\omega_{c\theta}$ are the relativistic electron cyclotron frequencies in the external vertical and toroidal magnetic fields, respectively, i.e.,

$$\omega_{cz} \equiv \frac{e\hat{B}_z}{\gamma_b mc}, \quad \omega_{c\theta} \equiv \frac{e\hat{B}_\theta}{\gamma_b mc}. \tag{21}$$

Here, $\hat{B}_z \equiv B_{0z}^{ext}(R_0,0)$ and $\hat{B}_\theta \equiv B_{0\theta}^{ext}(R_0,0)$. Expressing the external field index n in terms of the minor beam radii a and b, we find that Eq. (20) can be expressed as

$$\frac{\omega_r^2}{\omega_{cz}^2} = \frac{b^2}{a^2+b^2}\left(1 + \frac{\omega_{pe}^2}{\omega_{cz}^2}\left\{\Big[\beta_b^2 - (1-f)\Big] + \frac{a(b-a)}{b(a+b)}(1-f)\right\}\right),$$

$$\frac{\omega_z^2}{\omega_{cz}^2} = \frac{a^2}{a^2+b^2}\left(1 + \frac{\omega_{pe}^2}{\omega_{cz}^2}\left\{\Big[\beta_b^2 - (1-f)\Big] + \frac{b(a-b)}{a(a+b)}(1-f)\right\}\right). \tag{22}$$

The above expressions for ω_r^2 and ω_z^2 allow the traditional limits of circular cross section ($a = b$) and full nonneutrality ($f = 0$) to be taken easily.

D. Modified Betatron Equilibrium

The results in Sec. II.C can be simplified further for the special case of a modified betatron with circular cross section, i.e.,

$$\hat{B}_\theta \neq 0, \qquad a = b, \qquad n = 1/2. \tag{23}$$

In this case, the betatron frequencies in Eq. (20) can be expressed as $\omega_\beta^2 = \omega_r^2 = \omega_z^2$, which gives $\Omega_\beta^2 = \Omega_r^2 = \Omega_z^2$ in Eq. (19). Here, ω_β^2 and Ω_β^2 are defined by

$$\omega_\beta^2 \equiv \frac{1}{2}\omega_{cz}^2 + \frac{1}{2}\omega_{pe}^2\left[\beta_b^2 - (1-f)\right], \tag{24}$$

$$\Omega_\beta^2 \equiv \omega_b\omega_{c\theta} - \omega_b^2 + \omega_\beta^2. \tag{25}$$

Additional equilibrium properties can also be calculated from Eq. (9). For example, the average poloidal velocity of the electrons, $V_{0\phi}(r,z) = [\int d^3p\,(p_\phi/\gamma m)\,f_e^0]$ $/(\int d^3p\,f_e^0)$, can be approximated by

$$V_{0\phi}(r,z) = \omega_b\rho, \tag{26}$$

where $\rho = (r'^2 + z^2)^{1/2}$. Moreover, the equilibrium pressure tensor can be shown to be isotropic in the plane perpendicular to the toroidal axis of the ring. From Eq. (9), the effective transverse temperature profile, $T_{0\perp}(r,z) = [\int d^3p\,(p_r^2+p_z^2)\,f_e^0/2\gamma m)]$ $/(\int d^3p\,f_e^0)$, can be approximated by (for $\rho \leq a$)

$$T_{0\perp}(\rho) = \hat{T}_\perp\left(1 - \frac{\rho^2}{a^2}\right), \tag{27}$$

where

$$\hat{T}_\perp \equiv \frac{1}{2}\gamma_b m\Omega_\beta^2 a^2 = \frac{1}{2}\gamma_b m\omega_{c\theta}^2 r_L^2. \tag{28}$$

In Eq. (28), r_L is the characteristic thermal Larmor radius of the ring electrons in the toroidal magnetic field $\hat{B}_\theta$. Making use of Eqs. (25) and (28) and the condition that $\Omega_\beta^2 > 0$, the rotation frequency ω_b can be determined in terms of r_L. This gives

$$\omega_b = \hat{\omega}_b^{\pm} \equiv \frac{\omega_{c\theta}}{2}\left(1 \pm \left\{1 + \frac{2\omega_{cz}^2}{\omega_{c\theta}^2} - \frac{2\omega_{pe}^2}{\omega_{c\theta}^2}\left[(1-f) - \beta_b^2\right] - \left(\frac{2r_L}{a}\right)^2\right\}^{1/2}\right). \tag{29}$$

The two signs ($\pm$) in Eq. (29) represent fast ($+$) and slow ($-$) rotational equilibria. For the equilibrium to exist, it follows from Eq. (29) that the inequality

$$\frac{\omega_{pe}^2}{\omega_{cz}^2}\Big[(1-f)-\beta_b^2\Big] < 1+\frac{\omega_{c\theta}^2}{2\omega_{cz}^2}\left[1-\left(\frac{2r_L}{a}\right)^2\right] \tag{30}$$

must be satisfied.

E. Conventional Betatron Equilibrium

For the conventional betatron, we neglect beam rotation and set the toroidal magnetic field equal to zero in Secs. II.B and II.C, i.e.,

$$\begin{aligned} \hat{B}_\theta &= 0, \\ \omega_b &= 0. \end{aligned} \tag{31}$$

From Eqs. (19) and (20), it readily follows that

$$\begin{aligned} \Omega_r^2 &= \omega_r^2 = \omega_{cz}^2(1-n)+\omega_{pe}^2\frac{b}{a+b}\Big[\beta_b^2-(1-f)\Big], \\ \Omega_z^2 &= \omega_z^2 = \omega_{cz}^2 n+\omega_{pe}^2\frac{a}{a+b}\Big[\beta_b^2-(1-f)\Big], \end{aligned} \tag{32}$$

where n is the external field index defined in Eq. (8). Making use of Eq. (20), the condition for equilibrium to exist now reduces to the two conditions, $\omega_r^2 = \Omega_r^2 > 0$ and $\omega_z^2 = \Omega_z^2 > 0$, which give

$$\begin{aligned} \omega_{pe}^2\frac{b}{a+b}\Big[(1-f)-\beta_b^2\Big] &< \omega_{cz}^2(1-n), \\ \omega_{pe}^2\frac{a}{a+b}\Big[(1-f)-\beta_b^2\Big] &< \omega_{cz}^2 n. \end{aligned} \tag{33}$$

From Eq. (22), it follows that Eq. (33) can be expressed in the equivalent form

$$\begin{aligned} \omega_{pe}^2\left\{\Big[(1-f)-\beta_b^2\Big]+\frac{a(a-b)}{b(a+b)}(1-f)\right\} &< \omega_{cz}^2, \\ \omega_{pe}^2\left\{\Big[(1-f)-\beta_b^2\Big]+\frac{b(b-a)}{a(a+b)}(1-f)\right\} &< \omega_{cz}^2. \end{aligned} \tag{34}$$

Depending on the sign of $(a-b)$, we choose the stricter of the two conditions in Eq. (34) as the condition for the equilibrium to exist. Therefore, for $a > b$, the first equation from Eq. (34) is chosen, and the second equation is chosen for $b > a$. The above equations relate the maximum allowable equilibrium beam density to f, β_b, ω_{cz}, and n (or equivalently a and b). For the case of a circular beam with $a = b$ and $n = 1/2$, we note that the maximum allowable density for the modified betatron in Eq. (30) is higher than the maximum allowable density for the conventional betatron. This is due to the presence of the toroidal magnetic field in Eq. (30). Therefore, the modified betatron allows a higher limiting beam current. For the case where $\hat{B}_\theta/\hat{B}_z \gg 1$, the ratio of the modified to conventional betatron limiting currents is given by $\hat{B}_\theta^2/2\hat{B}_z^2$.

Additional equilibrium properties of the conventional betatron can also be evaluated. For example, the effective transverse temperature within the electron beam can be approximated by

$$T_{0\perp}(r,z) = \hat{T}_\perp\left[1-\left(\frac{r'^2}{a^2}+\frac{z^2}{b^2}\right)\right], \tag{35}$$

where

$$\hat{T}_\perp = \frac{1}{2}\gamma_b m\Omega_r^2 a^2. \tag{36}$$

Therefore, for the choice of equilibrium distribution function in Eq. (9), the transverse temperature for the conventional betatron is constant on elliptical surfaces that are concentric and confocal to the outer beam boundary.

III. ELECTROMAGNETIC DISPERSION RELATION FOR LONGITUDINAL PERTURBATIONS

In this section, we discuss the dispersion relation for small-amplitude perturbations about the equilibrium betatron configuration described in Sec. II.B. First, in Sec. III.A, the longitudinal dispersion relation is presented in the circular beam limit, neglecting the effects of slowly varying external accelerating fields ($\dot{\gamma}_b = 0 = \ddot{\gamma}_b$). The resulting dispersion relation [Eq. (45)] includes the influence of transverse electromagnetic effects, body-wave and surface-wave perturbations, a spread in canonical angular momentum, and a finite transverse emittance of the beam electrons. Then, in Sec. III.B, the longitudinal dispersion relation [Eq. (47)] is presented for the case where the beam cross section is allowed to be noncircular, and the effects of slowly varying external accelerating fields ($\dot{\gamma}_b \neq 0$, $\ddot{\gamma}_b \neq 0$) are included in the analysis.

In deriving the dispersion relation, a normal-mode approach is taken whereby all perturbed quantities are assumed to vary according to

$$\delta\psi(\mathbf{x},t) = \delta\hat{\psi}_\theta(r,z)\exp\Big[i(l\theta - \omega t)\Big]. \tag{37}$$

Here, ω is the complex oscillation frequency, and l is the toroidal mode number. In addition to the assumptions enumerated in Sec. II.A, the following assumptions are made in the stability analysis.

1. First, it is assumed that $\mathrm{Re}(\omega) \simeq l\omega_{cz}$ and that the waves are far removed from resonance with the transverse (r,z) motion of the electrons. This can be expressed as[7,16]

$$\left|\left(\frac{\omega_x}{\omega - l\omega_{cz}}\right)^2 - 1\right|, \quad \left|\left(\frac{\omega_y}{\omega - l\omega_{cz}}\right)^2 - 1\right|, \quad \left|\frac{\omega_x}{\omega}\right|, \quad \left|\frac{\omega_y}{\omega}\right| \gg \frac{a}{R_0}, \quad \frac{b}{R_0}, \tag{38}$$

where ω_x and ω_y are defined by

$$\omega_x^2 = \omega_r^2 + \frac{1}{4}\left(\frac{\dot{\gamma}_b}{\gamma_b}\right)^2 - \frac{1}{2}\left(\frac{\ddot{\gamma}_b}{\gamma_b}\right),$$

$$\omega_y^2 = \omega_z^2 + \frac{1}{4}\left(\frac{\dot{\gamma}_b}{\gamma_b}\right)^2 - \frac{1}{2}\left(\frac{\ddot{\gamma}_b}{\gamma_b}\right). \tag{39}$$

Note that ω_x and ω_y are similar to the betatron frequencies defined in Eq. (20), modified by the effects of the slow time variation of the betatron accelerating fields.

2. Second, the toroidal mode number l is assumed to be sufficiently small that

$$\frac{l}{\gamma_b}\frac{a_c}{R_0} \ll 1. \tag{40}$$

A. Circular Beam without Slowly Varying Accelerating Fields

In this section, the dispersion relation is presented for both the modified and conventional betatrons in the circular beam limit ($a = b$), neglecting the effects of slowly varying external accelerating fields ($\dot{\gamma}_b = 0 = \ddot{\gamma}_b$). Therefore, $\omega_\beta = \omega_r = \omega_z = \omega_x = \omega_y$, and $\Omega_\beta^2 = \Omega_r^2 = \Omega_z^2$. In this limit, the dispersion relation can be expressed as[7,8]

$$1 + \frac{\nu}{\gamma_b}\left(2\ln\frac{a_c}{a} + 1\right)\frac{k^2c^2}{\left(\omega - l\omega_{cz} + i\left|\mu k\Delta\right|/\gamma_b m R_0\right)^2}$$
$$\times\left[\mu\left(1 - \frac{\omega\beta_b}{ck}\right) + \frac{\omega\left(\omega - l\omega_{cz}\right)}{\gamma_b^2 k^2 c^2} - \frac{\omega_{pe}^2\omega_{cz}^2}{2\omega_\beta^2\Omega_\beta^2}\left(1 - \frac{\omega\beta_b}{ck}\right)^2\left(1 - \frac{a^2}{a_c^2}\right)\right] = 0, \tag{41}$$

where $k \equiv l/R_0$, Budker's parameter ν is defined in Eq. (4), the betatron frequency ω_β is defined in Eq. (24), the effective transverse oscillation frequency Ω_β is defined in Eq. (25), and μ is the traditional negative–mass parameter defined by

$$\mu = \frac{\omega_{cz}^2}{\omega_\beta^2} - \frac{1}{\gamma_b^2}. \tag{42}$$

It should be pointed out that transverse electromagnetic effects are included in the terms proportional to $(1 - \omega\beta_b/ck)$ in Eq. (41), and the terms proportional to μ and $\omega(\omega - l\omega_{cz})$ represent contributions from body–wave perturbations within the electron ring ($\rho < a$). On the other hand, the term proportional to $(1 - a^2/a_c^2)$ in Eq. (41) represents the contribution localized at the surface of the electron ring ($\rho = a$). The factor proportional to Δ in Eq. (41) arises from the spread in canonical angular momentum. Moreover, because the effective transverse temperature is proportional to Ω_β^2, transverse thermal effects are incorporated in the last term on the left–hand side of Eq. (41). Finally, the lowest–order effects of finite inverse aspect ratio a/R_0 are manifest in the factor ν/γ_b, which can be expressed as

$$\frac{\nu}{\gamma_b} = \frac{\beta_b^2}{4}\frac{\omega_{pe}^2}{\omega_{cz}^2}\frac{a^2}{R_0^2}. \tag{43}$$

It is convenient to introduce the normalized Doppler–shifted frequency χ defined by

$$\chi = \frac{\omega - l\omega_{cz}}{\omega_{cz}}. \tag{44}$$

Equation (41) can then be expressed in the equivalent form

$$\begin{aligned}
&\chi^2\left[1 + G_1\frac{\nu}{\gamma_b^3}\left(1 - \beta_b^2\gamma_b^4\frac{\omega_{pe}^2\omega_{cz}^2}{2\gamma_b^2\omega_\beta^2\Omega_\beta^2}G_2\right)\right] \\
&+l\chi\left[G_1\frac{\nu}{\gamma_b^3}\left(1 - \gamma_b^2\mu + 2\gamma_b^2\frac{\omega_{pe}^2\omega_{cz}^2}{2\gamma_b^2\omega_\beta^2\Omega_\beta^2}G_2\right) + 2i\,|\mu|\,\frac{\Delta}{\gamma_b m\beta_b c R_0}\right] \\
&+l^2\left[G_1\frac{1}{\beta_b^2}\frac{\nu}{\gamma_b^3}\left(\mu - \frac{\omega_{pe}^2\omega_{cz}^2}{2\gamma_b^2\omega_\beta^2\Omega_\beta^2}G_2\right) - \mu^2\left(\frac{\Delta}{\gamma_b m\beta_b c R_0}\right)^2\right] = 0,
\end{aligned} \tag{45}$$

where G_1 and G_2 are the geometric factors defined by

$$\begin{aligned}
G_1 &= 2\ln\frac{a_c}{a} + 1, \\
G_2 &= \left(1 - \frac{a^2}{a_c^2}\right),
\end{aligned} \tag{46}$$

and the definitions for ν, ω_β, Ω_β, and μ are defined in Eqs. (4), (24), (25), and (42), respectively. We note from Eq. (45) that χ scales linearly with the toroidal mode number l.

B. Noncircular Beam with Slowly Varying Accelerating Fields

The effects of noncircularity and slowly varying accelerating fields are now included in the dispersion relation. The appropriate generalization of Eq. (45) can be expressed as[7]

$$\begin{aligned}
&\chi^2\left[1 + G_1'\frac{\nu}{\gamma_b^3}\left(1 - \beta_b^2\gamma_b^4\frac{\omega_{pe}^2\omega_{cz}^2}{2\gamma_b^2\omega_x^2\Omega_r^2}G_2'\right)\right] \\
&+l\chi\left[G_1'\frac{\nu}{\gamma_b^3}\left(1 - \gamma_b^2\mu + 2\gamma_b^2\frac{\omega_{pe}^2\omega_{cz}^2}{2\gamma_b^2\omega_x^2\Omega_r^2}G_2'\right) + 2i\,|\mu|\,\frac{\Delta}{\gamma_b m\beta_b c R_0}\right] \\
&+l^2\left[G_1'\frac{1}{\beta_b^2}\frac{\nu}{\gamma_b^3}\left(\mu - \frac{\omega_{pe}^2\omega_{cz}^2}{2\gamma_b^2\omega_x^2\Omega_r^2}G_2'\right) - \mu^2\left(\frac{\Delta}{\gamma_b m\beta_b c R_0}\right)^2\right] = 0.
\end{aligned} \tag{47}$$

Here, the normalized Doppler–shifted frequency χ is defined in Eq. (44), ν is defined in Eq. (4), and the geometric factors G_1' and G_2' are defined by[7]

$$G_1' = 2\ln\frac{2a_c}{a+b} + 1,$$

$$G_2' = \frac{1}{a(a+b)}\left[a^2 - ab + 2b^2 - \frac{a(a+b)}{4a_c^2}\left(2b^2 + a^2\right)\right]. \tag{48}$$

The betatron frequency ω_x is defined in Eq. (39), which includes modifications due to the slowly varying accelerating fields and the noncircular cross section. The noncircular contributions to ω_x are manifest in the definition of ω_r in Eq. (20). In addition, the negative–mass parameter μ, which is modified by both effects, can be expressed as

$$\mu = \frac{\omega_{cz}^2}{\omega_x^2} - \frac{1}{\gamma_b^2}. \tag{49}$$

Note also that the Ω_r factor in Eq. (47) is modified by noncircular effects [see Eqs. (19) and (20)].

IV. STABILITY PROPERTIES: ANALYTICAL RESULTS

Stability properties for the modified and conventional betatron configurations are studied analytically in this section for the circular, nonaccelerating case ($a = b$, $\dot{\gamma}_b = 0 = \ddot{\gamma}_b$). First, in Sec. IV.A, an exact solution for the eigenfrequency ω is obtained from the dispersion relation in Eq. (45). Then, Secs. IV.B, IV.C, and IV.D address specific limiting cases which demonstrate the influence on stability behavior due to a spread in canonical angular momentum, transverse electromagnetic effects, and surface–wave perturbations, respectively. Finally, Secs. IV.E and IV.F address the effects of transverse beam temperature and inverse toroidal aspect ratio, respectively, and the corresponding stability boundaries are calculated analytically from the dispersion relation.

A. Exact Solution to the Dispersion Relation

In this section, the exact solution to the dispersion relation in Eq. (45) is obtained for both the modified and conventional betatron. The solution can be expressed in terms of the dimensionless variables l, γ_b, $\hat{a}$, $\hat{b}$, and μ, where

$$\hat{a} = \frac{\nu}{\gamma_b^3} G_1 = \frac{1}{4}\frac{\beta_b^2}{\gamma_b^2}\left(\frac{\omega_{pe}}{\omega_{cz}}\right)^2\left(\frac{a}{R_0}\right)^2\left(2\ln\frac{a_c}{a}+1\right) > 0,$$

$$\hat{b} = \frac{\omega_{pe}^2\omega_{cz}^2}{2\gamma_b^2\omega_\beta^2\Omega_\beta^2}\left(1-\frac{a^2}{a_c^2}\right). \tag{50}$$

The sign of $\hat{b}$ in Eq. (50) is determined by the sign of ω_β^2 [see Eq. (24)]. We define the dimensionless coefficients occurring in Eq. (45) by

$$A_\chi = 1 + \hat{a}\left(1-\beta_b^2\gamma_b^4\hat{b}\right),$$

$$B_\chi = \hat{a}\left[1-\gamma_b^2\left(\mu-2\hat{b}\right)\right],$$

$$C_\chi = \frac{\hat{a}\left(\mu-\hat{b}\right)}{\beta_b^2}, \tag{51}$$

$$\Delta_\chi = \frac{\Delta}{\gamma_b m\beta_b c R_0}.$$

Solving Eq. (45) for the complex eigenfrequency ω gives

$$\omega = l\omega_{cz}\left\{1 - \frac{(B_\chi + 2i\,|\mu|\,\Delta_\chi)}{2A_\chi} \pm \frac{\left[(B_\chi + 2i\,\mu|\,\Delta_\chi)^2 - 4A_\chi\left(C_\chi - \mu^2\Delta_\chi^2\right)\right]^{1/2}}{2A_\chi}\right\}, \tag{52}$$

where A_χ, B_χ, C_χ, Δ_χ, and μ [Eq. (42)] are real-valued quantities.

For zero spread in canonical angular momentum ($\Delta = 0$), the necessary and sufficient condition for instability ($\mathrm{Im}[\omega] > 0$) obtained from Eq. (52) is given by

$$B_\chi^2 - 4A_\chi C_\chi < 0. \tag{53}$$

This limiting case ($\Delta = 0$) is investigated further in Secs. IV.C–IV.F. In addition, Sec. IV.B investigates stability properties allowing a small, non–zero spread in canonical angular momentum ($\Delta \neq 0$).

B. Stabilizing Influence of a Small Spread in Canonical Angular Momentum

The influence of a spread in canonical angular momentum on stability behavior is investigated in this section. We assume sufficiently small Δ that

$$\Delta_\chi^2 \ll \left|\frac{B_\chi^2 - 4A_\chi C_\chi}{4\mu^2\,(A_\chi - 1)}\right|, \tag{54}$$

where Δ_χ is defined in Eq. (51). It can be shown that the necessary and sufficient condition for stability when $B_\chi^2 - 4A_\chi C_\chi < 0$ is given by

$$\frac{\Delta}{\gamma_b m\beta_b c R_0} > \frac{\left(4A_\chi C_\chi - B_\chi^2\right)^{1/2}}{2\,|\mu|}. \tag{55}$$

For typical betatron parameters, Eq. (55) can be approximated by

$$\frac{\Delta}{\gamma_b m\beta_b c R_0} \gtrsim \frac{8\,[2\ln(a_c/a) + 1]}{\beta_b^2\gamma_b^4}\left(\frac{\nu}{\gamma_b}\right)^2\left(\frac{R_0}{a}\right)^2 \ll 1. \tag{56}$$

Equation (56) states that a small spread (Δ) in canonical angular momentum indeed has a strong stabilizing effect in both modified and conventional betatron configurations.

C. Stabilizing Influence of Transverse Electromagnetic Effects

This section addresses the influence of transverse electromagnetic effects on stability behavior[7,8]. The transverse electromagnetic effect contributions are present in the terms in Eq. (45) proportional to ω/ck. By rewriting the dispersion relation using the dimensionless coefficients in Eq. (51), these contributions are included by way of the solitary $\hat{a}$ term in the definition of A_χ as well as the $\hat{a}(1-\gamma_b^2\mu)$ term in the definition of B_χ. To emphasize this effect, we take the limit where $\Delta = 0$ and $a \simeq a_c$. The limit $a \simeq a_c$ allows us to neglect the $\hat{b}$ terms from the coefficients in Eq. (51) which represent surface–wave contributions. In addition, the assumption that $\nu/\gamma_b \ll 1$ allows us to neglect the $\hat{a}$ term in A_χ. Within the context of these assumptions, it can be shown that two ranges of μ [Eq. (42)] exist for which the beam is stable: μ negative, and μ greater than some positive value.

For negative values of μ, the condition for stability ($\mu < 0$) is the traditional criterion for stabilization of the negative–mass instability[17]. For the modified betatron, the stability condition $\mu < 0$ combined with the condition for existence of the equilibrium [Eq. (30)] become

$$1 < \frac{\omega_{pe}^2}{\gamma_b^2\omega_{cz}^2} < 1 + \frac{\omega_{c\theta}^2}{2\omega_{cz}^2}\left[1 - \left(\frac{2r_L}{a}\right)^2\right], \tag{57}$$

where it has been assumed that $f = 0$. It is evident that the inequality in Eq. (57) can be satisfied provided $\omega_{pe}^2/\omega_{cz}^2$ is sufficiently large. Therefore, in the modified betatron, the negative–mass instability can be completely stabilized provided the equilibrium density and, thus, equilibrium self–field effects are sufficiently strong. On the other hand, in the conventional betatron, the condition $\mu < 0$ and the condition for existence of the equilibrium [Eqs. (33)] cannot be satisfied when $f = 0$. However, for $f \neq 0$, the condition $\mu < 0$ combined with the condition for existence of the equilibrium can be expressed as

$$\frac{\omega_{pe}^2}{\gamma_b^2\omega_{cz}^2}\left(\gamma_b^2 f - 1\right) > 2\gamma_b^2 - 1. \tag{58}$$

Equation (58) states that $f > 1/\gamma_b^2$ is a necessary condition for both equilibrium and stability when $\mu < 0$. Therefore, for $\Delta = 0$ and $a \simeq a_c$, a partially neutralizing ion

background must be included in the conventional betatron to stabilize the negative–mass instability. Assuming that sufficient charge neutralization is included, Eq. (58) can be satisfied provided $\omega_{pe}^2/\omega_{cz}^2$ is sufficiently large. Thus, the traditional negative–mass instability is completely stabilized in a conventional betatron provided the focusing effect of the equilibrium self–magnetic field exceeds the defocusing effect of the self–electric field ($f > 1/\gamma_b^2$), and the net self-focusing force is sufficiently strong.

In the regime where $\mu > 0$, for the case where $a = b$ and $\dot{\gamma}_b = 0 = \ddot{\gamma}_b$, there is a radical departure from the traditional negative–mass stability criterion[7,8]. In particular, due to transverse electromagnetic effects, we find from Eq. (45) that a threshold value of μ exists, above which the negative–mass instability is absent. For a given positive value of μ, the necessary and sufficient condition for stability can be expressed as

$$\frac{\nu}{\gamma_b} > \frac{4\mu/(\gamma_b^2 - 1)}{(\mu - 1/\gamma_b^2)^2[2\ln(a_c/a) + 1]}. \tag{59}$$

For an ultrarelativistic electron beam with $\gamma_b \gg 1$, Eq. (59) can be satisfied easily for both the modified and conventional betatron configurations provided the beam current (proportional to ν/γ_b) is sufficiently large.

D. Influence of Surface–Wave Perturbations on Stability Behavior

The influence of surface–wave perturbations on stability behavior is investigated in this section. The surface–wave effects are manifest in the $\hat{b}$ terms in Eq. (51). To emphasize the influence of these perturbations, it is assumed that the electron ring is fully nonneutral ($f = 0$), with no stabilizing canonical angular momentum spread ($\Delta = 0$). In addition, a moderate beam energy is assumed such that the stabilizing effect of transverse electromagnetic perturbations can be neglected. In this case, the solitary $\hat{a}$ term in the definition of A_χ is neglected, along with the $\hat{a}(1 - \gamma_b^2\mu)$ term in the definition of B_χ [see Eq. (51)].

The results fall into the two following categories: (a) the betatron focusing forces exceed the defocusing self–field forces ($\omega_\beta^2 > 0$), and (b) the betatron focusing forces are exceeded by the defocusing self–field forces ($\omega_\beta^2 < 0$). It should be noted that case (b) excludes the conventional betatron, since an equilibrium does not exist

when $f = 0$. Thus, case (b) ($\omega_\beta^2 < 0$) is referred to as the *modified betatron regime*. Moreover, case (a) ($\omega_\beta^2 > 0$) is referred to as the *conventional betatron regime*, since it is traditionally the regime in which a conventional betatron accelerator operates.

(a) Conventional Betatron Regime ($\omega_{cz}^2 > \omega_{pe}^2/\gamma_b^2$)**:** For a modified betatron operating in the conventional betatron regime, the necessary and sufficient condition for instability in Eq. (53) can be expressed as

$$\left(\frac{r_L}{a}\right)^2 > \left(1 - \frac{a^2}{a_c^2}\right) \frac{\omega_{cz}^2}{\omega_{c\theta}^2} \frac{\omega_{pe}^2/\omega_{cz}^2}{2\gamma_b^2 - 1 + \omega_{pe}^2/\gamma_b^2\omega_{cz}^2}, \tag{60}$$

where $\Omega_\beta^2 a^2 = \omega_{c\theta}^2 r_L^2$ has been used. For the case of a high–current electron beam with $\omega_{pe}^2/\gamma_b^2\omega_{cz}^2 \simeq 1$, Eq. (60) shows that surface–wave perturbations are easily stabilized for sufficiently small values of r_L^2/a^2. Therefore, when the betatron focusing forces are greater than defocusing self–field forces in the modified betatron, the surface–wave perturbations can stabilize the negative–mass instability provided the transverse temperature of the electrons is sufficiently small.

For a conventional betatron operating in the conventional betatron regime, $\Omega_\beta^2 = \omega_\beta^2$, and the necessary and sufficient condition for instability [Eq. (53)] can be expressed as

$$\frac{\omega_{pe}^2}{\gamma_b^2\omega_{cz}^2} < 1 + \left\{\left[\gamma_b^2 + \gamma_b^2\left(1 - \frac{a^2}{a_c^2}\right) - 1\right]^2 + 2\gamma_b^2 - 1\right\}^{1/2} - \gamma_b^2\left[1 + \left(1 - \frac{a^2}{a_c^2}\right)\right]. \tag{61}$$

When the electron ring is thin compared to the conductor radius ($a \ll a_c$), the instability condition can be further simplified to give

$$\frac{\omega_{pe}^2}{\gamma_b^2\omega_{cz}^2} < \left\{\left[2\gamma_b^2 - 1\right]^2 + 2\gamma_b^2 - 1\right\}^{1/2} - 2\gamma_b^2 + 1. \tag{62}$$

For a nonrelativistic, fully nonneutral conventional betatron ($\gamma_b \simeq 1$), the sufficient condition for stability combined with the condition for the existence of the equilibrium gives

$$\sqrt{2} - 1 < \omega_{pe}^2/\omega_{cz}^2 < 1. \tag{63}$$

On the other hand, for an ultrarelativistic, fully nonneutral conventional betatron ($\gamma_b^2 \gg 1$), the sufficient condition for stability and existence of the equilibrium becomes

$$1/2 < \omega_{pe}^2/\gamma_b^2\omega_{cz}^2 < 1. \tag{64}$$

These two conditions [Eqs. (63) and (64)] can be satisfied by sufficiently large values of $\omega_{pe}^2/\gamma_b^2\omega_{cz}^2$. Therefore, for a fully nonneutral ($f = 0$) conventional betatron with no spread in canonical angular momentum ($\Delta = 0$), the negative–mass instability can be completely stabilized provided the beam density is sufficiently large.

(b) Modified Betatron Regime ($\omega_{cz}^2 < \omega_{pe}^2/\gamma_b^2$)**:** Equilibrium does not exist for the conventional betatron when $f = 0$. Therefore, only the modified betatron configuration is considered here.

The instability condition [Eq. (53)] for a modified betatron operating in the modified betatron regime can be expressed as

$$\left(\frac{r_L}{a}\right)^2 < \left(1 - \frac{a^2}{a_c^2}\right) \frac{\omega_{cz}^2}{\omega_{c\theta}^2} \frac{\omega_{pe}^2/\omega_{cz}^2}{2\gamma_b^2 - 1 + \omega_{pe}^2/\gamma_b^2\omega_{cz}^2}, \tag{65}$$

where $\Omega_\beta^2 a^2 = \omega_{c\theta}^2 r_L^2$. Equation (65) shows that surface–wave perturbations can be stabilized provided r_L^2/a^2 is sufficiently large. Therefore, when the betatron focusing forces are exceeded by the defocusing self–field forces in the modified betatron, the surface–wave perturbations can be stabilized with a sufficiently large transverse electron temperature. From Eq. (57), when $a \simeq a_c$ (neglecting the effects of surface–wave perturbations), it was shown that the negative–mass instability is completely stabilized for sufficiently strong self–fields. Here, when surface–wave effects are included ($a < a_c$), we find that Eq. (65) is satisfied for sufficiently small values of r_L^2/a^2, and instability results. Therefore, for the case where $\omega_{cz}^2 < \omega_{pe}^2/\gamma_b^2$, we conclude that a sufficiently low effective transverse temperature elicits instability in a modified betatron. The surface–wave perturbation is manifest by the toroidal variation of the azimuthal electron velocity. This produces a perturbed charge and current density in the eigenvalue equation, resulting in a kink–type perturbation of the electron ring. The instability is referred to as a *radial kink instability* since it originates from a radial surface–wave perturbation. Therefore, it is concluded that the transverse temperature plays a major role in the stability properties of the modified betatron, since increasing the effective transverse temperature provides stabilization to the radial kink instability.

E. Influence of Transverse Temperature on Stability Behavior

The detailed effect of transverse temperature on stability behavior is studied in this section. To emphasize the effect, the influence of a spread in canonical angular momentum is neglected ($\Delta = 0$) and the instability criterion in Eq. (53) is investigated without any limitations on beam current or size. This contrasts with Sec. IV.D, which presented approximate stability criteria based on the assumption of moderate energy.

The transverse temperature at the center of the minor cross section of the beam in the modified and conventional betatron configurations can be expressed as $\hat{T}_\perp = \gamma_b m \Omega_\beta^2 a^2/2$ [see Eqs. (28) and (36)], where for the modified betatron $\Omega_\beta^2 a^2 = \omega_{c\theta}^2 r_L^2$ defines the transverse thermal Larmor radius (r_L) of the electrons.

For the modified betatron, it can be shown from Eq. (53) and Eqs. (50)-(51) that the necessary and sufficient condition for stability is given by

$$\left[\left(\frac{\omega_{c\theta}}{\omega_{cz}}\right)^2 \left(\frac{r_L}{a}\right)^2\right] \left\{4\mu - \hat{a}\left[\mu^2\gamma_b^2\left(\gamma_b^2 - 1\right) - 2\mu\left(\gamma_b^2 + 1\right) + \beta_b^2\right]\right\}$$

$$\leq \frac{2}{\gamma_b^2}\left(\frac{\omega_{pe}}{\omega_{cz}}\right)^2 \left(\frac{\omega_{cz}}{\omega_\beta}\right)^2 \left(1 - \frac{a^2}{a_c^2}\right). \tag{66}$$

In the modified betatron regime ($\omega_{cz}^2 < \omega_{pe}^2/\gamma_b^2$), when $f = 0$, both μ and ω_β^2 are negative. Therefore, since the transverse temperature is proportional to $\omega_{c\theta}^2 r_L^2$, Eq. (66) shows that a sufficiently large transverse temperature is needed to stabilize the beam. In the modified betatron regime, we note that the same conclusion was obtained from Eq. (65) in Sec. IV.D, which neglects transverse electromagnetic effects. Section IV.D showed that the destabilization was due to surface–wave perturbations. Moreover, for a modified betatron operating in the conventional betatron regime ($\omega_{cz}^2 > \omega_{pe}^2/\gamma_b^2$), when $f = 0$, both μ and ω_β^2 are positive. The corresponding stability analysis divides into two categories. For moderate beam current in a modified betatron [see Eq. (60) in Sec. IV.D], a sufficiently low transverse temperature is required for stabilization. However, for beam current above some critical value, Eq. (66) shows that the system is stable for all transverse temperatures.

For the conventional betatron, $\hat{T}_\perp$ is related to the beam density by Eq. (36). Thus, in principal, a condition on beam density for stability of the conventional betatron can be determined from Eq. (66).

F. Influence of Inverse Aspect Ratio on Stability Behavior

In this section the influence of inverse aspect ratio a/R_0 on stability behavior is studied. To emphasize the effect, the stabilizing influence of canonical angular momentum spread is neglected ($\Delta = 0$). For both the modified and conventional betatron configurations, it can be shown from Eq. (53) and Eqs. (50)-(51) that the system is stable provided

$$\left(\frac{a}{R_0}\right)^2 \left(\frac{1}{2}\frac{\beta_b}{\gamma_b}\right)^2 \left(\frac{\omega_{pe}}{\omega_{cz}}\right)^2 \left(2\ln\frac{a_c}{a}+1\right)\left[2\mu\left(\gamma_b^2+1\right)-\mu^2\gamma_b^2\left(\gamma_b^2-1\right)-4\gamma_b^2\hat{b}-\beta_b^2\right] \leq 4\left(\hat{b}-\mu\right), \tag{67}$$

where $\hat{b}$ is defined in Eq. (50).

For a fully nonneutral modified betatron operating in the modified betatron regime ($\omega_{cz}^2 < \omega_{pe}^2/\gamma_b^2$), μ and $\hat{b}$ are negative and we find three different types of behavior as the beam density is increased. First, for sufficiently low current that $\omega_{pe}^2/\gamma_b^2\omega_{cz}^2 \gtrsim 1$, it follows that $(\hat{b}-\mu) > 0$, and the right–hand side of Eq. (67) is negative; therefore, the beam is stable for all values of a/R_0. At low currents, stabilization at all aspect ratios results from the traditional mechanism for stabilizing the negative–mass instability (Sec. IV.C). As the beam density is increased, a second type of behavior occurs. The $(\hat{b}-\mu)$ term is now negative, and Eq. (67) shows that a sufficiently large value of a/R_0, which increases monotonically with $\omega_{pe}^2/\omega_{cz}^2$, is required for stabilization. As the density is increased even further, a critical value is approached above which the stability criterion in Eq. (67) is satisfied for no value of a/R_0.

However, for a modified betatron operating in the conventional betatron regime ($\omega_{cz}^2 > \omega_{pe}^2/\gamma_b^2$) (this also applies to a fully nonneutral conventional betatron which can *only* operate in this regime), both $(\hat{b}-\mu)$ and the term in brackets on the left hand side of Eq. (67) are negative. Thus, Eq. (67) predicts that a sufficiently large inverse aspect ratio a/R_0 is needed for stabilization. Moreover, the value of a/R_0 required for stability increases with increasing density. This result is consistent with the approximate analysis in Sec. IV.C.

V. STABILITY PROPERTIES: NUMERICAL RESULTS

Stability properties for the modified and conventional betatron configurations are studied numerically in this section by applying the dispersion relation in Eq. (47) to three betatron devices of current interest. The first device, studied in Sec. V.B, is the Naval Research Laboratory (NRL) modified betatron experiment. The NRL experiment will operate in a Phase I regime and a Phase II regime, where Phase II corresponds to higher current and higher energy. The second and third devices, studied in Sec. V.C, are the Phermex and Liner conventional betatrons at Los Alamos National Laboratory (LANL). The Liner device is presently a conceptual design, whereas the Phermex device is under construction. The projected operating parameters for these devices are shown in Table 1.

In Sec. V.A, the dimensionless parameters are identified that describe the modified and conventional betatrons within the context of the present analysis. In Secs. V.B and V.C, numerical results are presented describing the stability characteristics of the devices mentioned above. In particular, the regions of equilibrium and stability are plotted for the projected operating regimes of the various devices. In these plots, the region where both equilibrium and stability exist is represented as a shaded region. The curve representing the stability boundary is drawn as a solid line, whereas the curve representing the equilibrium boundary is drawn as a dashed line. Accompanying plots are also presented which show the $l = 1$ normalized growth rate $\mathrm{Im}\omega/\omega_{cz}$ over a range of equilibrium parameters.

A. Choice of Dimensionless Parameters

For convenience, we introduce the following sets of dimensionless parameters which are sufficient to describe the betatron configurations within the context of the present analysis. For the modified betatron with circular cross section ($a = b$), the choice of dimensionless parameters is

$$\frac{\omega_{pe}}{\omega_{cz}}, \quad \frac{\omega_{c\theta}}{\omega_{cz}}, \quad \gamma_b, \quad \frac{a}{R_0}, \quad \frac{a}{a_c}, \quad \frac{r_L}{a}, \quad f, \quad \frac{\Delta}{\gamma_b m \beta_b c R_0}, \quad F(\gamma_b, \dot{\gamma}_b, \ddot{\gamma}_b, \omega_{cz}), \qquad (68)$$

and for the conventional betatron ($\omega_b = 0$, $\omega_{c\theta} = 0$), the choice of dimensionless parameters is

$$\frac{\omega_{pe}}{\omega_{cz}}, \quad \gamma_b, \quad \frac{b}{a}, \quad \frac{\sqrt{ab}}{R_0}, \quad \frac{\sqrt{ab}}{a_c}, \quad f, \quad \frac{\Delta}{\gamma_b m \beta_b c R_0}, \quad F(\gamma_b, \dot{\gamma}_b, \ddot{\gamma}_b, \omega_{cz}). \qquad (69)$$

Here, $F(\gamma_b, \dot{\gamma}_b, \ddot{\gamma}_b, \omega_{cz})$ is defined by[7]

$$F(\gamma_b, \dot{\gamma}_b, \ddot{\gamma}_b, \omega_{cz}) \equiv \frac{1}{\omega_{cz}^2}\left[\frac{1}{4}\left(\frac{\dot{\gamma}_b}{\gamma_b}\right)^2 - \frac{1}{2}\left(\frac{\ddot{\gamma}_b}{\gamma_b}\right)\right]. \tag{70}$$

The quantity $F(\gamma_b, \dot{\gamma}_b, \ddot{\gamma}_b, \omega_{cz})$ represents the modification to the betatron frequencies due to slowly-varying accelerating fields [see Eq. (39)]. For the device parameters chosen in Table 1, the corresponding dimensionless parameters are summarized in Table 2. We note that the operating parameters specified in Table 2 correspond to ideal conditions with no background neutralizing ions ($f = 0$), no stabilizing spread in canonical angular momentum ($\Delta = 0$), and no external betatron acceleration ($F = 0$). We also note that the values of the transverse thermal Larmor radius terms (r_L/a) for the NRL modified betatron have been arbitrarily chosen in Table 2 to be just inside the stability boundary.

B. NRL Modified Betatron: Phase I and Phase II

The NRL modified betatron is presently operating in Phase I, the initial operating regime of the device. Phase II represents the second planned stage of operation, which corresponds to substantially increased current and energy (see Table 1). This section presents numerical results obtained from the dispersion relation in Eq. (45) ($a = b$ and $F = 0$) for both the Phase I and Phase II modified betatrons, with primary emphasis on Phase II. The dimensionless parameters used in the stability analysis are summarized in Table 2. The influence of transverse beam temperature (r_L/a) on stability behavior is first studied, followed by an investigation of the influence of inverse toroidal aspect ratio (a/R_0) on stability behavior. Finally, the stabilizing effect of a spread (Δ) in canonical angular momentum is examined.

Influence of Transverse Beam Temperature on Stability Behavior: In this section, the influence of transverse beam temperature on stability behavior is illustrated in Figs. 2–7. In these plots, the regions of equilibrium and stability are presented for r_L/a versus $\omega_{c\theta}/\omega_{cz}$, ω_{pe}/ω_{cz}, γ_b, a/a_c, and f. The equilibrium and stability boundaries are determined from Eqs. (30) and (66), respectively. The growth rate curves are then determined from Eq. (45) for values of r_L/a typical of the corresponding equilibrium and stability plots.

For Phase II, the regions of equilibrium and stability for r_L/a versus $\omega_{c\theta}/\omega_{cz}$ are illustrated in Fig. 2(a). The parameter regime in Fig. 2(a) represents the modified betatron regime ($\omega_{cz}^2 < \omega_{pe}^2/\gamma_b^2$), and for the values $r_L/a = 0.15$ and $\omega_{c\theta}/\omega_{cz} = 20$ chosen in Table 2, stable operation is predicted for the Phase II operating point. The analysis in Sec. IV.D predicts, for the modified betatron regime ($\omega_{cz}^2 < \omega_{pe}^2/\gamma_b^2$), that surface–wave perturbations exist which can be stabilized only by sufficiently large transverse beam temperature. Exactly this effect is seen in Fig. 2(a). Also, the stability boundary [from Eq. (66)] for r_L/a versus $\omega_{c\theta}/\omega_{cz}$ coincides exactly with a constant transverse beam temperature $\hat{T} = \gamma_b m\omega_{c\theta}^2 r_L^2/2$ (when γ_b is constant). The same qualitative behavior is found for Phase I parameters. Growth rate curves for the $l = 1$ mode are plotted versus $\omega_{c\theta}/\omega_{cz}$ in Fig. 2(b) for several values of r_L/a selected from Fig. 2(a). It can be seen that the maximum growth rate of the instability is modest, with values well below 1% of the cyclotron frequency ω_{cz} in the vertical field.

The influence of beam density for Phase I parameters is shown in the equilibrium and stability plot of r_L/a versus ω_{pe}/ω_{cz} in Fig. 3(a). The transition point at $\omega_{pe}/\omega_{cz} = 3$ corresponds to $\omega_{cz}^2 - \omega_{pe}^2/\gamma_b^2$ changing sign. As ω_{pe}/ω_{cz} is increased, the system changes from a conventional betatron regime to a modified betatron regime. The surface–wave analysis in Sec. IV.D predicts, in the conventional betatron regime ($\omega_{cz}^2 > \omega_{pe}^2/\gamma_b^2$), that the transverse beam temperature (proportional to r_L/a for $\omega_{c\theta}/\omega_{cz}$ constant) must be sufficiently small for stability. For the modified betatron regime, the opposite is predicted. Precisely this effect is seen in Fig. 3(a). The abruptness of the behavior about the transition point at $\omega_{cz}^2 = \omega_{pe}^2/\gamma_b^2$ is due to the fact that the negative mass parameter μ is not defined at this point [see Eq. (49)]. Curves of normalized growth rate versus ω_{pe}/ω_{cz} for selected values of r_L/a are presented in Fig. 3(b). As can be seen from Fig. 3(b), for Phase I parameters the normalized growth rate in the conventional betatron operating regime near transition can be well over 10%. However, in the modified betatron operating regime, $\mathrm{Im}\omega/\omega_{cz}$ never exceeds 7% as ω_{pe}/ω_{cz} is varied.

The influence of beam density on equilibrium and stability properties for the higher–current, higher–energy Phase II device is shown in Figs. 4(a) and 4(b). The transition point from the conventional to the modified betatron regime occurs at $\omega_{pe}/\omega_{cz} = 7.5$ for $\gamma_b = 7.5$. From Fig. 4(a), it is evident that a sufficiently high transverse beam temperature is also required to stabilize surface–wave perturbations in

the Phase II modified betatron regime. However, for operation in the conventional betatron regime ($\omega_{pe}/\omega_{cz} < 7.5$), the region just below the transition point is now altered. The result that requires a sufficiently small transverse temperature for stabilization is still evident for $\omega_{pe}/\omega_{cz} < 6.1$; however, a stable region appears for $6.1 < \omega_{pe}/\omega_{cz} < 7.5$, which corresponds to stabilization at any transverse temperature. This stable region is a consequence of the transverse electromagnetic effects discussed in Sec. IV.C. The stable region evident in Fig. 4(a) ($6.1 < \omega_{pe}/\omega_{cz} < 7.5$) coincides precisely with values predicted in Eq. (59). Thus, for a high energy beam, a stable region occurs in the conventional betatron regime of operation of the modified betatron due to the stabilizing influence of transverse electromagnetic effects. Corresponding growth rate curves for selected values of r_L/a are shown in Fig. 4(b) as a function of ω_{pe}/ω_{cz}. As illustrated in Fig. 4(b), Phase II also exhibits relatively large ($\approx 3\%$) normalized growth rate in the conventional betatron regime near transition compared with the growth rate in the modified betatron regime ($< 0.75\%$).

The regions of equilibrium and stability for r_L/a versus γ_b are illustrated in Fig. 5(a) for Phase II parameters. In this case, the transition point from the modified to the conventional betatron regime occurs when $\gamma_b = 38$, and corresponds precisely to the point where the stability curve approaches zero. [This is not evident in Fig. 5(a) due to the scale.] The modified betatron regime corresponds to $\gamma_b < 38$, where the influence of surface–wave perturbations requires that the transverse beam temperature be sufficiently large for stability. For $\gamma_b > 38$ (conventional betatron regime), Sec. IV.C predicts stability due to the influence of transverse electromagnetic effects. The stability boundary in the modified betatron regime shows that $r_L/a \propto \gamma_b^2$ for small values of γ_b, whereas, for γ_b approaching the transition energy, $r_L/a \propto 1/\gamma_b^2$. This follows from Eq. (65). The corresponding growth rate curves are plotted versus γ_b in Fig. 5(b). Note the rapid increase in growth rate at low energy as r_L/a is decreased. Although the growth rate can be high for low energies, increasing r_L/a above 0.15 yields moderate growth rates ($\mathrm{Im}\omega/\omega_{cz} < 2\%$). [Note from Fig. 5(a) that there is no instability for $r_L/a > 0.18$.]

Figure 6(a) illustrates how the equilibrium and stability regions are affected by the location of the conductor radius a_c. In particular, shown are plots of r_L/a versus a/a_c for Phase II parameters. The quantity a/a_c does not affect the sign of

$\omega_{cz}^2 - \omega_{pe}^2/\gamma_b^2$. Therefore, Fig. 6(a) represents only the modified betatron regime and shows the minimum value of transverse beam temperature required for stability. The minimum beam temperature required for stability is found to be proportional to $1 - a^2/a_c^2$, as predicted by Eq. (65). Thus, the destabilizing influence of surface perturbations is reduced as the conductor radius (a_c) approaches the outer beam radius (a). The corresponding normalized growth rate is plotted versus a/a_c in Fig. 6(b) for several values of r_L/a. For the values of r_L/a chosen, the growth rate is modest with $\mathrm{Im}\omega/\omega_{cz}$ less than 1%.

Next, the influence of charge neutralization is investigated. As a reminder, f represents the fraction of positively charged background ions present in the beam ($f = 0$ corresponds to no ions, $f = 1$ corresponds to complete charge neutrality). For Phase II, the regions of equilibrium and stability for r_L/a versus f are illustrated in Fig. 7(a). The point where the stability boundary approaches zero at $f = 0.017$ corresponds to the transition from the modified to the convention betatron regime. Because nonzero values of f are under consideration for Phase II, the transition point defined by $\omega_\beta^2 = 0$ must be calculated from the expression in Eq. (24). Thus, for the modified betatron regime ($f < 0.017$), the usual surface–wave effect dominates, and the transverse beam temperature must be sufficiently large for stabilization. However, the conventional betatron regime divides naturally into three regions. For $0.017 < f < 0.024$, due to the high current in Phase II, a stable region exists due to the influence of transverse electromagnetic effects and the fact that μ is positive and sufficiently large to satisfy Eq. (59). This stable region does not occur in a corresponding plot for Phase I. For $0.024 < f < 0.089$, μ is positive, but not large enough for Eq. (59) to be satisfied; in this case, electromagnetic effects do not stabilize the negative–mass instability. Thus, the stability boundary is determined in this region by surface–wave contributions, and a sufficiently low transverse beam temperature is required for stabilization. The remainder of the conventional betatron regime ($f > 0.089$) corresponds to $\mu < 0$, and stabilization is provided by the traditional negative–mass stability condition, $\mu < 0$. Several plots of growth rate versus f are presented in Fig. 7(b). The very rapid increase in growth rate for $r_L/a = 0.275$ and $r_L/a = 0.280$ correspond to the minimum of the unstable region in Fig. 7(b) for f in the range $0.024 < f < 0.089$. However, for operation in the modified betatron regime, $\mathrm{Im}\omega/\omega_{cz}$ stays below 0.5%.

Influence of Inverse Toroidal Aspect Ratio on Stability Behavior: The influence of inverse aspect ratio (a/R_0) on equilibrium and stability behavior is illustrated in Figs. 8(a) and 9(a) which show plots of a/R_0 versus ω_{pe}/ω_{cz} and γ_b, respectively. The equilibrium and stability boundaries are determined from Eqs. (30) and (67), respectively. The corresponding growth rate curves in Figs. 8(b) and 9(b) are determined from Eq. (45) for several values of a/R_0.

In Fig. 8(a), the equilibrium and stability boundaries for a/R_0 versus ω_{pe}/ω_{cz} are plotted for Phase II parameters. The point where the stability boundary first intersects the abscissa ($\omega_{pe}/\omega_{cz} = 7.5$) corresponds to the transition point from the conventional betatron regime to the modified betatron regime. Values below $\omega_{pe}/\omega_{cz} = 7.5$ correspond to the conventional betatron regime ($\mu > 0$), and stabilization is provided by transverse electromagnetic effects when a/R_0 is sufficiently large. By expressing ν/γ_b in terms of a/R_0 as in Eq. (43), it can be shown that the stability boundary for $\omega_{pe}/\omega_{cz} < 7.5$ corresponds to values of a/R_0 which provide the current required to satisfy the stability condition in Eq. (59). The modified betatron regime corresponds to $\omega_{pe}/\omega_{cz} > 7.5$. From the transition value at $\omega_{pe}/\omega_{cz} = 7.5$ to $\omega_{pe}/\omega_{cz} = 33$, the transverse beam temperature (corresponding to the choice of parameters in Table 2) is large enough to provide stabilization for all values of a/R_0. However, when $33 < \omega_{pe}/\omega_{cz} < 44$, thermal effects are not sufficient for stabilization, and larger values of a/R_0 are required for stabilization. This is a consequence of the higher energy of Phase II and does not occur in a corresponding plot for Phase I. For $\omega_{pe}/\omega_{cz} > 44$, an increase in the inverse aspect ratio is not sufficient to provide stabilization. Plots of the normalized growth rate versus ω_{pe}/ω_{cz} are presented in Fig. 8(b) for several values of a/R_0. Evidently, in the modified betatron regime, $\mathrm{Im}\omega/\omega_{cz}$ stays below 2%.

Figure 9(a) illustrates the energy dependence in Phase II by plotting the regions of equilibrium and stability for a/R_0 versus γ_b. The transition energy occurs at $\gamma_b = 38$, with the conventional betatron regime corresponding to $\gamma_b > 38$. Stability in this region is provided by transverse electromagnetic effects when a/R_0 corresponds to a sufficiently large current to satisfy Eq. (59). For the modified betatron regime ($\gamma_b < 38$), except in the region $3.1 < \gamma_b < 8.4$, the transverse beam temperature (prescribed in Table 2) is sufficiently large to stabilize surface–wave perturbations. This unstable range corresponds to the values predicted by

Eq. (62). Within this range, an increase in a/R_0 is not sufficient to stabilize the beam. Thus, the transverse beam temperature is too low in the modified betatron regime, the relatively weak stabilizing influence of toroidal aspect ratio may be too small to effectively stabilize the beam. The growth rate curves in Fig. 9(b) show how a decrease in the inverse aspect ratio (a/R_0) decreases the growth rate of the instability. Also, $\mathrm{Im}\omega/\omega_{cz}$ is below 3% for any values of a/R_0 considered for the modified betatron.

Stabilizing Influence of a Spread in Canonical Angular Momentum: For Phase I parameters, we now consider the stabilizing effect of a spread Δ in canonical angular momentum. (Keep in mind that $\Delta = 0$ has already been considered in Figs. 2–9.) The minimum value of Δ required for stabilization is evident from Fig. 10(a), which shows a plot of the stability boundary for $\Delta/\gamma_b m\beta_b cR_0$ versus ω_{pe}/ω_{cz}. It can be seen from Fig. 3(a) that Phase I operation at $a/R_0 = 0.065$ with $\Delta = 0$ is unstable below $\omega_{pe}/\omega_{cz} \simeq 3$. On the other hand, Fig. 10(a) shows that very modest values of canonical angular momentum spread (Δ) can stabilize the beam in this region. Our *a priori* assumption that $\Delta/\gamma_b m\beta_b cR_0$ be small is well justified in this case. Several growth rate curves are plotted versus ω_{pe}/ω_{cz} in Fig. 10(b). Evidently, the growth rate decreases rapidly with increasing (but small) values of $\Delta/\gamma_b m\beta_b cR_0$, and a modest spread in canonical angular momentum ($> 0.4\%$) keeps the growth rate below 1% of the cyclotron frequency ω_{cz}.

C. LANL Conventional Betatrons: Liner and Phermex

This section presents numerical results obtained from the dispersion relation in Eq. (47) for both the Liner and Phermex conventional betatron parameters. Presently, the LANL Liner conventional betatron is a conceptual design, whereas the Phermex conventional betatron is under construction. The "Liner" betatron is a liner driven electron ring accelerator, whereby an electron ring is injected azimuthally into a betatron magnetic field enclosed within a cylindrical conducting shell[18]. The conductor is then imploded, trapping the magnetic flux and accelerating the beam by the increasing vertical magnetic field. The "Phermex" betatron, which is the main emphasis of this section, corresponds to a conventional betatron in which an electron beam is injected into a betatron by the LANL Phermex electron linear accelerator[19]. The dimensionless parameters assumed in the present analysis

are listed in Table 2. The influence of inverse toroidal aspect ratio ($\sqrt{ab}/R_0$) on stability behavior is first studied. Then, for the Liner device only, the influence of slowly varying accelerating fields on stability behavior is investigated.

At the outset, it should be noted that the analysis predicts instability for the Liner parameters and stability for the Phermex parameters assumed in the present analysis (Table 2). The Liner design continues to evolve, and the parameters considered here only represent those used in the current studies.

Influence of Inverse Toroidal Aspect Ratio on Stability Behavior: In this section, the influence of inverse aspect ratio ($\sqrt{ab}/R_0$) on stability behavior is illustrated in Figs. 11–14. In these plots, the regions of equilibrium and stability are shown by plotting $\sqrt{ab}/R_0$ versus ω_{pe}/ω_{cz}, γ_b, b/a, and a/a_c. The equilibrium and stability boundaries are determined from Eqs. (34) and (47), respectively. The growth rate curves are then calculated numerically from Eq. (47) for the $l = 1$ mode for several values of $\sqrt{ab}/R_0$.

Figure 11(a) illustrates the regions of equilibrium and stability for $\sqrt{ab}/R_0$ versus ω_{pe}/ω_{cz} for Phermex. Because this is a conventional betatron with $f = 0$, it follows that $\omega_{cz}^2 > \omega_{pe}^2/\gamma_b^2$ and equilibrium does not exist for $\omega_{pe}/\omega_{cz} > 60$. From Sec. IV.D, Eq. (61) predicts that the region $43 < \omega_{pe}/\omega_{cz} < 60$ is stable to the radial kink instability. This region of stability is evident in Fig. 11(a). For $\omega_{pe}/\omega_{cz} < 43$, as predicted by Eq. (59), a larger inverse aspect ratio is required for stabilization of the negative–mass instability by transverse electromagnetic effects. The corresponding growth rate curves versus ω_{pe}/ω_{cz} are presented in Fig. 11(b) for several values of $\sqrt{ab}/R_0$. Note that the growth rates are extremely low ($\mathrm{Im}\omega/\omega_{cz}$ below 0.035%) in this case.

For Phermex, the scaling with energy is illustrated by the equilibrium and stability plot of $\sqrt{ab}/R_0$ versus γ_b in Fig. 12(a). From the condition $\omega_{cz}^2 > \omega_{pe}^2/\gamma_b^2$ (because $a = b$ is assumed), equilibrium does not exist for $\gamma_b < 1.22$. A stable region exists for $1.22 < \gamma_b < 1.73$ because of the influence of transverse electromagnetic effects. This is predicted by Eq. (61). On the other hand, for $\gamma_b < 1.73$, the inverse aspect ratio must be sufficiently large for stabilization by transverse electromagnetic effects. The corresponding plots of normalized growth rate versus γ_b are presented in Fig. 12(b) for several values of $\sqrt{ab}/R_0$. It is evident that $\mathrm{Im}\omega/\omega_{cz}$ can

increase to a relatively high value (10%) as the inverse aspect ratio increases above 0.10.

The effect of cross sectional beam shape on stability behavior is illustrated for Phermex in Fig. 13(a) where the regions of equilibrium and stability are plotted for $\sqrt{ab}/R_0$ versus b/a. Evidently, elongating the minor cross section of the beam radially (decreasing b/a) has a stabilizing effect. As stated in Sec. III.B, noncircularity enters the problem mathematically in the ω_x^2 term defined in Eq. (39). Also, the equilibrium boundaries in Fig. 13(a) [calculated from Eq. (34)] determine the limiting values of noncircularity for equilibrium to exist. Corresponding plots of the growth rate versus b/a are presented in Fig. 13(b) for several values of $\sqrt{ab}/R_0$. Note that the growth rate remains very low ($\mathrm{Im}\omega/\omega_{cz}$ below 0.03%) as b/a is varied.

Influence of Slowly Varying Accelerating Fields on Stability Behavior: The influence on stability behavior by slowly varying accelerating fields is investigated here for the Liner. As shown in Sec. III.B, this effect enters the dispersion relation in Eq. (47) through the ω_x^2 term defined in Eq. (39). The quantity F defined in Eq. (70) represents the contribution to ω_x^2 from slowly varying accelerating fields. Therefore, for a beam that satisfies the 2:1 betatron flux condition (constant radius acceleration) discussed in Sec. I, the effect of slowly varying accelerating fields can be determined by a detailed knowledge of the beam energy (γ_b) as a function of time (t). For the Liner, typical time histories of $\gamma_b(t)$ have been investigated[7], and the most dramatic effect (corresponding to a maximum of F) is found to occur just as the betatron acceleration process begins. In this regime, $F = -0.2$ represents a typical value. Figure 14 shows the effect on the stability region by plotting $\sqrt{ab}/R_0$ versus $\sqrt{ab}/a_c$ for $F = -0.2$ (solid line), and for $F = 0$ (dashed line). Evidently, for $F = -0.2$, the value of $\sqrt{ab}/R_0$ necessary for stability at the operating point of the device is decreased approximately by 25%. Thus, just as the acceleration process begins, the slowly varying accelerating fields have a stabilizing influence which is found to be significant. This is fortunate because the initial phase of the acceleration process is more likely to be unstable due to the lower beam energy.

VI. CONCLUSIONS

In this paper, equilibrium and stability properties have been investigated for an intense relativistic electron ring located at the midplane of an externally applied betatron field. In particular, the analysis is applicable to both modified and conventional betatron accelerators. The analysis was carried out within the framework of the Vlasov–Maxwell equations, including the important influence of intense equilibrium self fields. Two dispersion relations were presented for longitudinal perturbations and analyzed analytically and numerically. The first dispersion relation [Eq. (45)] is applicable to betatrons with circular beam cross section and does not include the effects of slowly varying accelerating fields. The second dispersion relation [Eq. (47)] includes the effects of noncircular cross section and slowly varying accelerating fields. The numerical investigations included studies of the Naval Research Laboratory's (NRL) modified betatron, and the Los Alamos National Laboratory's (LANL) Liner and Phermex conventional betatrons.

Section II summarized the equilibrium properties and basic assumptions, and Sec. III described the two dispersion relations for longitudinal perturbations. The formal stability analysis was carried out in Secs. IV and V. Stability properties for an intense relativistic electron ring in both the modified and conventional betatrons were investigated within the framework of the linearized Vlasov–Maxwell equations. The stability analysis was carried out for eigenfrequency ω close to harmonics of the relativistic cyclotron frequency ω_{cz}. Also included in the analysis was the influence of transverse electromagnetic effects and surface–wave perturbations. Detailed stability properties were investigated numerically in Sec. IV, leading to the following two main conclusions. First, for high–current and high–energy beams, neglecting surface–wave effects, it was found that transverse electromagnetic effects can stabilize the negative–mass instability when $\omega_{cz}^2 > \omega_{pe}^2/\gamma_b^2$ for both the modified and conventional betatrons. Second, the influence of surface–wave perturbations was investigated, neglecting the stabilizing influence of transverse electromagnetic effects (moderate energy beams). For $f = 0$ and $\Delta = 0$, two cases were considered: betatron focusing forces exceed defocusing self–field forces ($\omega_{cz}^2 > \omega_{pe}^2/\gamma_b^2$: conventional betatron regime); and betatron focusing forces are weaker than the defocusing self–field forces ($\omega_{cz}^2 < \omega_{pe}^2/\gamma_b^2$: modified betatron regime). For $\omega_{cz}^2 > \omega_{pe}^2/\gamma_b^2$, it was found that the ring can be stabilized by sufficiently low transverse beam temperature. However, for $\omega_{cz}^2 < \omega_{pe}^2/\gamma_b^2$, it was found that a sufficiently large transverse

temperature is required for stabilization of the radial kink instability. In addition, in Sec. IV, exact expressions were derived which describe the stability boundaries for the transverse beam temperature and the inverse aspect ratio.

Finally, Sec. V presented a full numerical investigation of the dispersion relation, where effects such as nonneutrality, noncircular beam cross section, canonical angular momentum spread, and slowly varying accelerating fields were included. The results were applied to three betatron devices. These included the NRL modified betatron (Phase I and Phase II) and the LANL Liner and Phermex conventional betatrons. The numerical investigations particularly emphasized the influence of transverse electromagnetic effects and surface–wave perturbations on stability behavior. The analysis showed, in the modified betatron regime ($\omega_{cz}^2 < \omega_{pe}^2/\gamma_b^2$), that surface–wave effects dominate, and a sufficiently high transverse beam temperature is necessary for stabilization. On the other hand, in the conventional betatron regime ($\omega_{cz}^2 > \omega_{pe}^2/\gamma_b^2$), surface–wave effects require a sufficiently low transverse beam temperature for stabilization. However, for sufficiently high–current beams, the system is stable at all transverse temperatures.

Other effects investigated numerically in Sec. V included: the stabilizing influence of a small spread Δ in canonical angular momentum; the influence of inverse aspect ratio a/R_0; the effect of the location of the conducting wall (a_c); the stabilizing effect in the conventional betatron of radially elongating the beam in the minor cross section; and the effect of slowly varying accelerating fields. Finally, stability behavior was investigated for the NRL modified betatron as the charge neutrality factor f is increased from $f = 0$ (pure electron beam) to $f = 1$ (fully neutralized beam).

ACKNOWLEDGEMENTS

This research was supported by the Office of Naval Research.

REFERENCES

[1] D. Chernin, Phys. Fluids **29**, 556 (1986).

[2] T. P. Hughes and B. B. Godfrey, IEEE Trans. Nucl. Sci. **NS–32**, 2495 (1985).

[3] C. A. Kapetanakos, P. Sprangle, S. J. Marsh, D. Dialetis, C. Agritellis, and A. Prakash, Part. Accel. **18**, 73 (1985).

[4] C. W. Roberson, J. A. Pasour, and C. A. Kapetanakos, *Free Electron Generators of Coherent Radiation* (Addison–Weseley Publishing Company, Reading, MA, 1982).

[5] P. Sprangle and C. A. Kapetanakos, J. Appl. Phys. **49**, 1 (1978).

[6] N. Rostoker, Comments Plasma Phys. **6**, 91 (1980).

[7] J. J. Petillo, *Massachusetts Institute of Technology*, Ph.D. Thesis, June 1986.

[8] H. S. Uhm, R. C. Davidson and J. J. Petillo, Phys. Fluids **28**, 2537 (1985).

[9] R. C. Davidson and H. S. Uhm, Phys. Fluids **25**, 2089 (1982).

[10] C. A. Kapetanakos, S. J. Marsh, and P. Sprangle, Part. Accel. **14**, 261 (1984).

[11] B. B. Godfrey and T. P. Hughes, Phys. Fluids **28**, 669 (1985).

[12] P. Sprangle and J. L. Vomvoridis, Part. Accel. **18**, 1 (1985).

[13] W. M. Manheimer and J. M. Finn, Part. Accel. **14**, 29 (1983).

[14] C. A. Kapetanakos, P. Sprangle, D. P. Chernin, S. J. Marsh, and I. Haber, Phys. Fluids **26**, 1634 (1983).

[15] J. J. Livingood, *Principles of Cyclic Particle Accelerators* (D. Van Nostrand Company, Inc., Princeton, NJ, 1961).

[16] H. S. Uhm and R. C. Davidson, Phys. Fluids **20**, 771 (1977).

[17] R. W. Landau and V. K. Neil, Phys. Fluids **9**, 2412 (1966).

[18] G. R. Gisler and R. J. Faehl, private communication (1985).

[19] G. R. Gisler, private communication (1985).

[20] R. C. Davidson, *Theory of Nonneutral Plasmas* (W. A. Benjamin, Inc., Reading, MA, 1974).

TABLE CAPTIONS

Table 1. Modified and conventional betatron machine parameters.

Table 2. Modified and conventional betatron dimensionless parameters.

Machine parameter		NRL		LANL	
		Phase I	Phase II	Liner	Phermex
Energy E	(MeV)	1	3.3	4.6	30
Current I	(kA)	2.5	10	0.2	1.7
Ring radius a	(cm)	1.5	1.5	0.5	1
Major radius R_0	(cm)	100	100	5	15
Torus radius a_c	(cm)	15	15	1.5	4
Vertical field $\hat{B}_z$	(G)	50	128	3,400	6,800
Toroidal field $\hat{B}_\theta$	(kG)	2.3	2.5	–	–

Table 1

Dimensionless parameter	NRL		LANL	
	Phase I	Phase II	Liner	Phermex
ω_{pe}/ω_{cz}	33	38	0.69	1.2
$\omega_{c\theta}/\omega_{cz}$	49	20	–	–
γ_b	3.0	7.5	10	60
$a/R_0,\ \sqrt{ab}/R_0$	0.015	0.015	0.10	0.067
$a/a_c,\ \sqrt{ab}/a_c$	0.10	0.10	0.33	0.25
b/a	1	1	1	1
r_L/a	0.065	0.15	–	–
f	0	0	0	0
$\Delta/\gamma_b m\beta_b c R_0$	0	0	0	0
$F(\gamma_b, \dot{\gamma}_b, \ddot{\gamma}_b, \omega_{cz})$	0	0	0	0

Table 2

FIGURE CAPTIONS

Fig. 1. Equilibrium ring geometry for the modified and conventional betatrons.

Fig. 2. (a) Regions of equilibrium and stability for r_L/a versus $\omega_{c\theta}/\omega_{cz}$ for the NRL Phase II modified betatron. The stability boundary (solid line) is obtained from the dispersion relation in Eq. (66) and the equilibrium boundary (dashed line) is obtained from Eq. (30) for $\omega_{pe}/\omega_{cz} = 38$, $\gamma_b = 7.5$, $a/R_0 = 0.015$, $a/a_c = 0.1$, $f = 0$, $\Delta/\gamma_b m\beta_b c R_0 = 0$, and $F = 0$ ($E = 3.3MeV$, $I = 10kA$, $a = 1.5cm$, $R_0 = 100cm$, and $a_c = 15cm$). (b) Curves of normalized growth rate $Im\omega/\omega_{cz}$ versus $\omega_{c\theta}/\omega_{cz}$ for $r_L/a = 0.01$, 0.03, 0.075, 0.15, and 0.225 for the NRL Phase II modified betatron. The growth rate curves are determined from the dispersion relation in Eq. (45) for $\omega_{pe}/\omega_{cz} = 38$, $\gamma_b = 7.5$, $a/R_0 = 0.015$, $a/a_c = 0.1$, $f = 0$, $\Delta/\gamma_b m\beta_b c R_0 = 0$, and $F = 0$ ($E = 3.3MeV$, $I = 10kA$, $a = 1.5cm$, $R_0 = 100cm$, and $a_c = 15cm$).

Fig. 3. (a) Regions of equilibrium and stability for r_L/a versus ω_{pe}/ω_{cz} for the NRL Phase I modified betatron. The stability boundary (solid line) is obtained from the dispersion relation in Eq. (66) and the equilibrium boundary (dashed line) is obtained from Eq. (30) for $\omega_{c\theta}/\omega_{cz} = 49$, $\gamma_b = 3$, $a/R_0 = 0.015$, $a/a_c = 0.1$, $f = 0$, $\Delta/\gamma_b m\beta_b c R_0 = 0$, and $F = 0$ ($E = 1MeV$, $a = 1.5cm$, $R_0 = 100cm$, $a_c = 15cm$, and $\hat{B}_\theta = 2.3kG$). (b) Curves of normalized growth rate $Im\omega/\omega_{cz}$ versus ω_{pe}/ω_{cz} for $r_L/a = 0.01$, 0.015, 0.045, 0.055, and 0.060 for the NRL Phase I modified betatron. The growth rate curves are determined from the dispersion relation in Eq. (45) for $\omega_{c\theta}/\omega_{cz} = 49$, $\gamma_b = 3$, $a/R_0 = 0.015$, $a/a_c = 0.1$, $f = 0$, $\Delta/\gamma_b m\beta_b c R_0 = 0$, and $F = 0$ ($E = 1MeV$, $a = 1.5cm$, $R_0 = 100cm$, $a_c = 15cm$, and $\hat{B}_\theta = 2.3kG$).

Fig. 4. (a) Regions of equilibrium and stability for r_L/a versus ω_{pe}/ω_{cz} for the NRL Phase II modified betatron. The stability boundary (solid line) is obtained from the dispersion relation in Eq. (66) and the equilibrium boundary (dashed line) is obtained from Eq. (30) for $\omega_{c\theta}/\omega_{cz} = 20$, $\gamma_b = 7.5$, $a/R_0 = 0.015$, $a/a_c = 0.1$, $f = 0$, $\Delta/\gamma_b m\beta_b c R_0 = 0$, and $F = 0$ ($E = 3.3MeV$, $a = 1.5cm$, $R_0 = 100cm$, $a_c = 15cm$, and $\hat{B}_\theta = 2.5kG$). (b) Curves of normalized growth

rate $Im\omega/\omega_{cz}$ versus ω_{pe}/ω_{cz} for $r_L/a = 0.01, 0.03, 0.075$, and 0.15 for the NRL Phase II modified betatron. The growth rate curves are determined from the dispersion relation in Eq. (45) for $\omega_{c\theta}/\omega_{cz} = 20$, $\gamma_b = 7.5$, $a/R_0 = 0.015$, $a/a_c = 0.1$, $f = 0$, $\Delta/\gamma_b m\beta_b c R_0 = 0$, and $F = 0$ ($E = 3.3MeV$, $a = 1.5cm$, $R_0 = 100cm$, $a_c = 15cm$, and $\hat{B}_\theta = 2.5kG$).

Fig. 5. (a) Regions of equilibrium and stability for r_L/a versus γ_b for the NRL Phase II modified betatron. The stability boundary (solid line) is obtained from the dispersion relation in Eq. (66) and the equilibrium boundary (dashed line) is obtained from Eq. (30) for $\omega_{pe}/\omega_{cz} = 38$, $\omega_{c\theta}/\omega_{cz} = 20$, $a/R_0 = 0.015$, $a/a_c = 0.1$, $f = 0$, $\Delta/\gamma_b m\beta_b c R_0 = 0$, and $F = 0$ ($I = 10kA$, $a = 1.5cm$, $R_0 = 100cm$, $a_c = 15cm$, and $\hat{B}_\theta = 2.5kG$). (b) Curves of normalized growth rate $Im\omega/\omega_{cz}$ versus γ_b for $r_L/a = 0.01$, 0.03, 0.075, and 0.15 for the NRL Phase II modified betatron. The growth rate curves are determined from the dispersion relation in Eq. (45) for $\omega_{pe}/\omega_{cz} = 38$, $\omega_{c\theta}/\omega_{cz} = 20$, $a/R_0 = 0.015$, $a/a_c = 0.1$, $f = 0$, $\Delta/\gamma_b m\beta_b c R_0 = 0$, and $F = 0$ ($I = 10kA$, $a = 1.5cm$, $R_0 = 100cm$, $a_c = 15cm$, and $\hat{B}_\theta = 2.5kG$).

Fig. 6. (a) Regions of equilibrium and stability for r_L/a versus a/a_c for the NRL Phase II modified betatron. The stability boundary (solid line) is obtained from the dispersion relation in Eq. (66) and the equilibrium boundary (dashed line) is obtained from Eq. (30) for $\omega_{pe}/\omega_{cz} = 38$, $\omega_{c\theta}/\omega_{cz} = 20$, $\gamma_b = 7.5$, $a/R_0 = 0.015$, $f = 0$, $\Delta/\gamma_b m\beta_b c R_0 = 0$, and $F = 0$ ($E = 3.3MeV$, $I = 10kA$, $a = 1.5cm$, $R_0 = 100cm$, and $\hat{B}_\theta = 2.5kG$). (b) Curves of normalized growth rate $Im\omega/\omega_{cz}$ versus a/a_c for $r_L/a = 0.03, 0.075, 0.125$, and 0.140 for the NRL Phase II modified betatron. The growth rate curves are determined from the dispersion relation in Eq. (45) for $\omega_{pe}/\omega_{cz} = 38$, $\omega_{c\theta}/\omega_{cz} = 20$, $\gamma_b = 7.5$, $a/R_0 = 0.015$, $f = 0$, $\Delta/\gamma_b m\beta_b c R_0 = 0$, and $F = 0$ ($E = 3.3MeV$, $I = 10kA$, $a = 1.5cm$, $R_0 = 100cm$, and $\hat{B}_\theta = 2.5kG$).

Fig. 7. (a) Regions of equilibrium and stability for r_L/a versus f for the NRL Phase II modified betatron. The stability boundary (solid line) is obtained from the dispersion relation in Eq. (66) and the equilibrium boundary (dashed line) is obtained from Eq. (30) for $\omega_{pe}/\omega_{cz} = 38$, $\omega_{c\theta}/\omega_{cz} = 20$, $\gamma_b = 7.5$,

$a/R_0 = 0.015$, $a/a_c = 0.1$, $\Delta/\gamma_b m\beta_b cR_0 = 0$, and $F = 0$ ($E = 3.3MeV$, $I = 10kA$, $a = 1.5cm$, $R_0 = 100cm$, $a_c = 15cm$, and $\hat{B}_\theta = 2.5kG$). (b) Curves of normalized growth rate $Im\omega/\omega_{cz}$ versus f for $r_L/a = 0.03$, 0.075, 0.125, 0.275, and 0.280 for the NRL Phase II modified betatron. The growth rate curves are determined from the dispersion relation in Eq. (45) for $\omega_{pe}/\omega_{cz} = 38$, $\omega_{c\theta}/\omega_{cz} = 20$, $\gamma_b = 7.5$, $a/R_0 = 0.015$, $a/a_c = 0.1$, $\Delta/\gamma_b m\beta_b cR_0 = 0$, and $F = 0$ ($E = 3.3MeV$, $I = 10kA$, $a = 1.5cm$, $R_0 = 100cm$, $a_c = 15cm$, and $\hat{B}_\theta = 2.5kG$).

Fig. 8. (a) Regions of equilibrium and stability for a/R_0 versus ω_{pe}/ω_{cz} for the NRL Phase II modified betatron. The stability boundary is obtained from the dispersion relation in Eq. (67) and equilibrium exists everywhere within the figure from Eq. (30) for $\omega_{c\theta}/\omega_{cz} = 20$, $\gamma_b = 7.5$, $a/a_c = 0.1$, $r_L/a = 0.15$, $f = 0$, $\Delta/\gamma_b m\beta_b cR_0 = 0$, and $F = 0$ ($E = 3.3MeV$, $a = 1.5cm$, $a_c = 15cm$, and $\hat{B}_\theta = 2.5kG$). (b) Curves of normalized growth rate $Im\omega/\omega_{cz}$ versus ω_{pe}/ω_{cz} for $a/R_0 = 0.0075$, 0.015, and 0.03 for the NRL Phase II modified betatron. The growth rate curves are determined from the dispersion relation in Eq. (45) for $\omega_{c\theta}/\omega_{cz} = 20$, $\gamma_b = 7.5$, $a/a_c = 0.1$, $r_L/a = 0.15$, $f = 0$, $\Delta/\gamma_b m\beta_b cR_0 = 0$, and $F = 0$ ($E = 3.3MeV$, $a = 1.5cm$, $a_c = 15cm$, and $\hat{B}_\theta = 2.5kG$).

Fig. 9. (a) Regions of equilibrium and stability for a/R_0 versus γ_b for the NRL Phase II modified betatron. The stability boundary (solid line) is obtained from the dispersion relation in Eq. (67) and the equilibrium boundary (dashed line) is obtained from Eq. (30) for $\omega_{pe}/\omega_{cz} = 38$, $\omega_{c\theta}/\omega_{cz} = 20$, $a/a_c = 0.1$, $r_L/a = 0.15$, $f = 0$, $\Delta/\gamma_b m\beta_b cR_0 = 0$, and $F = 0$ ($I = 10kA$, $a = 1.5cm$, $a_c = 15cm$, and $\hat{B}_\theta = 2.5kG$). (b) Curves of normalized growth rate $Im\omega/\omega_{cz}$ versus γ_b for $a/R_0 = 0.0075$, 0.015, 0.03, and 0.10 for the NRL Phase II modified betatron. The growth rate curves are determined from the dispersion relation in Eq. (45) for $\omega_{pe}/\omega_{cz} = 38$, $\omega_{c\theta}/\omega_{cz} = 20$, $a/a_c = 0.1$, $r_L/a = 0.15$, $f = 0$, $\Delta/\gamma_b m\beta_b cR_0 = 0$, and $F = 0$ ($I = 10kA$, $a = 1.5cm$, $a_c = 15cm$, and $\hat{B}_\theta = 2.5kG$).

Fig. 10. (a) Regions of equilibrium and stability for $\Delta/\gamma_b m\beta_b cR_0$ versus ω_{pe}/ω_{cz} for the NRL Phase I modified betatron. The stability boundary is obtained from

the dispersion relation in Eq. (45) and equilibrium exists everywhere within the figure from Eq. (30) for $\omega_{c\theta}/\omega_{cz} = 49$, $\gamma_b = 3$, $a/R_0 = 0.015$, $a/a_c = 0.1$, $r_L/a = 0.065$, $f = 0$, and $F = 0$ ($E = 1MeV$, $a = 1.5cm$, $R_0 = 100cm$, $a_c = 15cm$, and $\hat{B}_\theta = 2.3kG$). (b) Curves of normalized growth rate $Im\omega/\omega_{cz}$ versus ω_{pe}/ω_{cz} for $\Delta/\gamma_b m\beta_b c R_0 = 0.001$, 0.002, 0.003, and 0.004 for the NRL Phase I modified betatron. The growth rate curves are determined from the dispersion relation in Eq. (45) for $\omega_{c\theta}/\omega_{cz} = 49$, $\gamma_b = 3$, $a/R_0 = 0.015$, $a/a_c = 0.1$, $r_L/a = 0.065$, $f = 0$, and $F = 0$ ($E = 1MeV$, $a = 1.5cm$, $R_0 = 100cm$, $a_c = 15cm$, and $\hat{B}_\theta = 2.3kG$).

Fig. 11. (a) Regions of equilibrium and stability for $\sqrt{ab}/R_0$ versus ω_{pe}/ω_{cz} for the LANL Phermex conventional betatron. The stability boundary (solid line) is obtained from the dispersion relation in Eq. (47) and the equilibrium boundary (dashed line) is obtained from Eq. (34) for $\gamma_b = 60$, $\sqrt{ab}/a_c = 0.25$, $b/a = 1$, $f = 0$, $F = 0$, and $\Delta/\gamma_b m\beta_b c R_0 = 0$, ($E = 30MeV$, $a = b = 1cm$, and $a_c = 4cm$). (b) Curves of normalized growth rate $Im\omega/\omega_{cz}$ versus ω_{pe}/ω_{cz} for $\sqrt{ab}/R_0 = 0.001$, 0.010, 0.030, 0.0666, and 0.10 for the LANL Phermex conventional betatron. The growth rate curves are determined from the dispersion relation in Eq. (47) for $\gamma_b = 60$, $\sqrt{ab}/a_c = 0.25$, $b/a = 1$, $f = 0$, $F = 0$, and $\Delta/\gamma_b m\beta_b c R_0 = 0$ ($E = 30MeV$, $a = b = 1cm$, and $a_c = 4cm$).

Fig. 12. (a) Regions of equilibrium and stability for $\sqrt{ab}/R_0$ versus γ_b for the LANL Phermex conventional betatron. The stability boundary (solid line) is obtained from the dispersion relation in Eq. (47) and the equilibrium boundary (dashed line) is obtained from Eq. (34) for $\omega_{pe}/\omega_{cz} = 1.2$, $\sqrt{ab}/a_c = 0.25$, $b/a = 1$, $f = 0$, $\Delta/\gamma_b m\beta_b c R_0 = 0$, and $F = 0$ ($I = 1.7kA$, $a = b = 1cm$, and $a_c = 4cm$). (b) Curves of normalized growth rate $Im\omega/\omega_{cz}$ versus γ_b for $\sqrt{ab}/R_0 = 0.010$, 0.030, 0.066, 0.10 for the LANL Phermex conventional betatron. The growth rate curves are determined from the dispersion relation in Eq. (47) for $\omega_{pe}/\omega_{cz} = 1.2$, $\sqrt{ab}/a_c = 0.25$, $b/a = 1$, $f = 0$, $\Delta/\gamma_b m\beta_b c R_0 = 0$, and $F = 0$ ($I = 1.7kA$, $a = b = 1cm$, and $a_c = 4cm$).

Fig. 13. (a) Regions of equilibrium and stability for $\sqrt{ab}/R_0$ versus b/a for the LANL Phermex conventional betatron. The stability boundary (solid line) is obtained from the dispersion relation in Eq. (47) and the equilibrium boundary (dashed line) is obtained from Eq. (34) for $\omega_{pe}/\omega_{cz} = 1.2$, $\gamma_b = 60$,

$\sqrt{ab}/a_c = 0.25$, $f = 0$, $\Delta/\gamma_b m\beta_b c R_0 = 0$, and $F = 0$ ($E = 30MeV$, $I = 1.7kA$, and $a_c = 4cm$). (b) Curves of normalized growth rate $Im\omega/\omega_{cz}$ versus b/a for $\sqrt{ab}/R_0 = 0.001$, 0.010, 0.020, 0.0250, and 0.0275 for the LANL Phermex conventional betatron. The growth rate curves are determined from the dispersion relation in Eq. (47) for $\omega_{pe}/\omega_{cz} = 1.2$, $\gamma_b = 60$, $\sqrt{ab}/a_c = 0.25$, $f = 0$, $\Delta/\gamma_b m\beta_b c R_0 = 0$, and $F = 0$ ($E = 30MeV$, $I = 1.7kA$, and $a_c = 4cm$).

Fig. 14. Stability regions of $\sqrt{ab}/R_0$ versus $\sqrt{ab}/a_c$ for $F = -0.2$ and $F = 0$ for the LANL Liner conventional betatron. The stability boundaries are obtained from the dispersion relation in Eq. (47) and the equilibrium is defined everywhere in the region shown. The parameters chosen are $\omega_{pe}/\omega_{cz} = 0.69$, $\gamma_b = 10$, $b/a = 1$, $f = 0$, and $\Delta/\gamma_b m\beta_b c R_0 = 0$, where $F = -0.2$ corresponds to the solid curve and $F = 0$ corresponds to the dashed curve ($E = 4.6MeV$, $I = 0.2kA$, and $a = b = 0.5cm$).

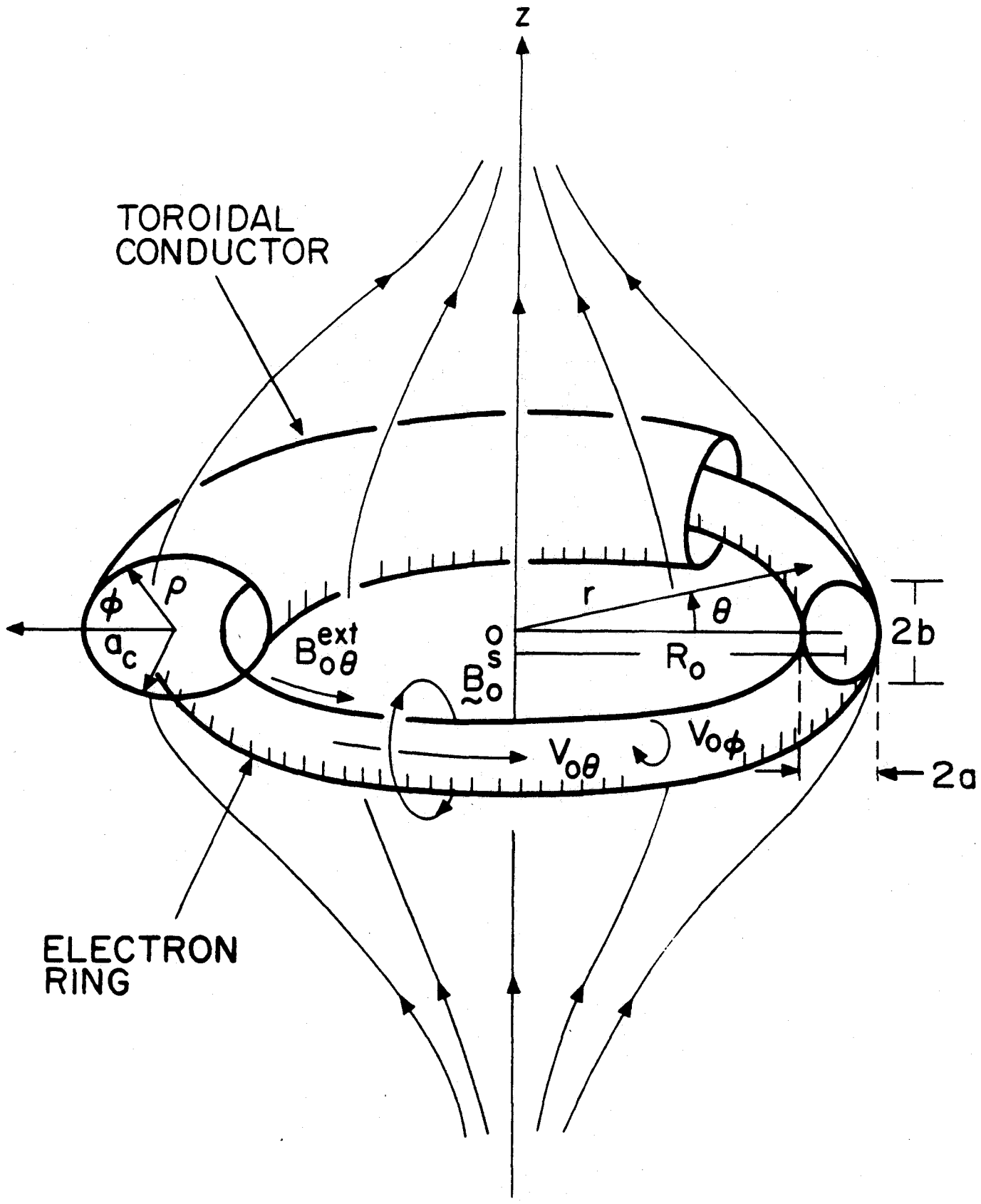
z
TOROIDAL
CONDUCTOR
ϕ
ρ
a_c
$B_{o\theta}^{ext}$
o
s
B_o
r
θ
R_o
2b
$V_{o\theta}$
$V_{o\phi}$
2a
ELECTRON
RING

Fig. 1

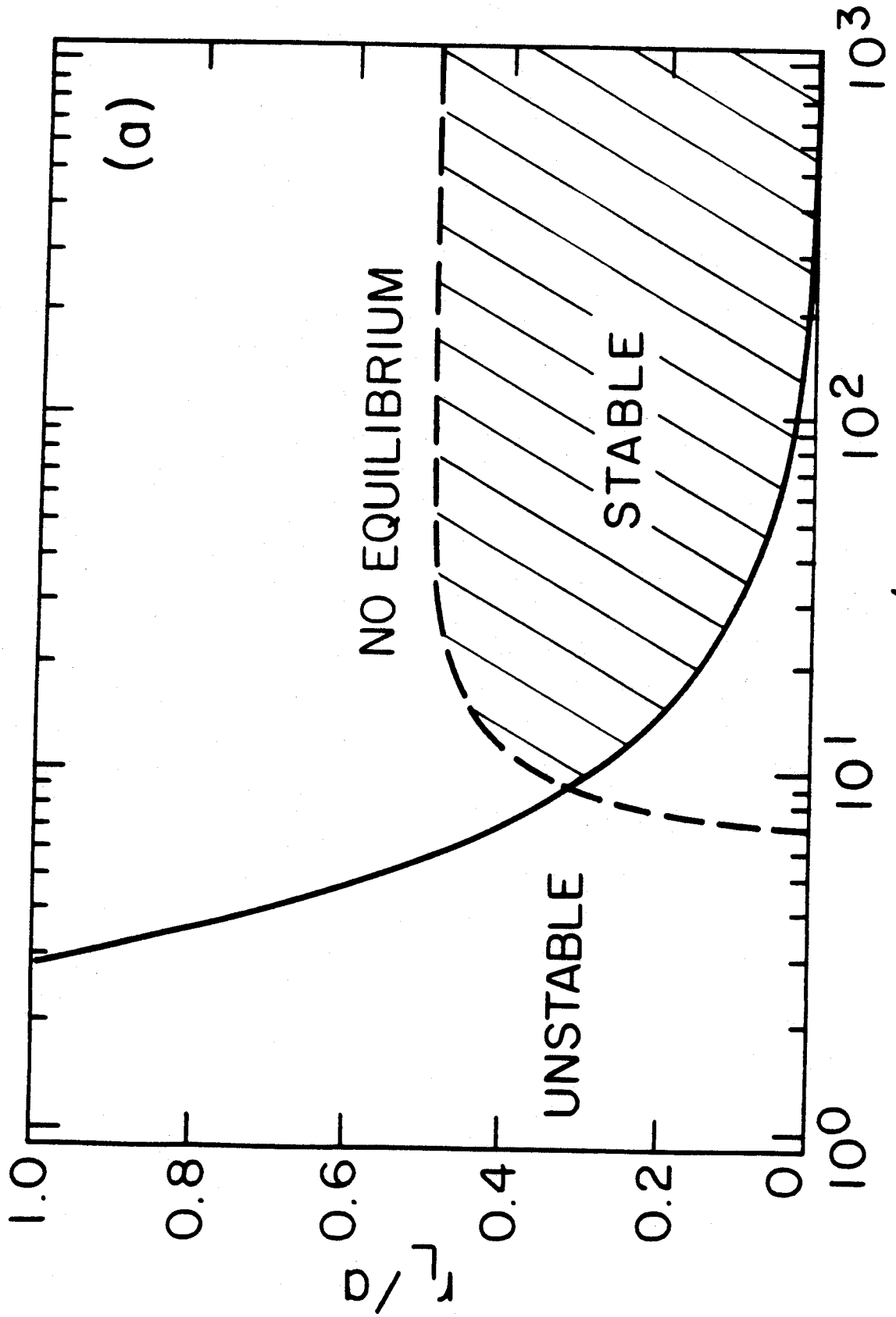
(a)
NO EQUILIBRIUM
STABLE
UNSTABLE
Γ/Γ_d
$\omega_{c\theta}/\omega_{cz}$
1.0
0.8
0.6
0.4
0.2
0
10^0
10^1
10^2
10^3

Fig. 2(a)

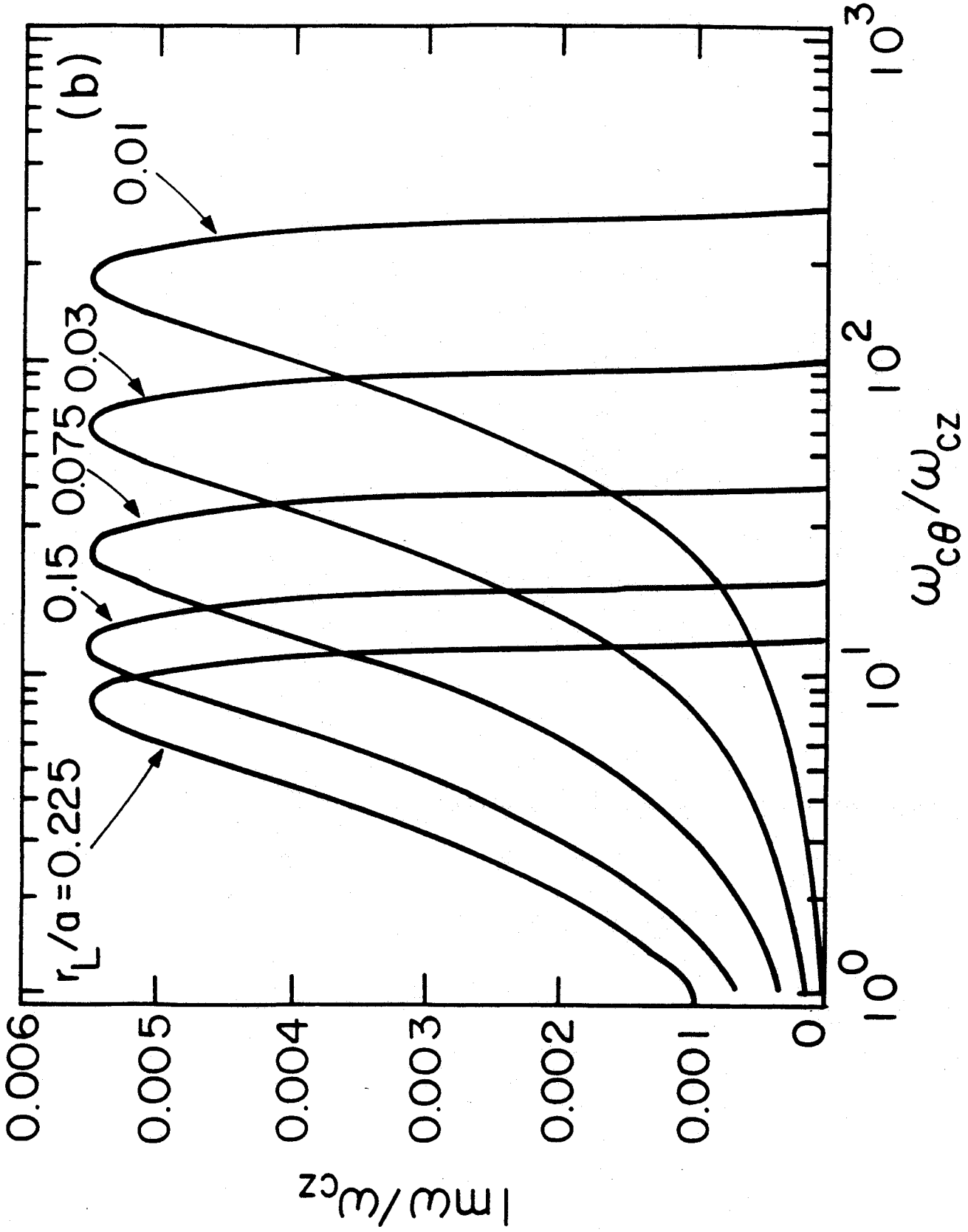
(b)
$r_L/a = 0.225$
0.15
0.075
0.03
0.01
$\omega_{c\theta}/\omega_{cz}$
$\mathrm{Im}\omega/\omega_{cz}$
0.006
0.005
0.004
0.003
0.002
0.001
0
10^0
10^1
10^2
10^3

Fig. 2(b)

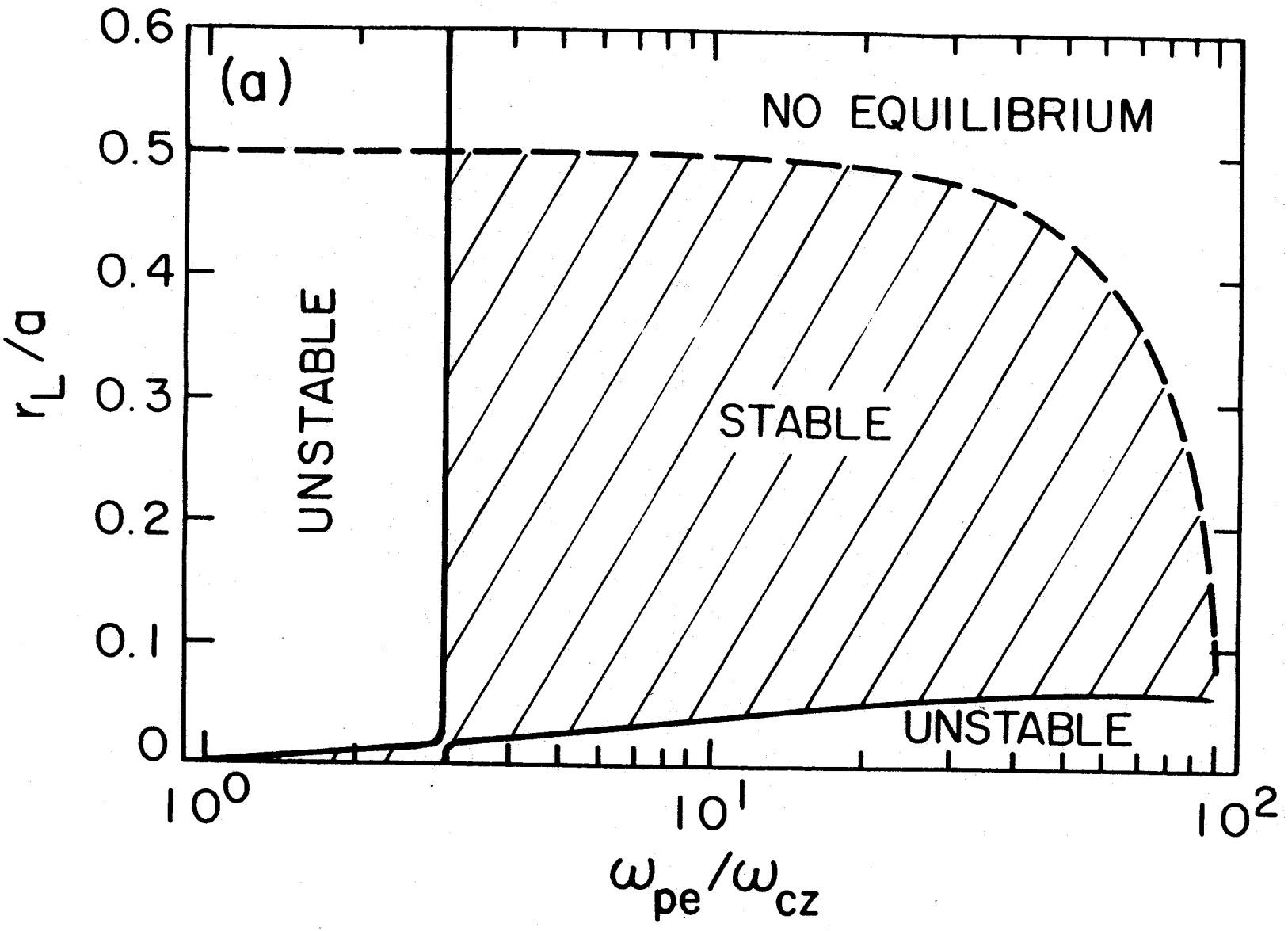
(a)
NO EQUILIBRIUM
UNSTABLE
STABLE
UNSTABLE
0.6
0.5
0.4
0.3
0.2
0.1
0
r_L/a
10^0
10^1
10^2
ω_{pe}/ω_{cz}

Fig. 3(a)

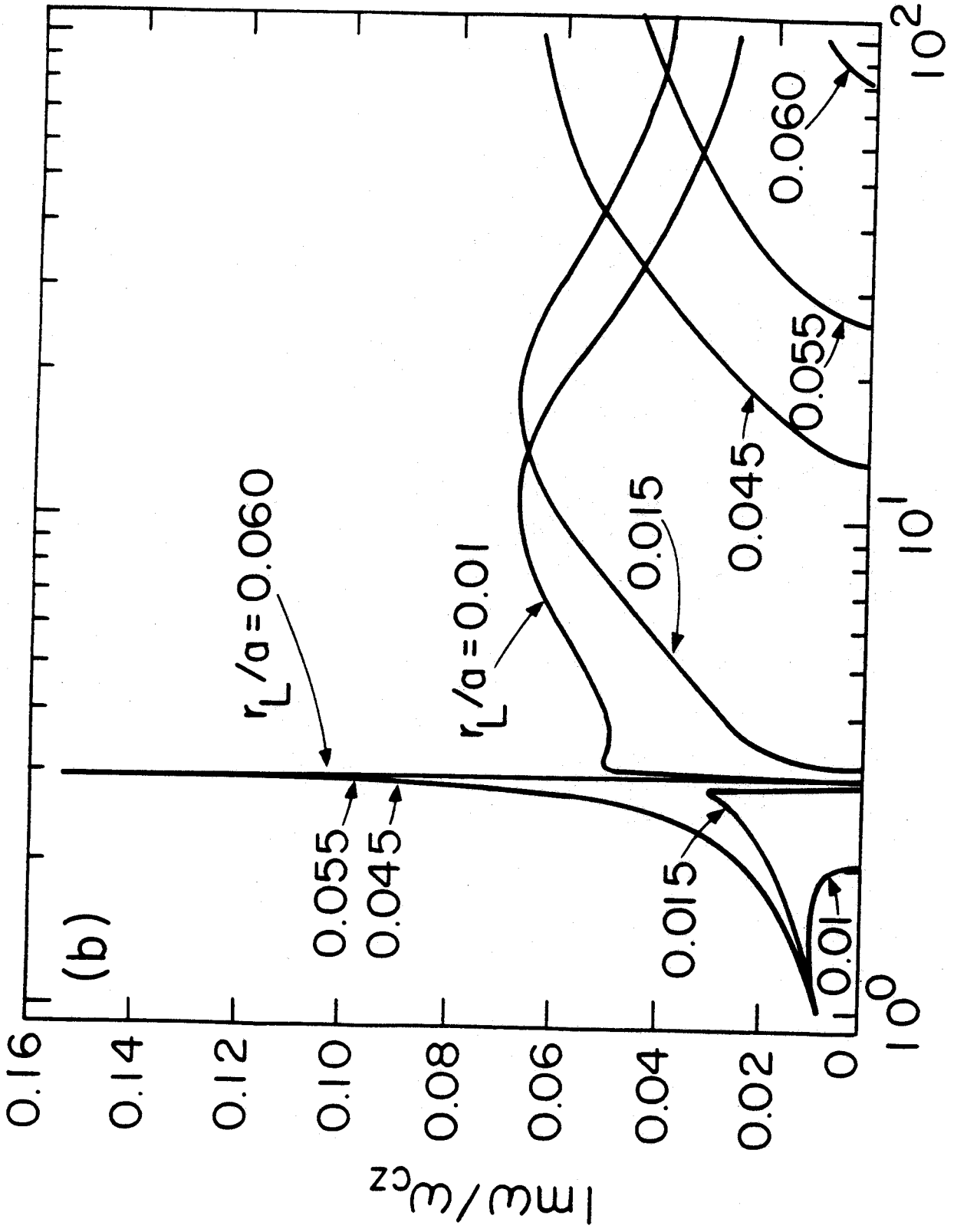
(b)
$r_L/a = 0.060$
$r_L/a = 0.01$
0.055
0.045
0.015
0.01
0.015
0.045
0.055
0.060
ω_{pe}/ω_{cz}
$\mathrm{Im}\omega/\omega_{cz}$
0.16
0.14
0.12
0.10
0.08
0.06
0.04
0.02
0
10^0
10^1
10^2

Fig. 3(b)

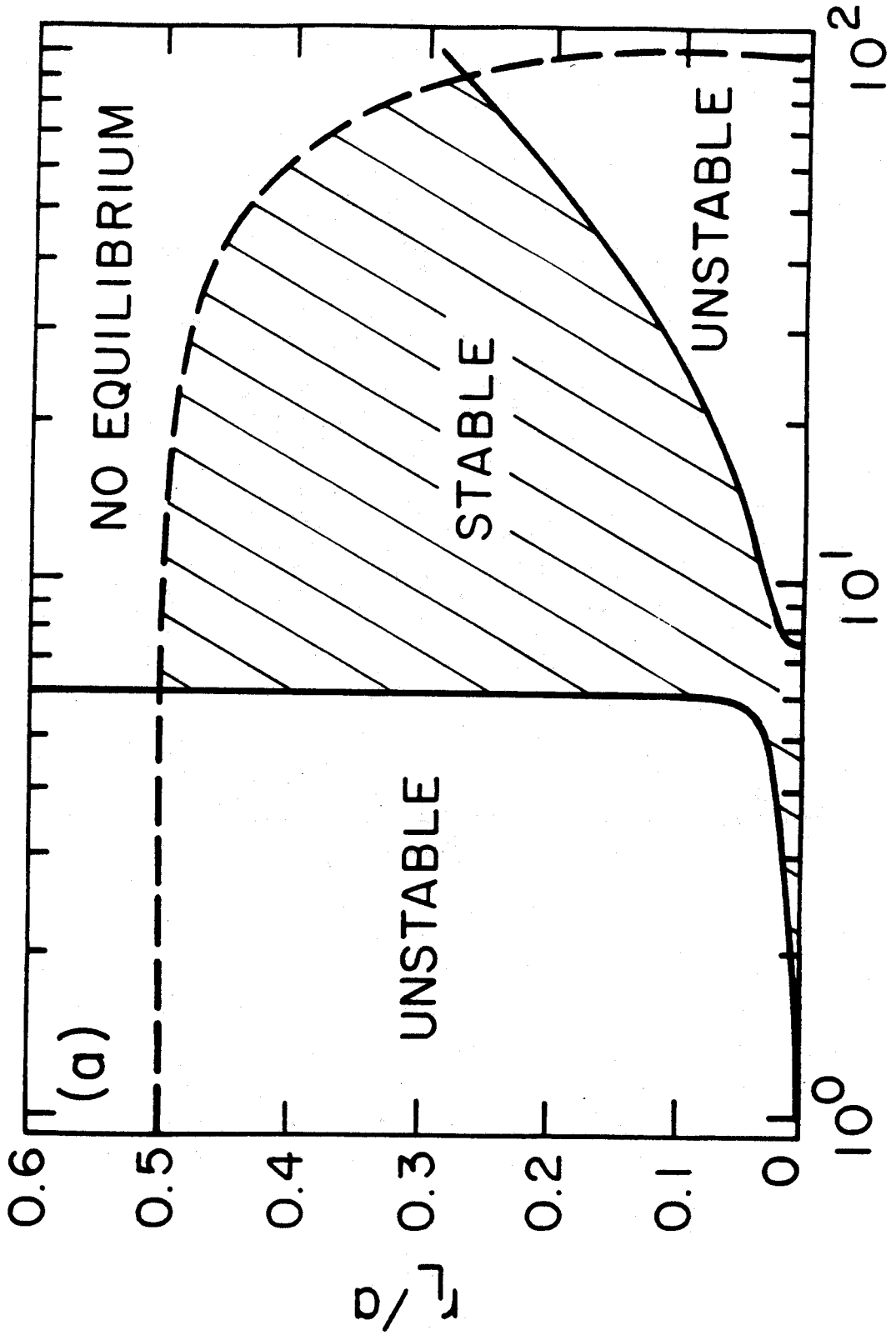
NO EQUILIBRIUM
STABLE
UNSTABLE
UNSTABLE
(a)
0.6
0.5
0.4
0.3
0.2
0.1
0
10^0
10^1
10^2
ω_{pe}/ω_{cz}
Γ/Ω

Fig. 4(a)

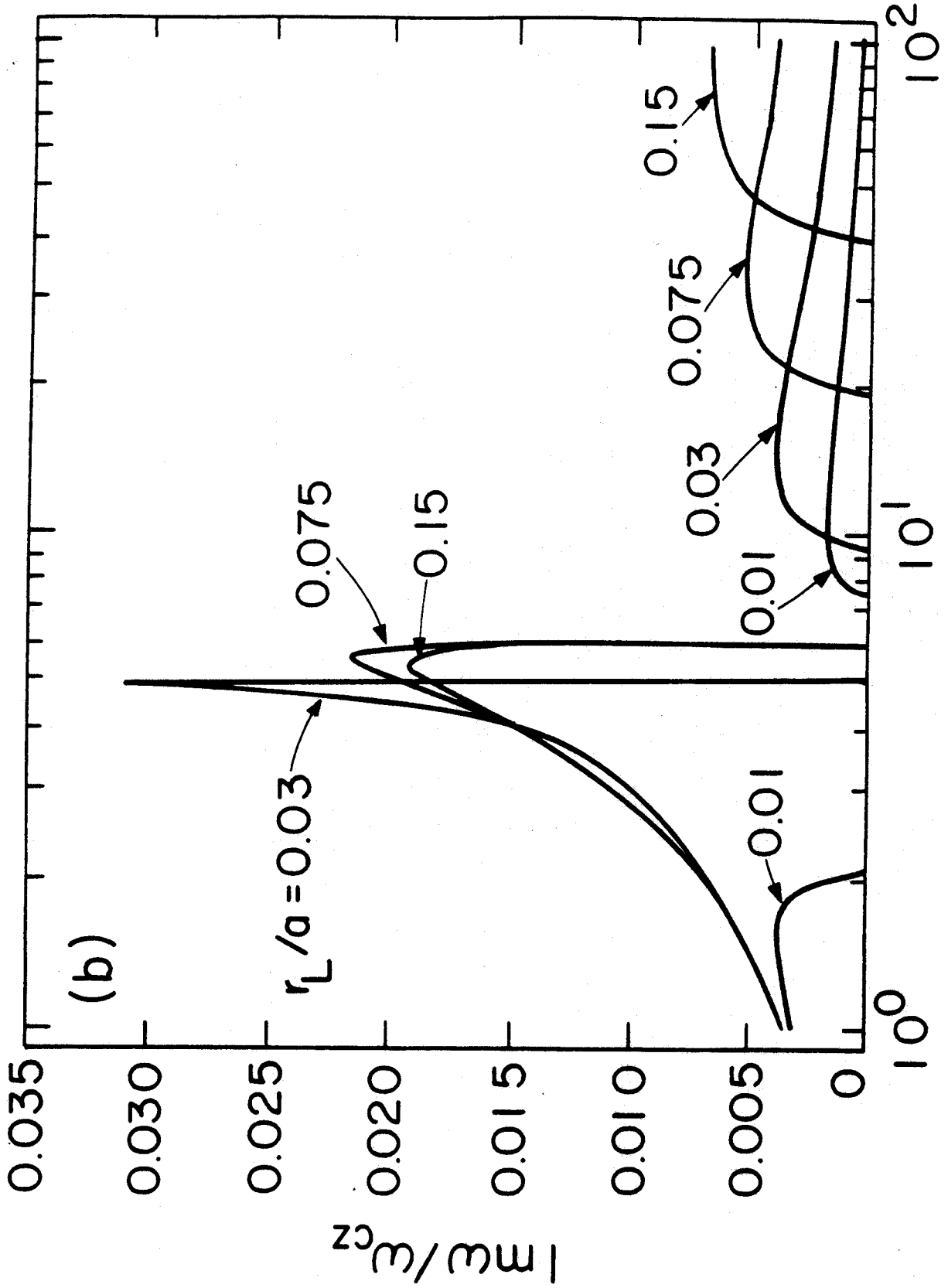
(b)
$r_L/a = 0.03$
0.075
0.15
0.01
0.03
0.075
0.15
0.01
$\mathrm{Im}\omega/\omega_{cz}$
ω_{pe}/ω_{cz}
0.035
0.030
0.025
0.020
0.015
0.010
0.005
0
10^0
10^1
10^2

Fig. 4(b)

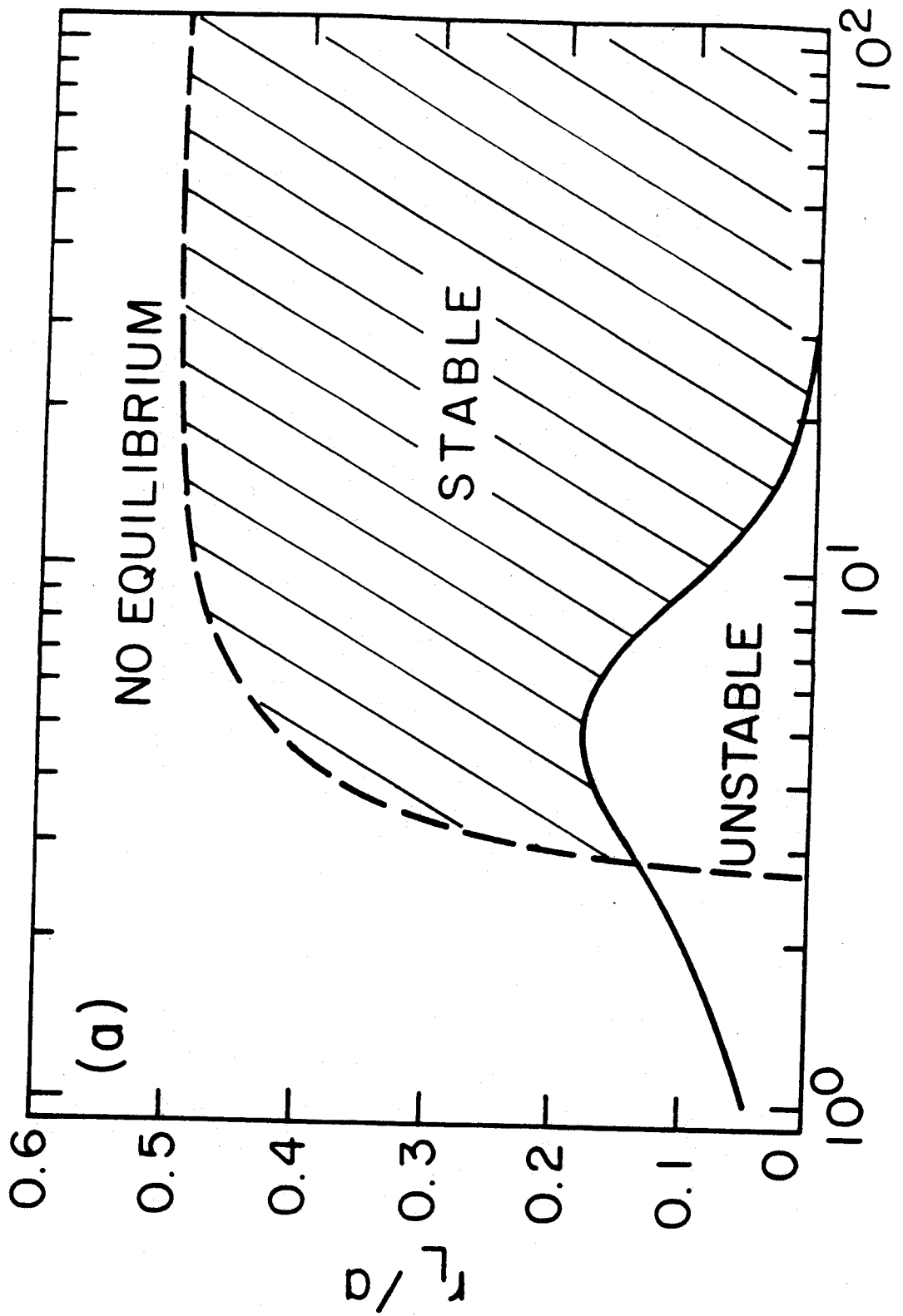
(a)
NO EQUILIBRIUM
STABLE
UNSTABLE
Γ_L/α
γ_b
0
0.1
0.2
0.3
0.4
0.5
0.6
10^0
10^1
10^2

Fig. 5(a)

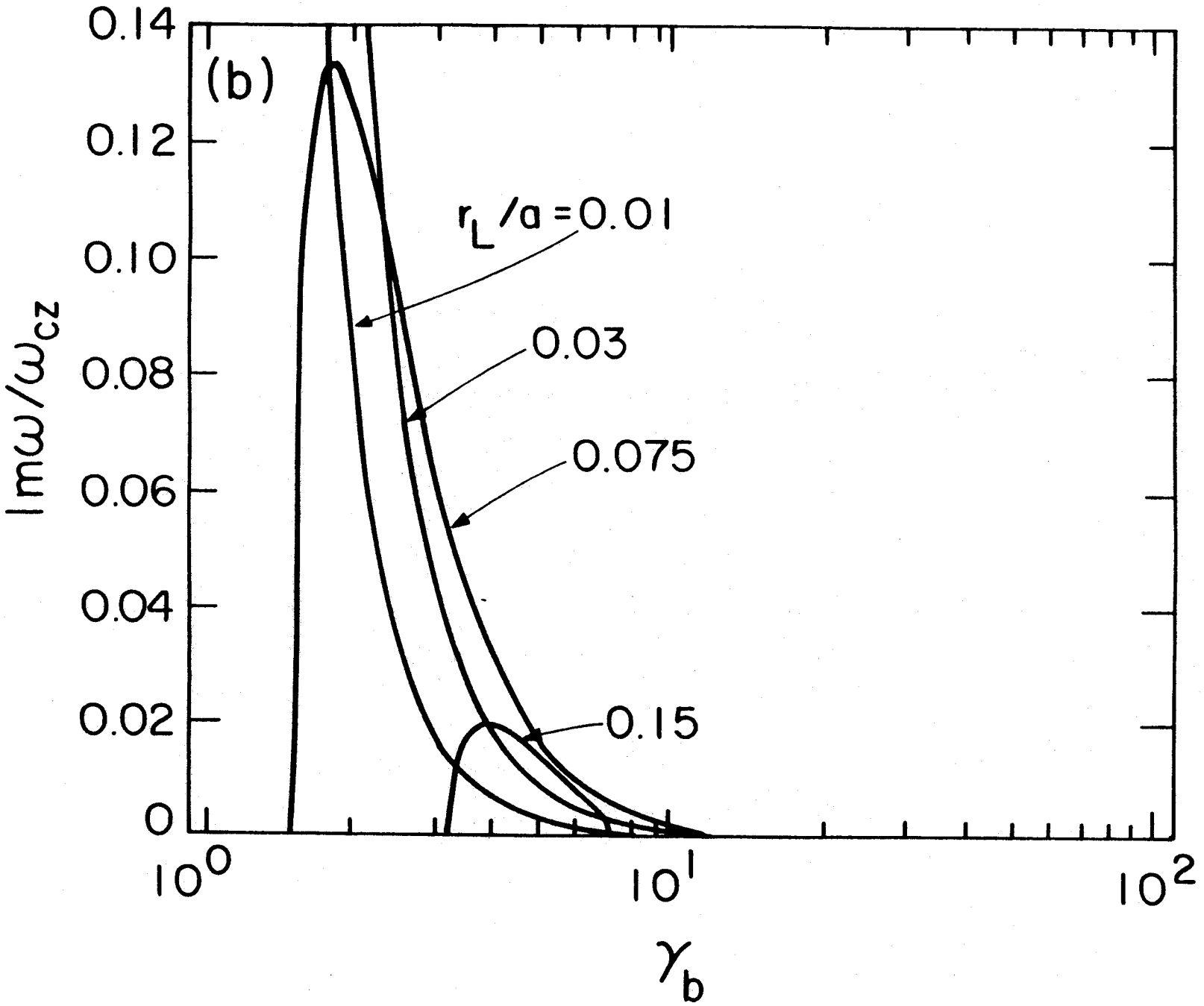
(b)
0.14
0.12
0.10
0.08
0.06
0.04
0.02
0
$\mathrm{Im}\omega/\omega_{cz}$
$r_L/a = 0.01$
0.03
0.075
0.15
10^0
10^1
10^2
γ_b

Fig. 5(b)

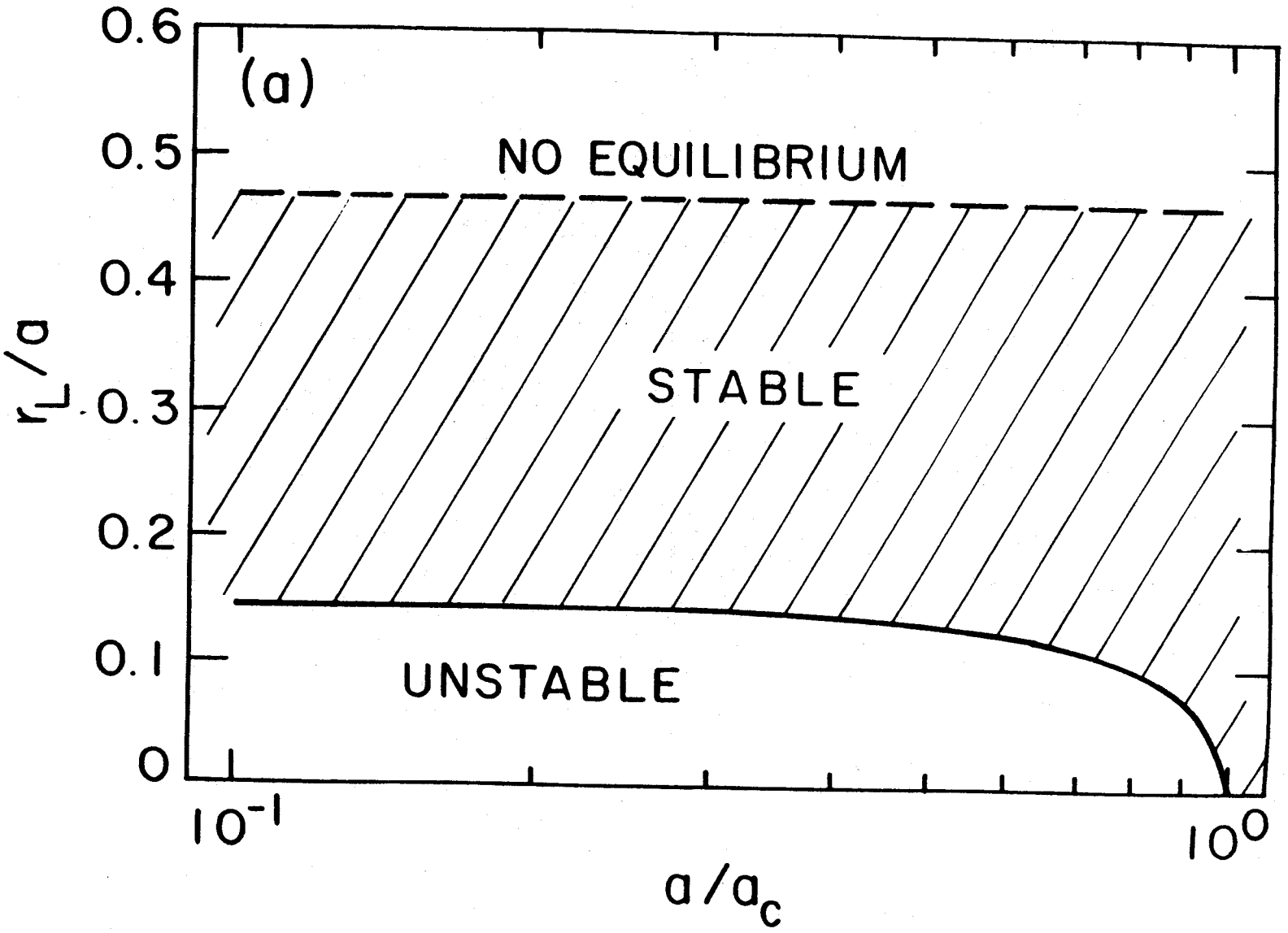
(a)
NO EQUILIBRIUM
STABLE
UNSTABLE
0.6
0.5
0.4
0.3
0.2
0.1
0
r_L/a
10^{-1}
10^{0}
a/a_c

Fig. 6(a)

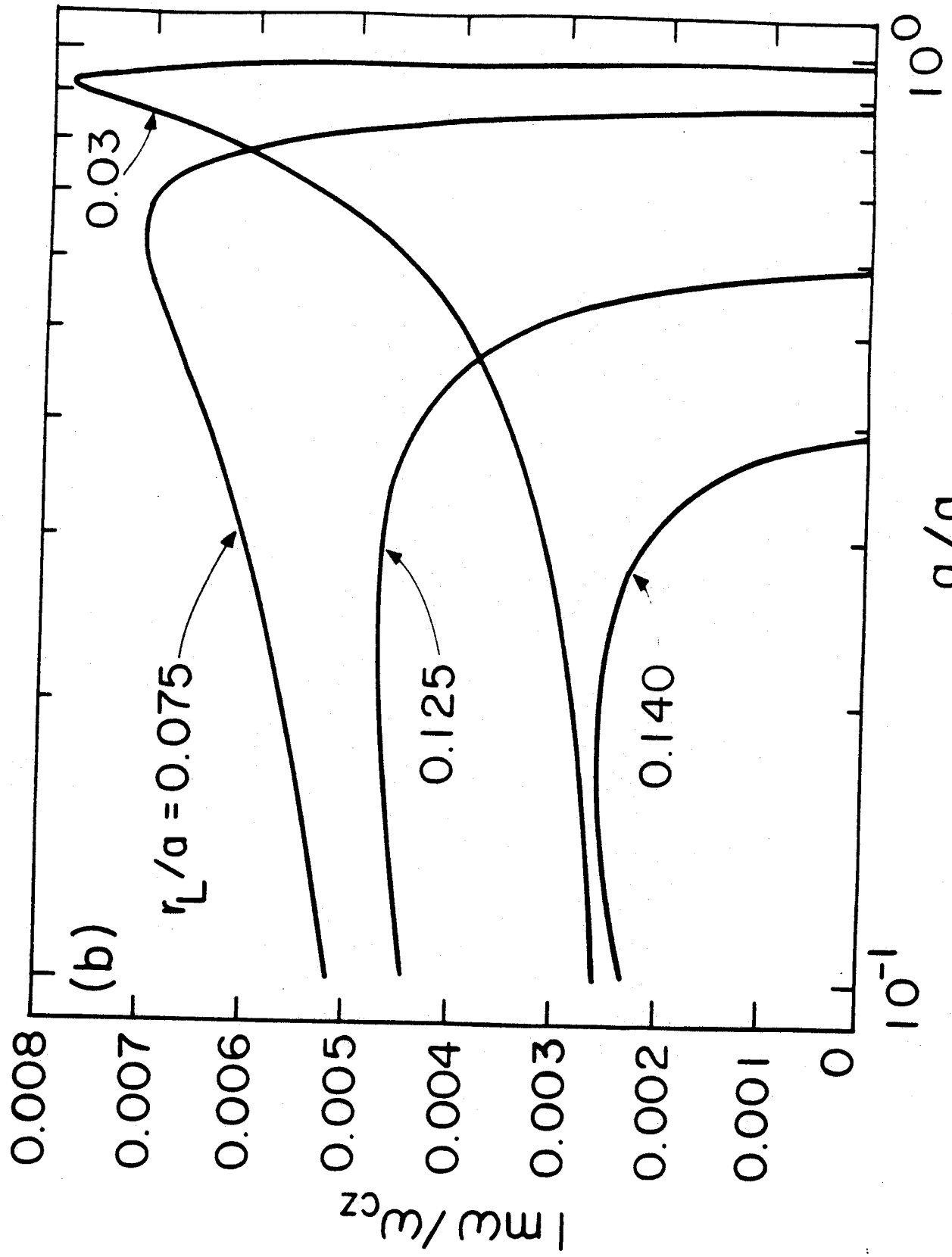
(b)
$r_L/a = 0.075$
0.03
0.125
0.140
$\mathrm{Im}\,\omega/\omega_{cz}$
0.008
0.007
0.006
0.005
0.004
0.003
0.002
0.001
0
10^{-1}
10^{0}
a/a_c

Fig. 6(b)

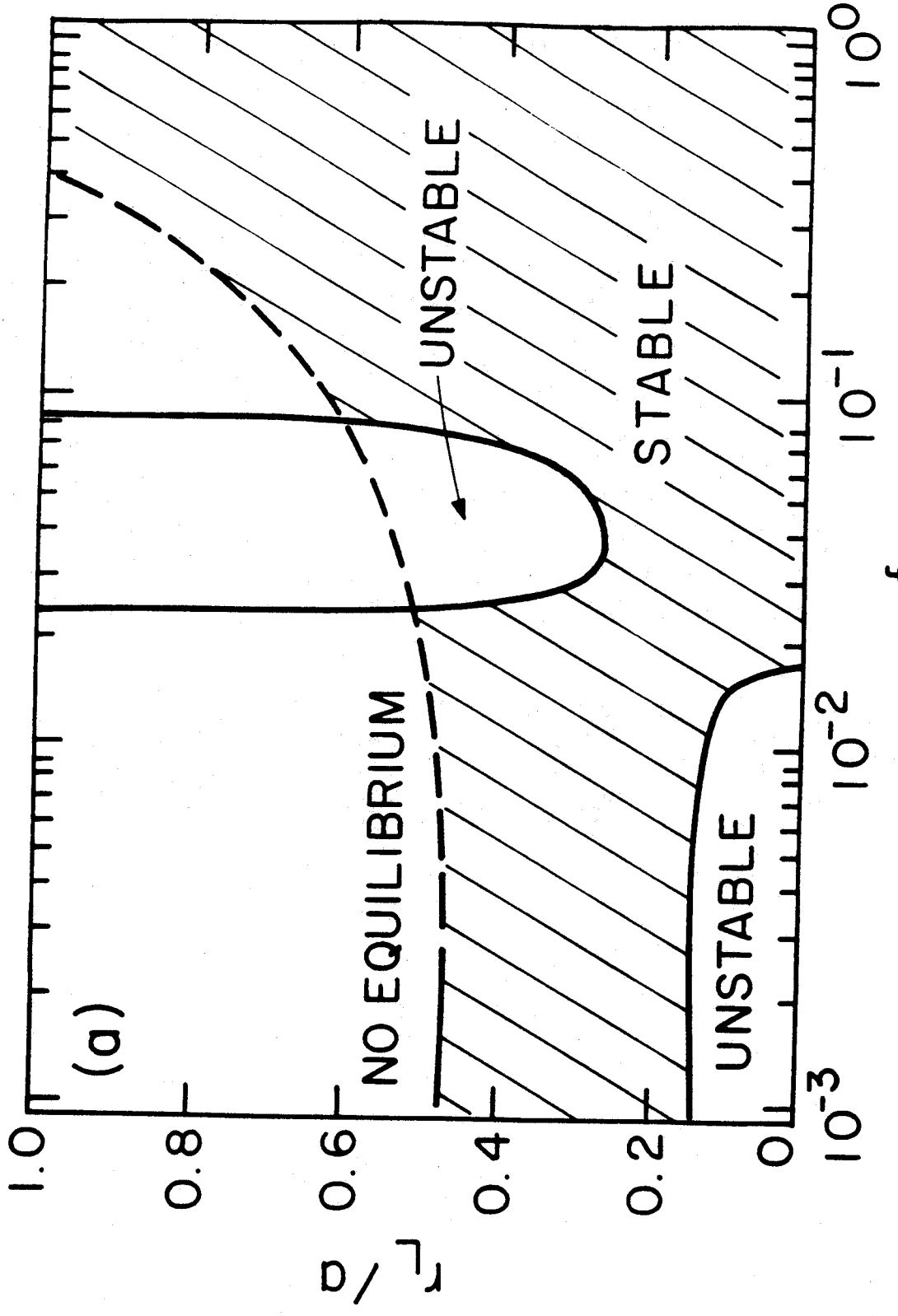
(a)
NO EQUILIBRIUM
UNSTABLE
STABLE
UNSTABLE
r_L/a
f
1.0
0.8
0.6
0.4
0.2
0
10^{-3}
10^{-2}
10^{-1}
10^{0}

Fig. 7(a)

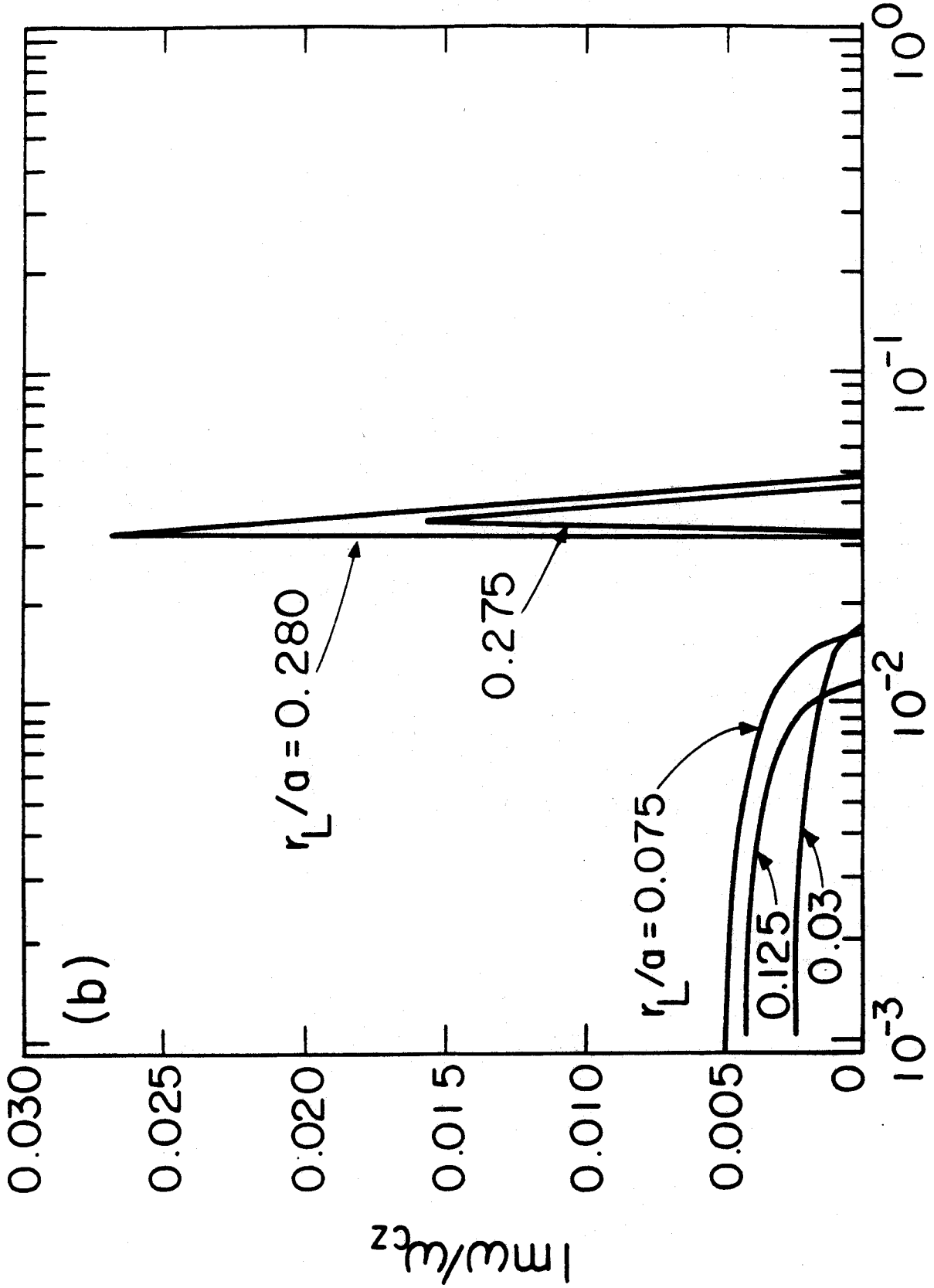
(b)
$r_L/a = 0.280$
0.275
$r_L/a = 0.075$
0.125
0.03
$\mathrm{Im}\omega/\omega_{cz}$
f
0.030
0.025
0.020
0.015
0.010
0.005
0
10^{-3}
10^{-2}
10^{-1}
10^{0}

Fig. 7(b)

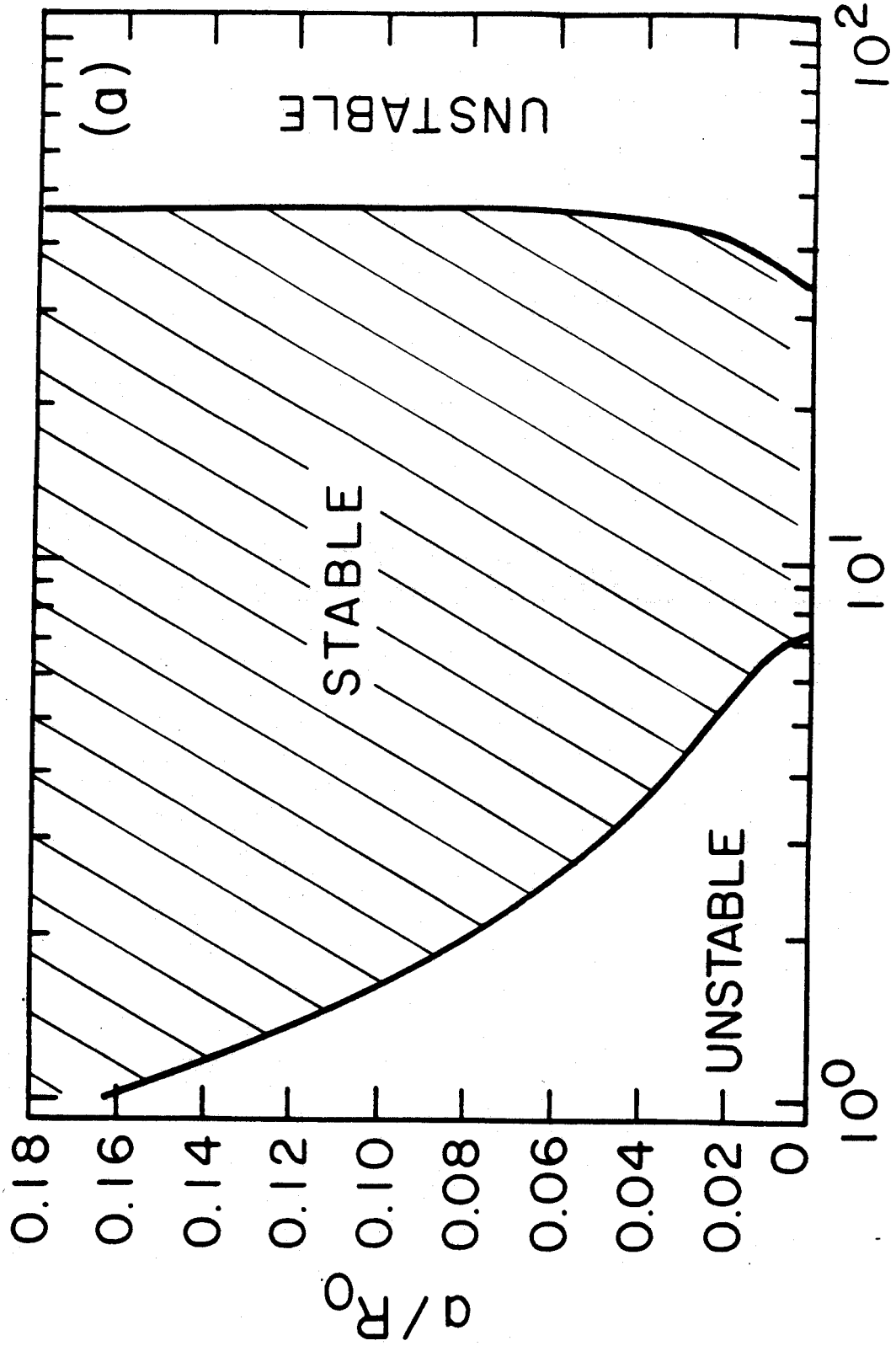
(a)
UNSTABLE
STABLE
UNSTABLE
0.18
0.16
0.14
0.12
0.10
0.08
0.06
0.04
0.02
0
a/R_o
10^0
10^1
10^2
ω_{pe}/ω_{cz}

Fig. 8(a)

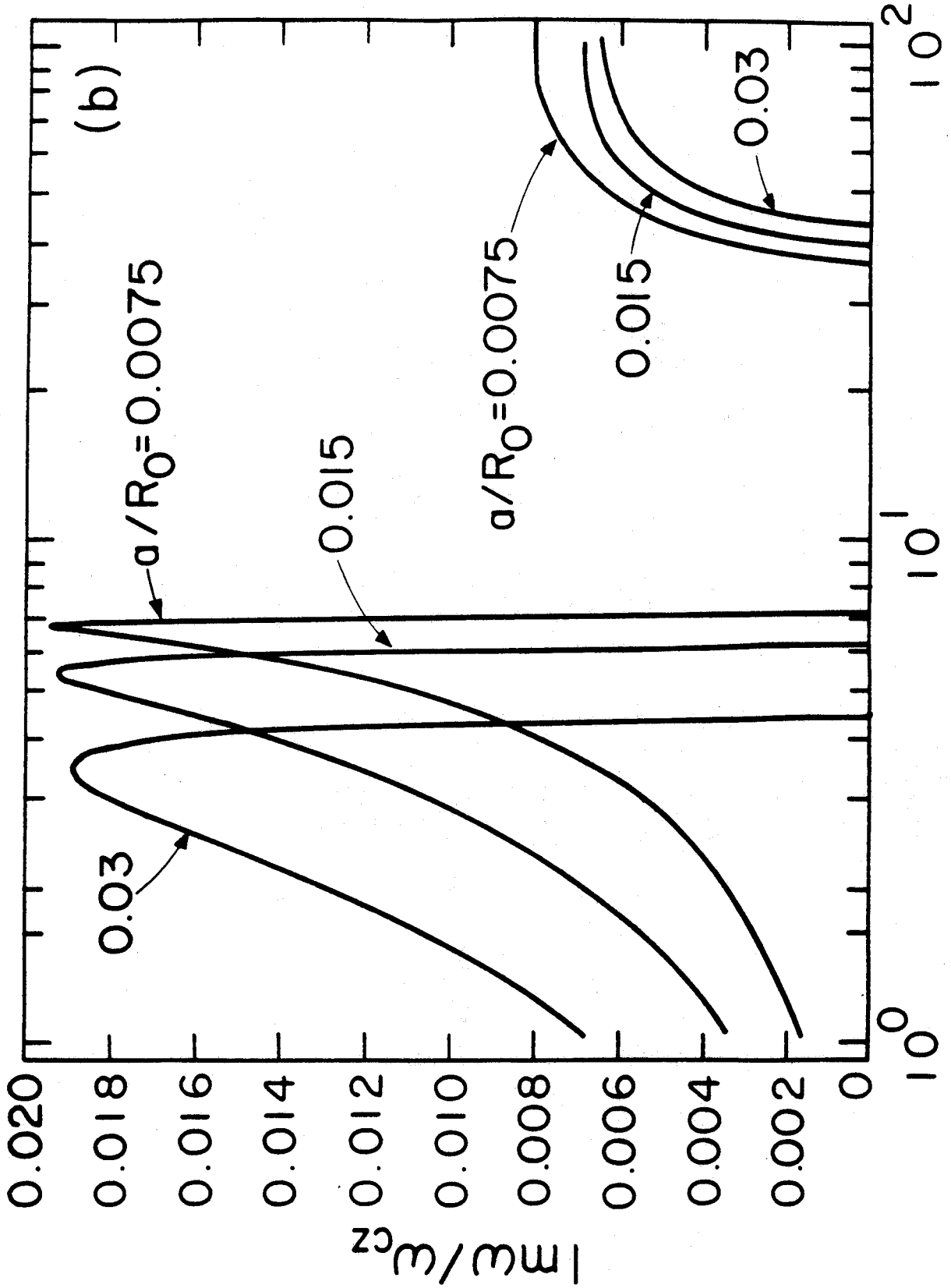
(b)
a/R_O=0.0075
0.015
0.03
a/R_O=0.0075
0.015
0.03
Im ω/ω_cz
ω_pe/ω_cz
0.020
0.018
0.016
0.014
0.012
0.010
0.008
0.006
0.004
0.002
0
10^0
10^1
10^2

Fig. 8(b)

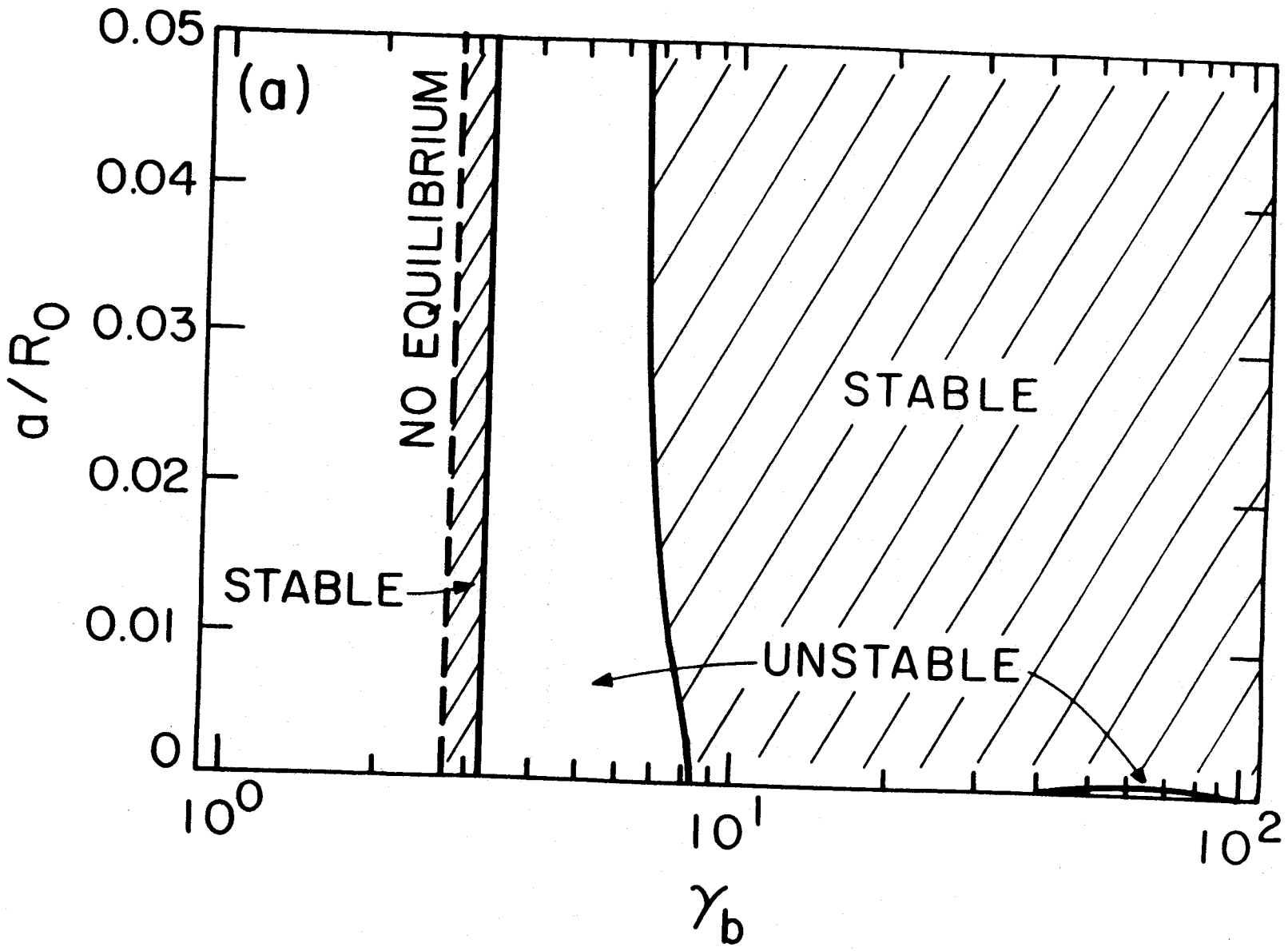
(a)
NO EQUILIBRIUM
STABLE
STABLE
UNSTABLE
0.05
0.04
0.03
0.02
0.01
0
a/R0
10^0
10^1
10^2
γb

Fig. 9(a)

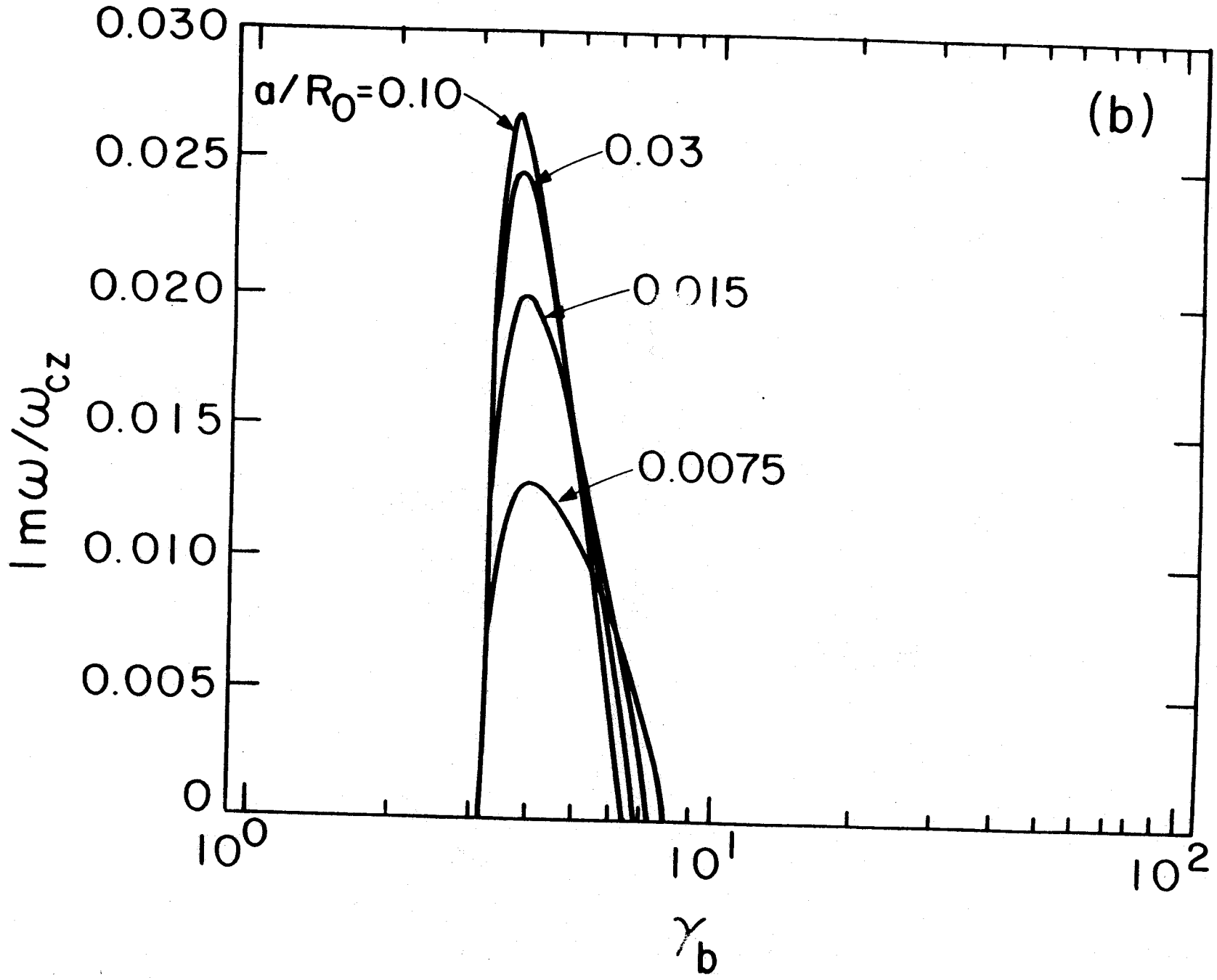
0.030
0.025
0.020
0.015
0.010
0.005
0
$a/R_0=0.10$
0.03
0.015
0.0075
(b)
$Im\omega/\omega_{cz}$
10^0
10^1
10^2
γ_b

Fig. 9(b)

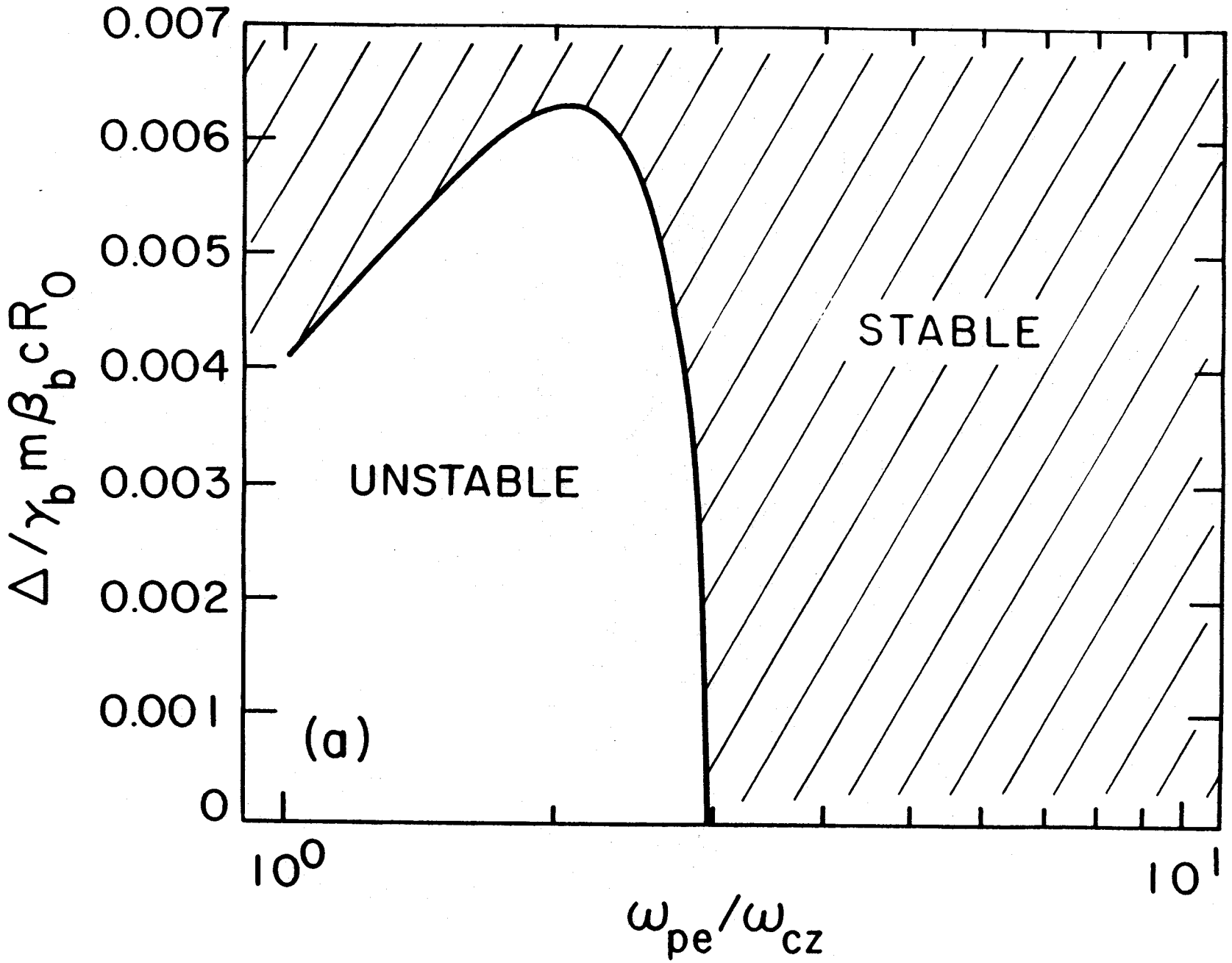
0.007
0.006
0.005
0.004
0.003
0.002
0.001
0
$\Delta/\gamma_b m\beta_b cR_0$
UNSTABLE
STABLE
(a)
10^0
10^1
ω_{pe}/ω_{cz}

Fig. 10(a)

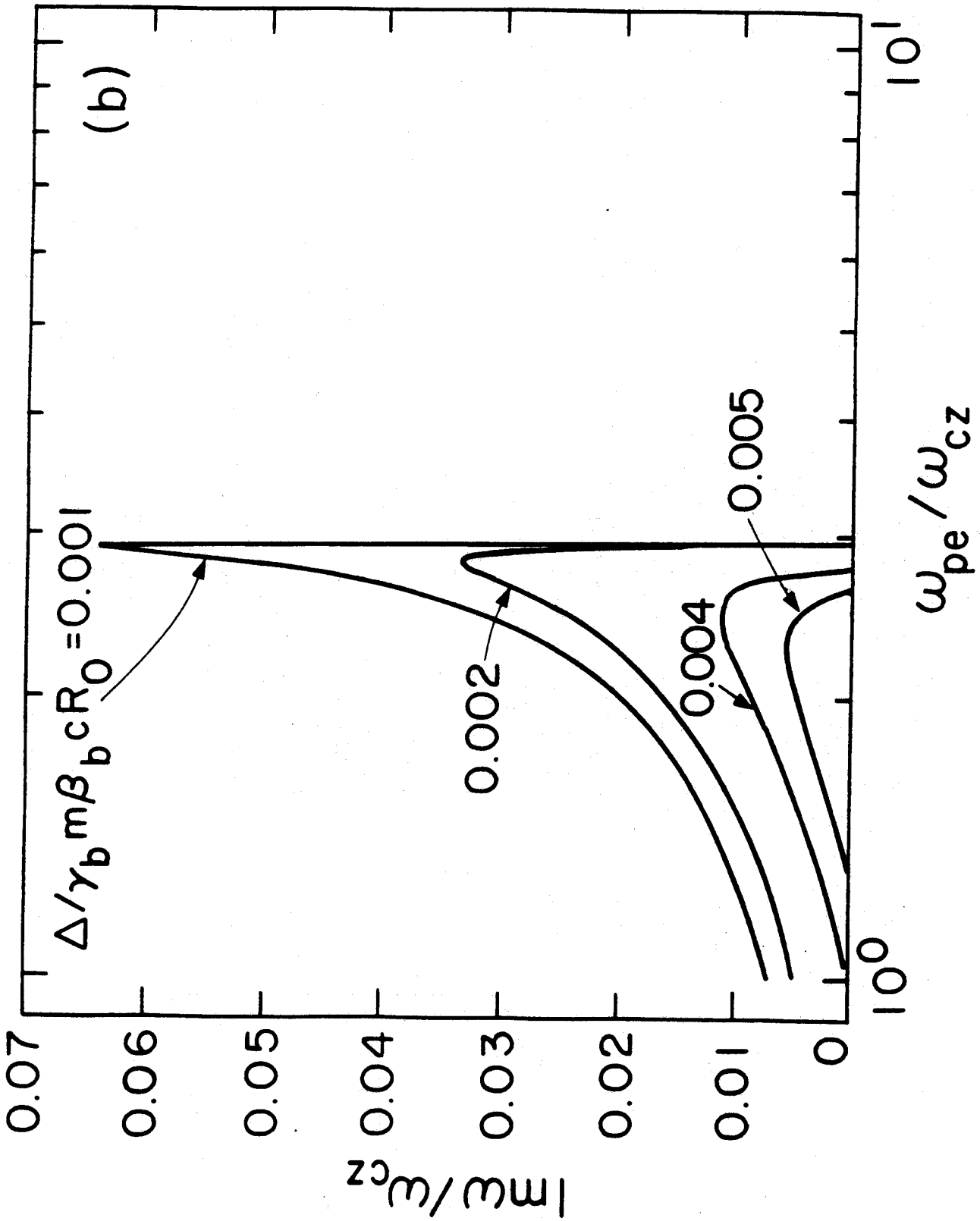
(b)
$\Delta/\gamma_b m\beta_b cR_o = 0.001$
0.002
0.004
0.005
ω_{pe}/ω_{cz}
$\mathrm{Im}\omega/\omega_{cz}$
0.07
0.06
0.05
0.04
0.03
0.02
0.01
0
10^0
10^1

Fig. 10(b)

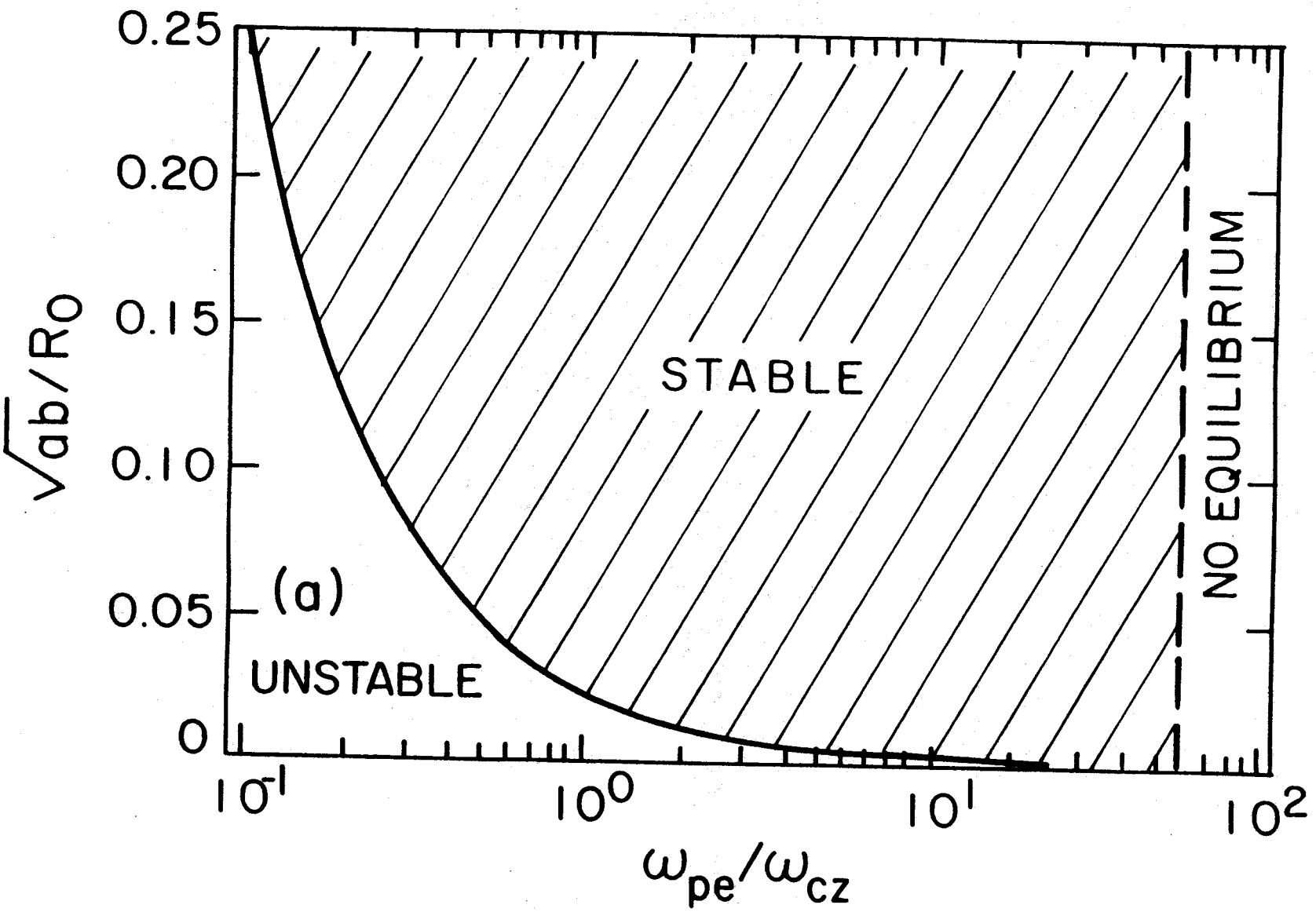
0.25
0.20
0.15
0.10
0.05
0
$\sqrt{ab}/R_0$
STABLE
NO EQUILIBRIUM
(a)
UNSTABLE
10^{-1}
10^{0}
10^{1}
10^{2}
ω_{pe}/ω_{cz}

Fig. 11(a)

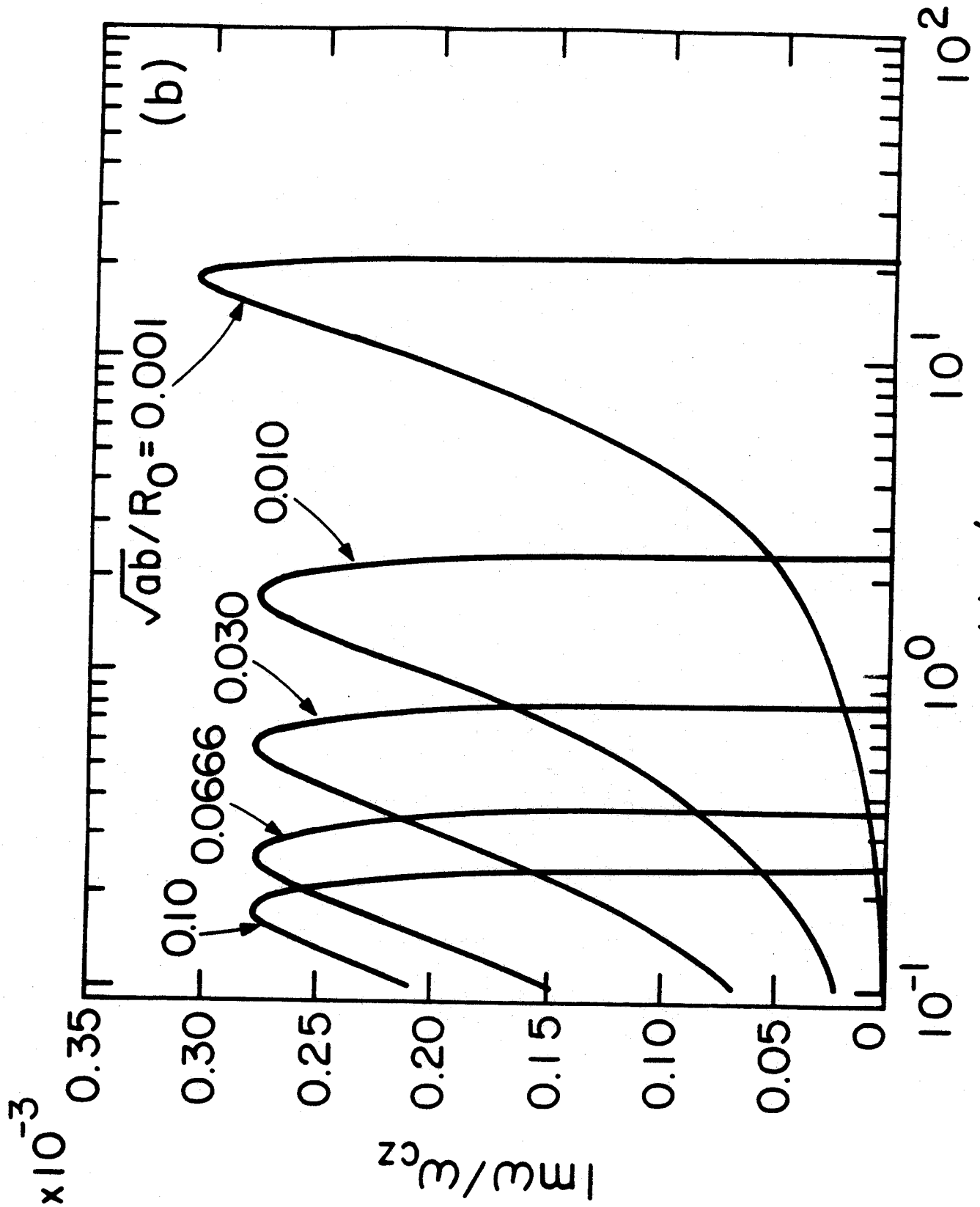
(b)
$\sqrt{ab}/R_0 = 0.001$
0.010
0.030
0.0666
0.10
ω_{pe}/ω_{cz}
$\mathrm{Im}\omega/\omega_{cz}$
$\times 10^{-3}$
0.35
0.30
0.25
0.20
0.15
0.10
0.05
0
10^{-1}
10^{0}
10^{1}
10^{2}

Fig. 11(b)

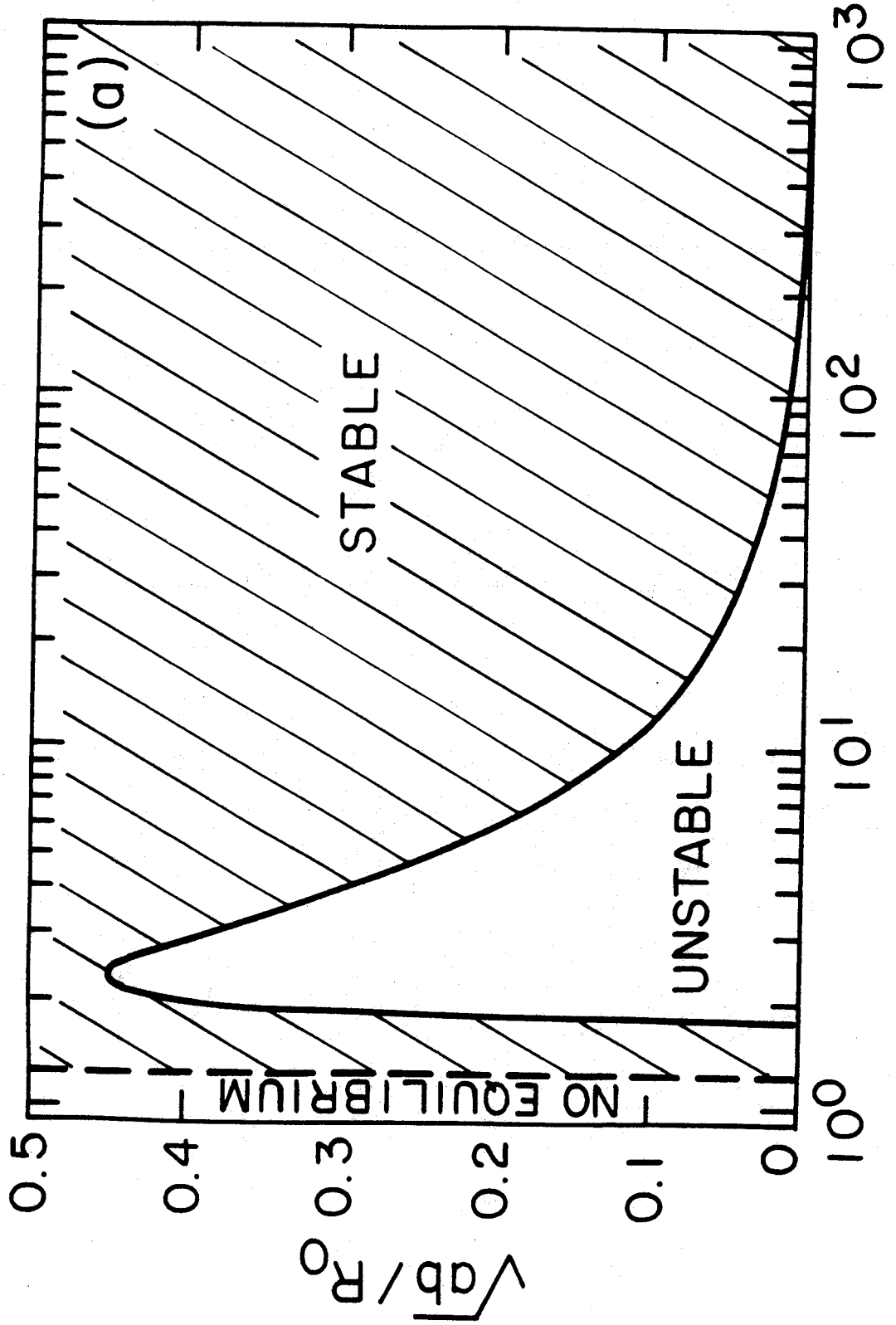
(a)
STABLE
UNSTABLE
NO EQUILIBRIUM
0.5
0.4
0.3
0.2
0.1
0
10^0
10^1
10^2
10^3
γ_b
$\sqrt{ab}/R_o$

Fig. 12(a)

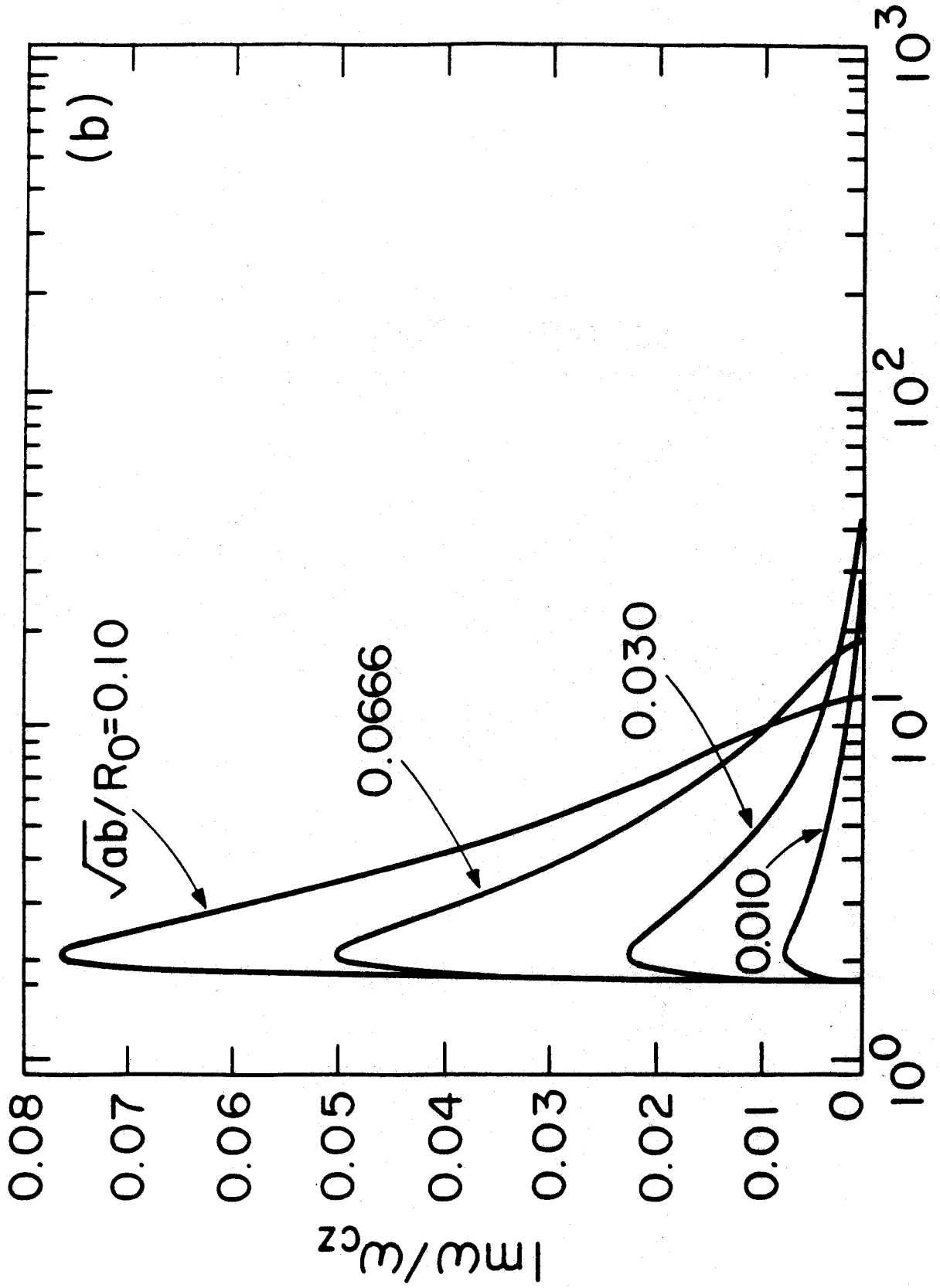
(b)
$\sqrt{ab}/R_0$=0.10
0.0666
0.030
0.010
γ_b
$\mathrm{Im}\omega/\omega_{cz}$
0.08
0.07
0.06
0.05
0.04
0.03
0.02
0.01
0
10^0
10^1
10^2
10^3

Fig. 12(b)

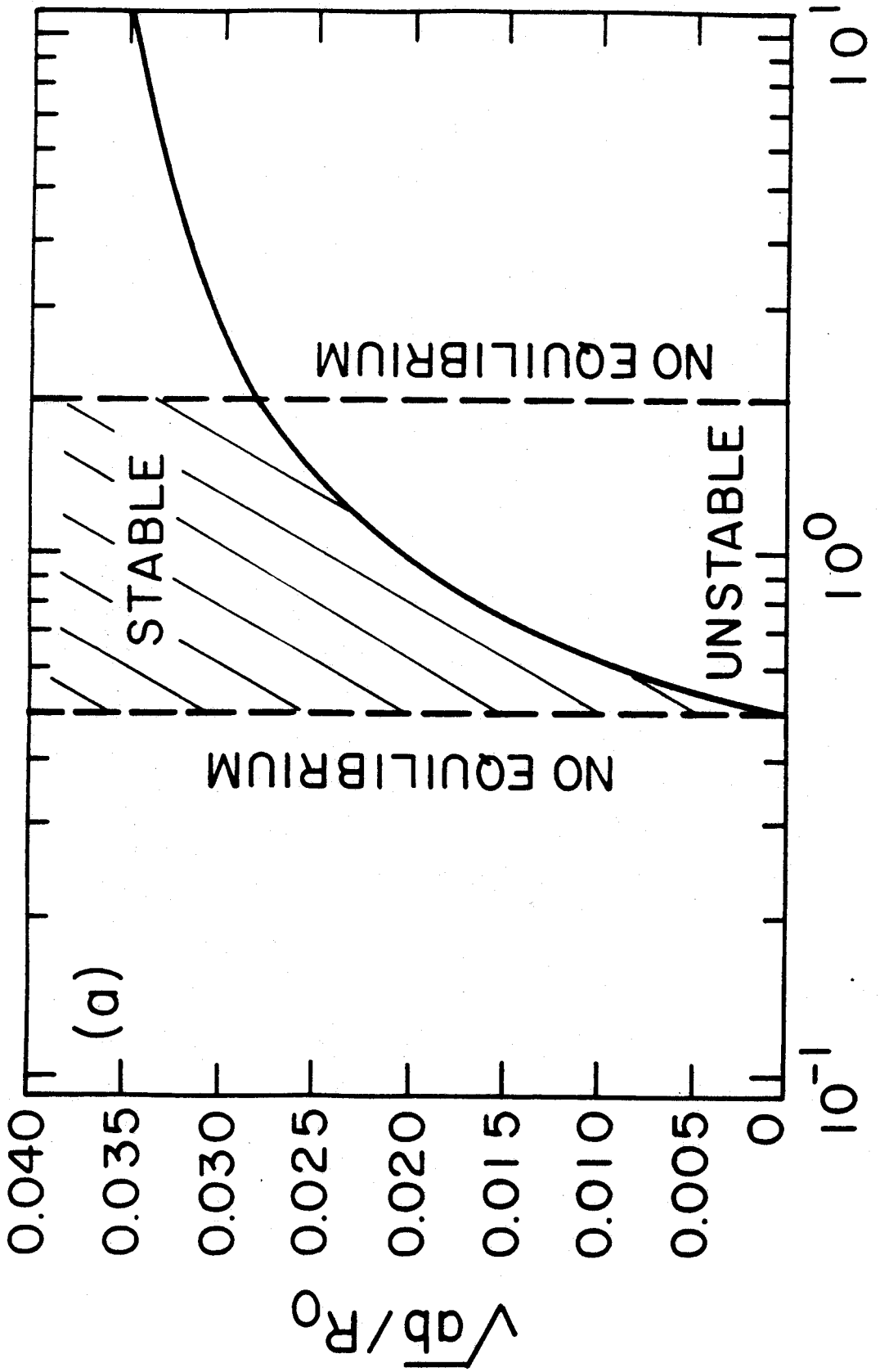
(a)
NO EQUILIBRIUM
STABLE
UNSTABLE
NO EQUILIBRIUM
$\sqrt{ab}/R_o$
b/a
0.040
0.035
0.030
0.025
0.020
0.015
0.010
0.005
0
10^{-1}
10^{0}
10^{1}

Fig. 13(a)

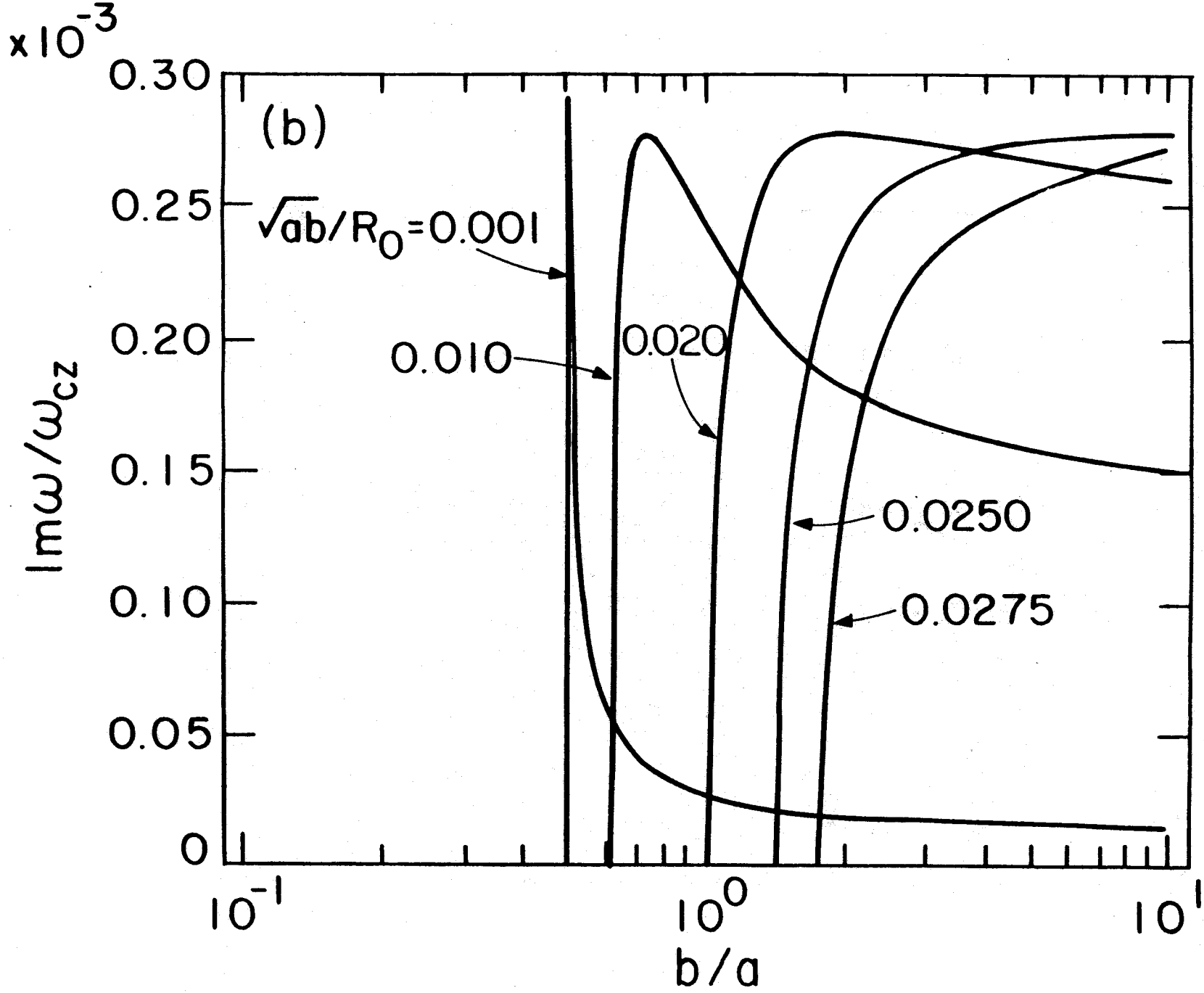
x10^-3
0.30
0.25
0.20
0.15
0.10
0.05
0
(b)
√ab/R0=0.001
0.010
0.020
0.0250
0.0275
Imω/ωcz
10^-1
10^0
10^1
b/a

Fig. 13(b)

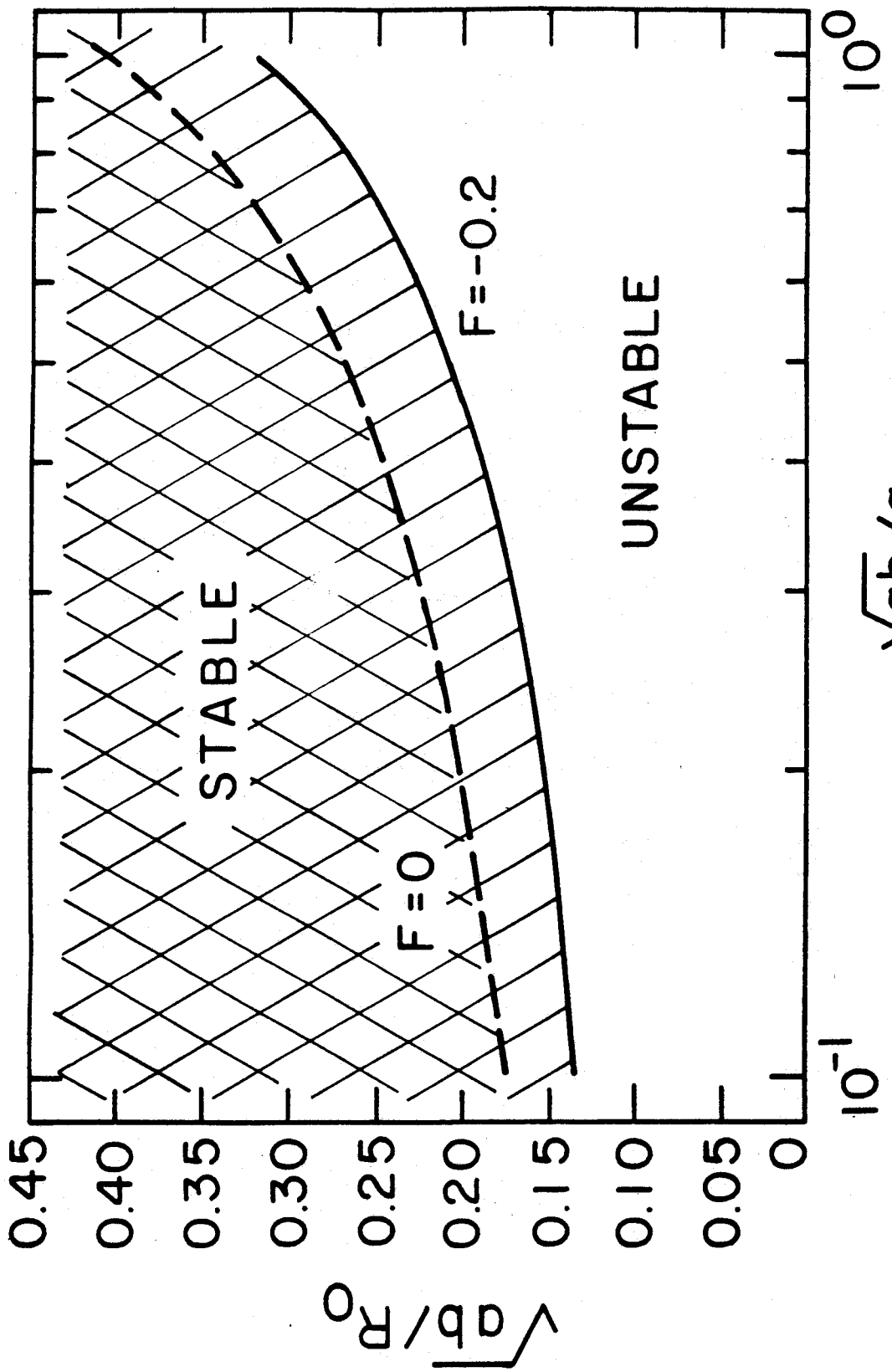
STABLE
UNSTABLE
F=0
F=-0.2
0.45
0.40
0.35
0.30
0.25
0.20
0.15
0.10
0.05
0
10^{-1}
10^{0}
$\sqrt{ab}/R_0$
$\sqrt{ab}/a_c$

Fig. 14